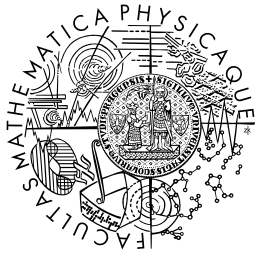

FACULTY
OF MATHEMATICS
AND PHYSICS
Charles University

DOCTORAL THESIS

Matěj Jan Morávek

Study of plasma in the mixtures with molecular gas at wide pressure range

Department of Surface and Plasma Science

Supervisor of the doctoral thesis:	doc. RNDr. Věra Hrachová, CSc.
Study programme:	Physics
Study branch:	Physics of Plasma and Ionized Media

Prague 2021

I declare that I carried out this doctoral thesis independently, and only with the cited sources, literature and other professional sources.

I understand that my work relates to the rights and obligations under the Act No. 121/2000 Sb., the Copyright Act, as amended, in particular the fact that the Charles University has the right to conclude a license agreement on the use of this work as a school work pursuant to Section 60 subsection 1 of the Copyright Act.

In Prague 20. 5. 2021 Matěj Jan Morávek

Title: Study of plasma in the mixtures with molecular gas at wide pressure range

Author: Matěj Jan Morávek

Department: Department of Surface and Plasma Science

Supervisor: doc. RNDr. Věra Hrachová, CSc., Department of Surface and Plasma Science

Abstract: The positive column of DC glow discharge sustained in oxygen and oxygen-nitrogen mixtures has been studied in two discharge tubes of the same shape made from different materials (Silica and Pyrex glass) for total pressures 650 – 2000 Pa and discharge currents up to 40 mA. Various parameters of the discharge – axial electric field strength, concentration of electrons and emission spectra – were studied with emphasis placed on transition region between low- and high-gradient form of the positive column. We have focused on the qualitative and quantitative analysis of the differences in emission spectra for both particular forms and the transitional region between them. The impact of 1 % admixture of nitrogen was also studied.

Keywords: Low-temperature plasma Oxygen DC Glow discharge Optical emission spectroscopy

In the first place I thank my supervisor, doc. RNDr. Věra Hrachová, CSc. for her patience and many advices she gave me during the past many years we worked together. I would also like to thank to RNDr. Adolf Kaňka, Dr. and Mgr. Lukáš Schmiedt, PhD. for teching me how to work with the laboratory equipment and their help with maintenance. I also thank to Mgr. Marek Laca, PhD. for his invaluable theoretical insight and help with some of the MatLab finesses. I also thank doc. Mgr. Pavel Kudrna, Dr. for his help with the microwave resonator and for lending the service program. Last but not least I must thank to my loving wife for her patience with which she let me pursue this long-time goal.

Contents

Introduction

This work is mostly a compilation of the experimental results obtained in the DC Glow Discharge (DC GD) in the pure oxygen and in the mixture of oxygen with nitrogen. This work follows the main research aim of the laboratory of doc. Hrachová at the Department of the Surface and Plasma Science of the Faculty of Mathematics and Physics of the Charles University in Prague. The main aim of my work was to broaden the previously (and usually) studied pressure region of few torrs (hundreds of pascals) to the region of middle pressure as high as our apparatus will be able to sustain the discharge. We found the limits of our apparatus around 2 kPa of total pressure, so the presented results are mainly from the region 650 Pa - 2000 Pa.

What makes this region technically interesting is the possibility of operation of the many technological and industrial processes which use the DC GD in oxygen (such as plasma etching [1], sterilization of the surfaces [2] etc.) with lower demands on the vacuum system.

However in this region the oxygen DC glow discharge shows unusual behaviour. Next to the so-called H-form of positive column, the so-called T-form emerges. These forms differ mainly by optical emission and axial electric field (for more about the forms see section 1.2). The cause of the simultaneous occurrence of these forms one next to the other in the same discharge and their distinct separation by a transitional region is a great unknown till these days.

This work is divided into five chapters. Chapter 1 presents short historical overview of the DC GD research from the very beginning to the present day with an emphasis on the work made in our laboratory.

Chapters 2 and 3 describe the diagnostic methods used and the experimental apparatus respectively. The optical emission spectroscopy, which was the main experimental method used, is described in detail.

The results and their discussion are divided into three sections according to the gas composition in the discharge: section 4.1 covers the results obtained in pure oxygen, section 4.2 covers the results obtained in oxygen-nitrogen mixture (99:1) and 4.3 compares the results of the previous two. Each chapter is divided into subsections according to the experimental method used.

The main results are summarized in the Conclusion on page 70.

The main aim of this work was to provide comprehensive study of the oxygen DC Glow Discharge, not only to provide basis for modelling in order to describe the positive column of the discharge in the two forms and the transitional region inbetween them.

1. DC Glow Discharge in Oxygen - the overview

The low temperature plasma of DC Glow Discharge in oxygen and its mixtures with other gases (e.g. N_2, Cl_2, SF_6 and others) at low pressures historically plays important role in many both industrial and research processes. Among these let us mention plasma etching [3], [4], plasma oxidation [5], thin layer deposition [1], formation of superconducting materials [6] and sterilization [2], [7]. The discharge sustained in mixtures of rare and molecular gases (for example $O_2 - Ne$ mixture, $O_2 - Ar$ mixture) can also be utilized as working environment of gas lasers [8].

In the last decades the move for transferring these applications into higher pressures that are not so susceptible to impurities and need cheaper equipment stimulated the research into atmospheric pressure discharges and discharges sustained at medium pressures. The properties and even behaviour of the discharge changes significantly with increasing pressure, hence our study pushes previous research made at our laboratory to higher pressure range. We will try to summarize the most important facts about glow discharge in pure oxygen in following subsections.

1.1 Pure Oxygen discharge

DC Glow discharge can be sustained under wide pressure range from few Pa up to few tens of kPa. The typical structure of the glow discharge consists of cathode areas (Aston dark space, cathode glow, cathode dark space, negative glow, Faraday space), positive column and anode area (anode glow and anode dark space) [9]. Spatial range of the particular areas depends foremost on the size of discharge area (i.e. distance of the driving electrodes) and on the working pressure.

Considering low pressures (below few hundreds Pascals), the glow oxygen discharge can exist with so-called long cathode fall where the cathode area occupates majority of the discharge volume at the expense of the positive column. The form with the long cathode fall can be also distinguished by the values of driving voltage for particular discharge current, which are of one order of magnitude higher than in the standard form. This behaviour is rather common also for glow discharges sustained in other gases [10]. With increasing pressure, the discharge stabilizes in the standard form with widely spread diffusion-controlled positive column, which can get contracted to the axis of the discharge for high pressures [9].

The glow discharge in oxygen is a complex medium containing electrons and both neutral and charged atomic and molecular species of both positive and negative charge. It has been found that the degree of dissociation of the molecular oxygen to atomic oxygen increases with increasing current [11] and slightly decreases with pressure.

The effect of gas impurities on the oxygen dissociation was studied e.g. in [12]. The authors concluded that the better was the vacuum purity of the discharge system before filling with oxygen, the lower the oxygen dissociation.

To describe and explain the experimental results, several theoretical models of pure oxygen discharge were created (e.g. [13] or lately [14]). In [13] authors presented one-dimensional self-consistent model is based on the solution of Boltzmann's kinetic equation for electrons and set of balance equations for molecular oxygen O_2 in ground electronic state and excited states O_2 $(a^1\Delta)$ and $O_2(a^1\Sigma)$, for atomic oxygen O, ozone O_3 and O^- anions. Interactions between electrons and vibrationally excited O_2 molecules in a ground quantum state were also taken into account. This model was able to determine transport parameters of electrons (mean value of energy, drift velocity) as well as dependence of reaction rate constants on the value of electrical field strength.

In [14] and in similar model for oxygen-argon mixture [15], Laca proposed a fluid model based on the moments of the Boltzmann's kinetic equation for electrons and set of balance equations for molecular oxygen O_2 in ground electronic state and excited states O_2 $(a^1\Delta)$ and $O_2(a^1\Sigma)$, for atomic oxygen O, ozone O_3 and O^- anions. Interactions with the wall of dicharge tube were also incorporated. This model was able to determine transport parameters of electrons (mean value of energy, drift velocity) in radial direction of cylindrical discharge. Knowing these factors, it was also possible to specify importance of each single process for all species included (creation and extinction of particles) and to obtain radial profiles of their densities. The most important result is the Bessel profile of ions and flat profile of kinetic temperature, which was confirmed, among others, in this study.

By these analyses, the dissociation of O_2 and O_2 $(a^1\Delta)$ by impact of an electron was found to be the main process for creation of the atomic oxygen:

$$e^- + O_2 \rightarrow e^- + O + O, \tag{1.1}$$

$$e^- + O_2\ (a^1\Delta) \rightarrow e^- + O + O. \tag{1.2}$$

The surface re-association was found as the most important process for the atomic oxygen extinction:

$$O + wall \rightarrow \frac{1}{2}O_2. \tag{1.3}$$

As it was stated above, the important part of oxygen discharge are negative oxygen ions (O^-, O_2^-, O_3^-). Their density easily reaches and can be even greater than the electron density in some cases. High values of rate coefficient of the dissociative attachment of electrons by O_2 molecules or $O_2(a^1\Delta)$ metastables are the main reasons.

For the value of reduced electric field (over 5000 V/m in standard discharge), three-body collision also plays an important role:

$$e + O_2 + O_2 \rightarrow O_2^- + O_2. \tag{1.4}$$

The presence of negative ions in the discharge can affect discharge properties such as conductivity, electrical field strength and also ambipolar diffusion, which is the key process for the space distribution of charged particles in the positive column of DC Glow Discharge. Study of radial distribution of charged particles is therefore one of the very important topics.

1.2 H-form and T-form of oxygen discharge

One of the important parameters of positive column is the axial electric field strength E or reduced electric field E/N, which corresponds to the energy dissipated to the discharge. When Güntershultze studied the dependence of electric field strength on discharge current in the oxygen [16], he noticed previously unseen behaviour of the positive column of the discharge. Besides standard positive column with values of electric field strength E of about 2000 V/m, another 'form' of the oxygen discharge was observed. This form was distinguished by the colour of emitted light as well as by significantly lower values of the electric field strength E (about 650 V/m). These forms were observed not only under the same conditions, but coexisting in the same discharge. For the widest discharge tube (radius 45 mm), only the form with lower values of E appeared independently on the discharge current used (25 mA and 50 mA). For the tube with the radius of 15 mm, this anomalous form appeared only after the discharge ignition but immediately collapsed into the form with higher values of E. For the narrowest tube with radius of 4.1 mm this form was not present at all.

This study was followed by a study made by Seeliger and Wichmann [17], who investigated the influence of the pressure and discharge current on the existence of the forms in the tubes 50 –120 cm long with the inner diameter of 10, 30 and 60 mm, respectively. They used pressure range of 0.5 – 7 Torr (or 66.5 Pa - 931 Pa) and employed discharge current up to 250 mA. The observed difference in values of the axial electric field strength E in the respective forms was systematically about one order of magnitude. According to the values of E authors named the forms as the *H-* and *T-form*: high-gradient form with electrical field strength of about kV/m was called the H-form (from the German 'hoch', i.e. high) and the low-gradient form with electrical field strength of about hundreds of V/m was called the T-form (from the German word 'tief', i.e. low). It was found that the low-gradient T-form appeared at higher pressures and lower current densities compared to the H-form. Moreover, authors managed to set such values of pressure and discharge current, that the both forms existed simultaneously, each in different part of the discharge tube. Seeliger and Wichman also analysed emission spectra of the discharge in the visible range of the wavelengths. They found mainly spectral lines corresponding to the transitions between quantum states of the neutral atomic oxygen in the H-form, while in the T-form the band of the so-called first negative system (see e.g. [18]) originating from the deexcitation of the O_2^+ molecular excited states was prominent.

Pekárek and Šícha [19] investigated the presence of ionization waves (or striations) in the positive column for the pressure 2 Torr (266 Pa) and discharge current 9.5 mA when both forms were present in the positive column. They concluded that the positive column of the H-form was homogeneous, while ionization waves were observed in the T-form. Unlike striations which are common in the rare gases or in hydrogen, the existence of the ionization waves in the T-form of the oxygen discharge was limited only to certain distance from the cathode.

Řezáčová studied the electron density in the both forms for pressures 2 – 7 Torr (266 Pa - 931 Pa) and discharge currents up to 40 mA by the means of microwave toroidal resonator [20]. Lower electron density was found in the H-form than in the T-form. The transition of one type of the discharge to another

at the pressure of 0.35 Torr (46.5 Pa) was also observed. The electron density in both forms was measured for discharge current of 21.5 mA, when gradient in the positive column was 9 V/cm. The value of electron density in both forms was found to be $n_e = 1.109$ cm^{-3}, which was in good agreement with another study made by Drost et. al [21].

Keren [22] employed quadrupole mass spectrometer for mass analysis of positive ions both in the T- and H-forms of the glow discharge in pure oxygen for the pressure 2,5 Torr (332.5 Pa) and for the discharge current 10 mA. The discharge tube used for the measurements was of the inner diameter of 33 mm. Positive ions O_2^+ and O^+ were found in the T-form, while only O_2^+ ions were observed in the H-form under the same conditions. The mass spectrometer was also used by Kocian and Mayor for the analysis of oxygen atom, O^+ and O^- ions density in the both forms [23]. Authors used an oxygen-nitrogen mixture with 0.4 % of N_2. Plasma was generated in a Pyrex discharge tube with inner diameter of 60 mm by DC glow discharge in the pressure range of 0,05 – 5 Torr (6.65 - 665 Pa) with discharge currents 20 – 200 mA. The experiment was realized in the flowing regime. Authors found out that in the low-gradient T-form the degree of dissociation of the molecular oxygen decreased with increasing discharge current, while in the high-gradient H form the degree of dissociation increased with increasing discharge current. It was also found that the density of O^- ions increased in the H-form with discharge current, while O^+ ions density was very small there (authors mentioned the value 0.001 for the O^+ to neutral atoms density ratio).

The complex investigation of the glow discharge in oxygen with respect to the existence of the high- and low-gradient forms was presented by Dettmer [24], who experimentally studied and mathematically modelled oxygen discharge in a quartz discharge tube with inner diameter of 19 mm and anode-cathode distance of 505 mm. The measurements were realized in flowing regime for pressure range of 1 – 10 Torr (133 - 1330 Pa) and for current densities up to 35 mA/cm^2. Moreover, a cooling system was utilized to maintain the discharge tube and the wall on the temperature near that of tap water. The H-form was present at higher currents and lower pressures while the T-form was observed at lower currents and higher pressures. The H-form exhibited stable characteristics while the low-gradient T-form was observed to be unstable, exhibiting both periodic or aperiodic oscillations. The periodic oscillations existed only at certain frequencies or modes. The discharge impedance was the function of the frequency. Mass spectra measurements indicated that the atomic oxygen density increased significantly when the discharge transitioned from the T- to the H-form. Solutions of the Boltzmann kinetic equation indicated that the electron energy distribution function exhibited a characteristic intermediate between the Maxwellian and Druyvesteyn distribution.

Chemistry model results presented in the work showed O_2^+ to be the dominant positive ion and the O^- to be the dominant negative ion in both forms. The transition from the stable to unstable form was found to be related to the two criteria: the dominance of the derivative of the attachment coefficient with respect to E/N over that of the ionization coefficient, and the equivalence of the negative ion and electron number densities. The metastable $O_2(a^1\Delta)$ was found to be important in the discharge for two reasons: the two-step ionization was required together with the direct ionization to match the experimental electron density

measurements; second, the inclusion of the metastable molecule as the primary electron donor was required to match the transition points determined in the experiment with those determined from the model.

Latest inquiry was made by Schmiedt et al. [25]. Authors studied the DC Glow discharge in pure oxygen and in oxygen-argon mixture. Using optical emission spectrometry together with double-probe measurements enabled identification of another parameter that could be used to discern between the H- and T-form – the ratio of intensity atomic oxygen line triplets O I (^5P) (head at 777.2 nm) and O I (^3P) (head at 844.7 nm). It was found that in the H-form, the intensity ratio O I (^5P)/O I (^3P) was roughly 1, in the T-form it was almost twice as large. This parameter can therefore be used for determination of the state of the discharge column without the need for probe measurements, which disturbs plasma and can even lead to collapse of the T-form.

1.3 Oxygen-Nitrogen discharge

The oxygen-nitrogen mixture was widely studied in many works (e.g. flowing discharge [26], stationary discharge [27]). The importance of the study of especially small nitrogen additions stems from the fact that nitrogen (and water vapors) present the most common impurity in the vacuum systems. V. Guerra and J. Loureiro presented model of oxygen-nitrogen discharge plasma in [28]. This self-consistent one dimensional model predicts the concentrations of N_2, O_2, NO, NO_2, N_2O, NO_3, N_2O_5 a O_3 molecules in ground state and in excited states $N_2(A^3\Sigma, B^3\Pi, a'^1\Sigma, a^1\Pi, C^3\Pi, a''^1\Sigma)$ and $O_2(a^1\Delta, b^1\Sigma)$, O and N atoms in ground state and in excited states $N(^2D, ^2P)$, $O(^1D, ^1S)$ and concentrations of electrons and ions N_2^+, $N_2^+(B)$, N_4^+, O^+, O_2^+, NO^+, O^-. The calculations took into consideration also vibrational kinetics of nitrogen molecules and heat transfer. Using this model the main processes affecting the composition of the discharge were described.

This model showed that the E/N was decreasing with increasing ratio of oxygen to nitrogen. This was explained with lower ionization potential of dioxygen with respect to dinitrogen. The changes in E/N affected also the concentration of free electrons through changes in the drift velocity of electrons (in order to maintain fixed current density, the concentration of electrons has to adjust).

In this model is also described steep rise in the concentration of atomic oxygen when small addition of nitrogen is introduced into oxygen discharge. It is explained with lowering of the efficiency of wall recombination of oxygen (1.3) by the equivalent nitrogen wall reassociation process

$$N + wall \rightarrow \frac{1}{2}N_2 \tag{1.5}$$

because of occupancy of the wall recombination centers by nitrogen atoms [29].

1.4 Objectives of this thesis

The DC Glow discharge in oxygen and the phenomenon of simultaneous occurrence of H- and T-form was previously studied in our laboratory at lower

pressures, where the H-form is dominant. In order to understand the nature of the T-form and especially the boundary transitional region between the respective forms, the aim of this work is to study oxygen discharge at as high pressures as our equipment enables to facilitate the occurrence of the T-form and its stability. Other parameters of the discharge such as geometry, gas purity etc. are kept constant to enable comparison with previous work.

The main objectives of the thesis are therefore to study:

- The DC Glow Discharge in pure oxygen and in the oxygen-nitrogen mixture (ratio 99:1) using optical emission spectrometry with respect to the simultaneous occurrence of the H- and T-form of the positive column in medium pressures.
- The transitional region between said forms using optical emission spectrometry and toroidal resonator.
- Effect of the nitrogen addition on the T-form occurrence, as well as on discharge parameters.
- Effect of the discharge tube material.

2. Diagnostic methods

This chapter lists diagnostic methods along with deeper notes regarding necessary calculations.

2.1 Double probe compensation method

The double probe compensation method as is described in [9] was utilized in order to determine axial electric field strength. This is an important parameter used to describe energetic terms inside the discharge plasma. In order to be able to compare discharges of different type and geometry, John Sealy Townsend proposed the use of reduced electric field E/N, i.e. electric field strength divided by numerical density of gas in discharge. In low temperature plasmas with low ionization, the density of neutral gas is used. The unit, townsend is defined e. g. in [9] as

$$1\ Td = 10^{-21}\ V \cdot m^2 = 10^{-17}\ V \cdot cm^2.$$

The double probe compensation method is simple to perform and interpret as long as certain conditions are met. These conditions include stable discharge without ionization waves and as small probes as possible with the same dimensions and positioning in the discharge. A DC voltage from an adjustable source separate from the discharge source is then put on the probes and adjusted so that the current in the circuit formed by the source – probe – plasma – probe is zero. The voltage of the source is then equal to the potential difference in the discharge plasma between the probes positions (see schematics of the circuit in the fig. 3.3).

The numerical density of the gas was calculated from total pressure p (measured using capacitance gauge) and neutral gas temperature T (calculated from rotational temperature of oxygen molecules, see section 2.2.2) using the ideal gas formula

$$p = nk_BT, \tag{2.1}$$

where n is the numerical density in unit volume and k_B is the Boltzmann constant.

2.2 Optical emission spectroscopy

The optical emission spectroscopy is efficient method with the benefit of being totally passive - by simply examining the emitted radiation it does not affect the discharge in any way. It also enables us to deduce chemical and energetic ratios in the plasma.

The limitations are systematic (inability to measure non-emitting species, such as particles in their ground states) and technological - in our case of low emission intensity, high time requirements. Exposition times up to 100 s per scan were necessary in order to achieve reasonable resolution of the spectra in some cases (the radial measurements).

2.2.1 Concentration measurements

When using properly calibrated equipment, it is possible to calculate absolute concentrations of the emitting species (for more details about how the equipment used in this work was calibrated see Section 3.3.3, page 24).

When the equipment is calibrated, we are able to convert counts per second to the actual watts. With the spectrum in watts per wavelength, we can integrate over the emission lines and thus get emitted intensity I^m_{if}. This can be also calculated as

$$I^m_{if} = C \cdot I^0_{if} = C \cdot n_i \cdot V \cdot A_{if} \cdot h\nu_{if}, \tag{2.2}$$

where I^0_{if} is the actual intensity emitted from the volume V, n_i is the concentration of the emitting species, A_{if} is the Einstein coefficient of spontaneous emission from a state i to a state f, ν_{if} is the corresponding frequency of the emitted radiation, h is the Planck constant and C is a geometric coefficient of the setup. This geometric coefficient C needs to be calculated by other means, e.g. using simulation.

Different C and V were used for measurements along the discharge axis and perpendicularly to it, respectively. These were determined by collaborating ing. Jiří Čáp from Czech Technical University, Faculty of Mechanical Engineering in his 3D ray-tracing model (for more details see section 3.3.3).

In this work, concentrations of the atomic oxygen in the states O I ($3p\ ^5P$), O I ($3s\ ^3P$) and oxygen molecule in the state O_2 ($b\ ^1\Sigma^+_g$) were calculated using spectral lines and coefficients mentioned in the table 2.1.

Table 2.1: Table of emission lines and bands used to calculate concentration of excited species in the discharge.

Particle	Line/band	λ_{if} $[nm]$	Transition	A_{if} $[s^{-1}]$	Ref.	Note
O	Triplet at 777 nm	777.194	$3p\ ^5P \rightarrow\ 3s\ ^5S^0$	$3.69 \cdot 10^7$	[30]	
		777.417				
		777.539				
	Triplet at 845 nm	844.625	$3p\ ^3P \rightarrow\ 3s\ ^3S^0$	$3.22 \cdot 10^7$	[30]	Merged into one line
		844.636				
		844.676				
O_2	Atmospheric band	759 - 774	$b\ ^1\Sigma_g^+(v=0) \rightarrow X\ ^3\Sigma_g^-(v=0)$	$8.5 \cdot 10^{-2}$	[31]	

2.2.2 Rotational temperature

In the DC Glow Discharges in oxygen and its mixtures an important band of lines is almost always present in the wavelength range 759 - 774 nm. This so-called Atmospheric Band (A-band) of oxygen molecule is formed by transition of electrons from excited rotational levels. Since they are usually well resolved (at least the ${}^{P}P$ and ${}^{P}Q$ branches), we can use them to analyse the rotational energy and temperature (supposing steady-state regime and therefore Boltzmann energy distribution again).

We can again use the right part of the equation (2.2) where we introduce the formula for population of rotational levels, thus getting for the transition from level J_i to J_f (see [32])

$$I_{J_iJ_f} = C \cdot \nu^4_{J_iJ_f} \cdot S_J \cdot e^{-\frac{F_J}{k_B T_{rot}}}, \tag{2.3}$$

where $\nu_{J_iJ_f}$ is the frequency of the transition emission, S_J is Hönl-London factor (part of Einstein's spontaneous emission coef. A that is related to the rotational quantum number J_i, [32]), F_J is the energy of the quantum state J_i, k_B is Boltzmann thermodynamic constant and T_{rot} is the rotational temperature. This equation can again be reformulated as an equation of pyrometric line

$$\ln\left(\frac{I_{J_iJ_f}}{S_J}\right) = C'\left(\nu^4_{J_iJ_f}\right) - \frac{F_J}{k_B T_{rot}}. \tag{2.4}$$

The $C'\left(\nu^4_{J_iJ_f}\right)$ might as well be taken for constant, because of the small frequency range of the A-band. Similarly to the determination of vibrational temperature, the rotational temperature can be derived by linear regression from the Boltzmann plot of $ln\left(\frac{I_{J_iJ_f}}{S_J}\right)$ vs. F_J. An example of A-band with corresponding Boltzmann plot can be seen in Fig 2.1.

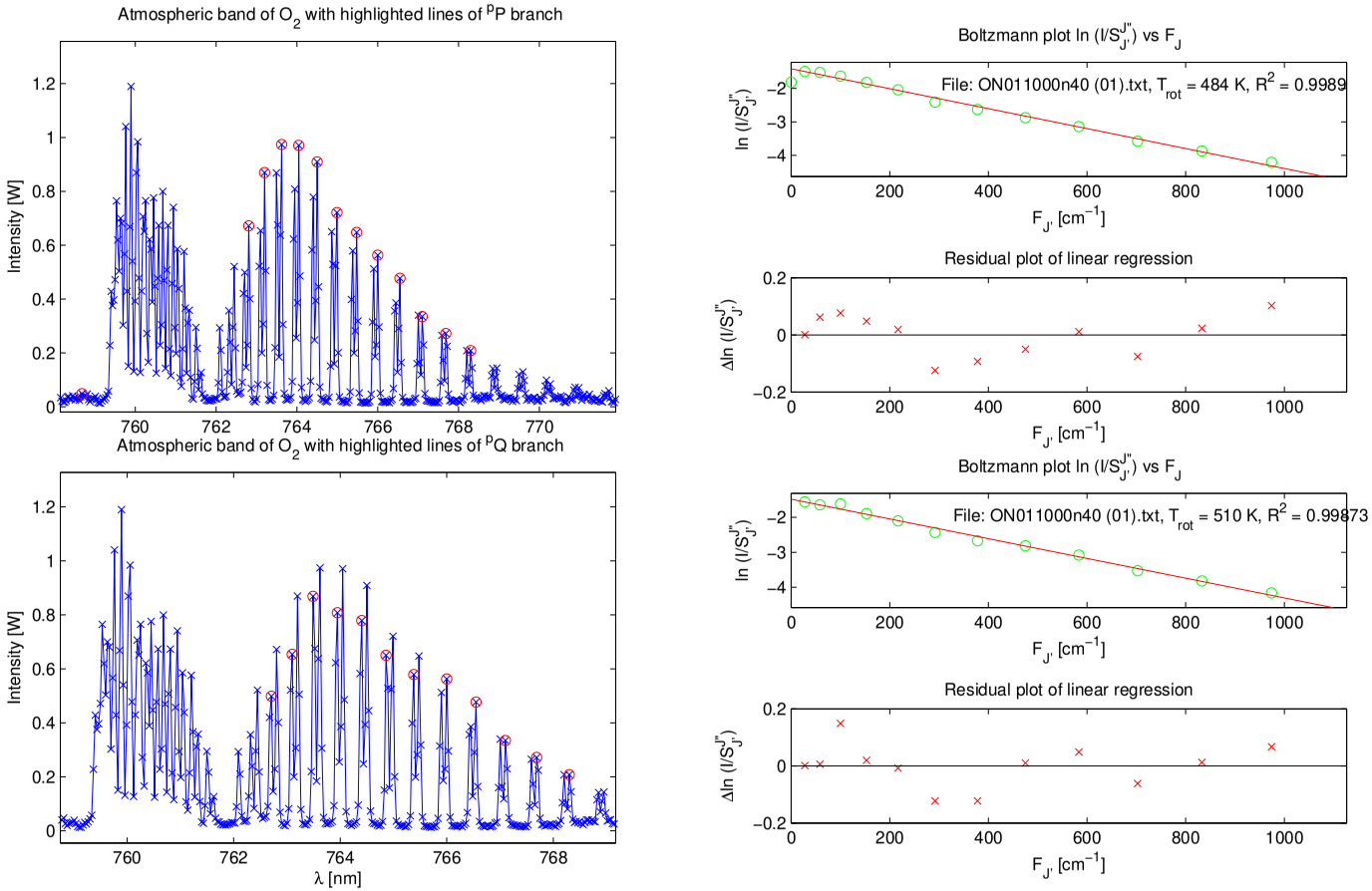

Figure 2.1: *The Atmospheric band of oxygen molecule with indicated ${}^{P}P$ and ${}^{P}Q$ branches, corresponding Boltzmann plots and calculated rotational temperature. Oxygen-nitrogen mixture (99:1), total pressure 1000 Pa, discharge current 40 mA. The figure shown is an example of the output of the MatLab script TrotO2v5 created by author for analysis of the spectra.*

The importance of the rotational temperature of oxygen molecules lies in the fact, that due to low Einstein coefficient (see Table 2.1), the mean lifetime of the excited molecules reaches few seconds, thus leaving enough time for them to reach thermal equilibrium with the kinetic temperature of their surroundings (in low- to medium-pressure glow discharge plasma this means neutral gas). Therefore the rotational temperature of oxygen can be used as indirect measurement of the kinetic temperature of the neutral gas [33].

For the calculation of Hönl-London factors S_J were used formulas as determined by Schlapp [34] and verified by Miller [35], shown in the table 2.2. The energy levels E_J were calculated using formula

$$E_J = B_{\nu'=0} \cdot J \cdot (J+1) - D_{\nu'=0} \cdot (J \cdot (J+1))^2, \tag{2.5}$$

where $B_{\nu'=0} = 1.39138\ cm^{-1}$ and $D_{\nu'=0} = 5.486 \cdot 10^{-6}\ cm^{-1}$ are constants taken from [31].

Table 2.2: Formulas for calculation of the Hönl-London factors S_J, [34]

Branch	S_J
${}^{P}P$	$0.5 \cdot (J_f + 1)$
${}^{P}Q$	$0.5 \cdot (J_f + 0.75)$
${}^{R}Q$	$0.5 \cdot (J_f + 0.25)$
${}^{R}R$	$0.5 \cdot J_f$

2.3 Microwave resonator

In order to gain insight into as many parameters as possible and especially their change along the transitional region between T- and H-form, last diagnostic method applied were microwave resonance measurements using toroidal microwave resonator with thin opening as described in [36].

The method is based on the change of resonance parameters of an electromagnetic resonator, when the permitivity inside changes. The change in permitivity is a result of introduction of conductive plasma. If the empty resonator is described with circular resonance frequency ω_0 and quality Q_0 then the changes in the circular frequency and quality $\Delta\omega$ and $\Delta(Q^{-1})$ can be calculated as

$$\frac{\Delta\omega}{\omega} = -\frac{2\pi}{\omega_0}\frac{\int_{V_p}\sigma_i E^2 dV}{\int_V E^2 dV}, \tag{2.6}$$

$$\Delta\left(\frac{1}{Q}\right) = \frac{4\pi}{\omega_0}\frac{\int_{V_p}\sigma_r E^2 dV}{\int_V E^2 dV}, \tag{2.7}$$

$$\Delta\omega = \omega - \omega_0, \tag{2.8}$$

$$\Delta\left(\frac{1}{Q}\right) = \frac{1}{Q} - \frac{1}{Q_0}, \tag{2.9}$$

where V is the volume of the entire resonator, V_p is the volume of the plasma inside the resonator, E the intensity of electrical high-frequency field and $\sigma = \sigma_r + j\sigma_i$ is the complex plasma admittance.

In real-life measurements it is impossible (and impractical) to measure directly $\Delta\omega = \omega - \omega_0$, because the frequency difference is caused not only by plasma presence, but also by the presence of the neutral gas and experimental equipment. Therefore the common practice is to measure the resonant frequency with plasma (ω) and the resonant frequency of the resonator with discharge tube and gas without the discharge (ω_{np}) and use $\Delta\omega' = \omega - \omega_{np}$ which represents the change due to plasma itself.

It is noteworthy that the above mentioned set of equations enables also the calculation of the collision frequency of the electrons and heavy particles in plasma ν (see equation (2.10)).

Since the high frequency plasma admittance σ can be calculated using simple relation

$$\sigma = \sigma_r + j\sigma_i = \frac{n_e e^2}{m_e} \cdot \frac{\nu - j\omega}{\nu^2 + \omega^2}, \tag{2.10}$$

where e is the elementary charge, m_e electron mass, ν is collision frequency of electrons with heavy particles and n_e is the sought electron concentration. The formula and following formulas in this section are in CGS system of units as is usual in literature (e.g. [9]).

After we calculate the necessary integrals and measure the change in frequency, we should be able to determine the n_e. The admittance of the plasma is a function of the concentration of electrons which is not necessarily constant over plasma column cross-section even in such electronegative plasma as is the positive column of a discharge in oxygen. Hence the profile function of the electrons needs to be estimated. The correct profile can be assumed using Schottky's theory, which leads to Bessel distribution in cylindrical geometry due to ambipolar diffusion. This fact was confirmed for the conditions of DC Glow Discharge in oxygen by Laca et al. using computer modelling [14]. Therefore the dependence of admittance σ on distance from discharge axis r may be expressed as

$$\sigma(r) = \frac{n_0 e^2}{m_e} \cdot \frac{\nu - j\omega}{\nu^2 + \omega^2} \cdot J_0\left(2.405 \cdot \frac{r}{R}\right), \tag{2.11}$$

where n_0 is the concentration of electrons on the discharge axis, J_0 is the Bessel function of zero order and R is the radius of plasma column.

If we introduce (2.11) into (2.6) and rearrange, we get

$$n_0 = \Delta\omega' \cdot \omega_{np} \cdot \frac{m_e}{e^2} \cdot \frac{\int_V E^2 dV}{\int_{V_p} J_0\left(2.405 \cdot \frac{r}{R}\right) E^2(r,z) dr dz} = \Delta\omega' \cdot \omega_{np} \cdot \frac{m_e}{e^2} \cdot \frac{1}{\alpha}, \tag{2.12}$$

where the fraction α is dimension-less function of the resonator geometry and dimensions.

It is therefore necessary to calculate the volume integrals for the particular resonator and the frequency of self-oscillation ω_0. Let

$$I_1(U,V) = \int_V E^2 dV, \tag{2.13}$$

$$I_2(U,r,z) = \int_{V_p} J_0\left(2.405 \cdot \frac{r}{R}\right) E^2(r,z) dr dz. \tag{2.14}$$

To be able to perform any meaningful calculations, we assume that the electric field between the 'tips' of the resonator is quasistationary and it can be treated as capacitor connected in parallel to the radial line [36]. The integrals (2.13) and (2.14) can be and need to be treated differently from here onward.

2.3.1 Empty resonator - $I_1(U, V)$

The integral $I_1(V)$ represents energy stored in the empty resonator, i.e. resonator filled with only electromagnetic waves, hence it is calculated over whole volume of the resonator. The rather complicated construction of toroidal resonator (see Fig. 3.7) means that in order to calculate I_1 it was split into four integrals that could be calculated analytically (see [36] for more details on the calculations). In order to calculate these integrals, the frequency of self-resonance ω_0 has to be determined - in our case it was calculated using the method described in [36]. The final value of I_1 is therefore only function of the resonator dimensions V and the amplitude of the driving voltage U.

2.3.2 Conductor in the resonator - $I_2(U, r, z)$

The integral (2.14) presents much more complicated problem. On one side the integral volume V_p is much simpler as it is only the interaction region - the cylinder of plasma in our case. One problem that needs to be assessed is the problem of setting the boundary along the resonator axis. Šícha et al. shows this as a significant advantage of the toroidal resonator, where the interaction region is easily confined inside the resonator cavity due to thin opening, through which the resonator and plasma interacts [37].

On the other side the electric field inside the cavity cannot be calculated analytically due to the effect of Besselian distribution of the electron concentration J_0 over the plasma cross-section, so the whole integral needs to be computed numerically. The electric field inside the plasma can be computed by means of electron optics formulas for bi-cylindrical electrostatic lens of the same diameter in the quasistationary state. According to the [38] the potential in the position (r, z) of the axial symmetric field may be expressed by the series

$$U(r,z) = \sum_{n=0}^{\infty} (-1)^n \frac{U_0(z)^{(2n)}}{(n!)^2} \cdot \left(\frac{r}{2}\right)^{2n}, \tag{2.15}$$

where $U_0(z)$ is the potential distribution along the axis of symmetry z and $U_0(z)^{(2n)}$ are even derivatives in the position z.

For the bi-cylindrical lens of inner diameter R that are separated by s which is negligible to R, the potential $U_0(z)$ can be expressed as (from [38], this is different formula than the one used in [36], which is only approximative):

$$U_0(z) = U \cdot \tanh\left(1.315 \cdot \frac{z}{R}\right), \tag{2.16}$$

where $\tanh(x)$ is the hyperbolic tangent of x. The value of E^2 was then calculated using my own MatLab script and the derivatives of $U_0(z)$ were calculated using Wolfram Mathematica online [39].

2.3.3 Double-probe characteristic

In order to confirm the correctness of our calculations, two controls were performed. One was simply using the parameters of the Šícha's resonator as is described in [40] and comparing our results to the ones given in the article. This

test was satisfying if we take into account much better precision with which the calculations we can do now compared to the methods used in 1966.

The second control was performed by using double-probe V-A characteristic to determine the n_0 by substantially different method. The method of calculation of the electron concentration is described e.g. in [9], p. 121. Since these methods enables us to calculate only ion concentration n_i, these control measurements were performed in pure argon discharge, 50 Pa, where we can safely assume $n_i = n_e$. The results obtained are shown in Table 2.3. It can be seen, that the results obtained using the Langmuir probes and using the toroidal resonator are in sufficient agreement.

Table 2.3: The comparison of electron density n_e measured using toroidal resonator and ion density n_i measured using double-probe method. The distance between the places of measurement was 1.5 cm.

Resonator - $n_e[cm^{-3}]$	2 probes - $n_i[cm^{-3}]$	$\Delta[cm^{-3}]$	Δ_{rel}
$3.00 \cdot 10^9 \pm 2.66 \cdot 10^4$	$4.05 \cdot 10^9 \pm 1.25 \cdot 10^8$	$1.05 \cdot 10^9$	26%
$2.98 \cdot 10^9 \pm 2.67 \cdot 10^4$	$4.09 \cdot 10^9 \pm 8.00 \cdot 10^7$	$1.11 \cdot 10^9$	27%
$3.05 \cdot 10^9 \pm 2.73 \cdot 10^4$	$3.09 \cdot 10^9 \pm 1.10 \cdot 10^8$	$4.09 \cdot 10^7$	1%

3. Experimental Setup

This chapter considers experimental set-up used. It describes in detail each of the various technics used.

3.1 Discharge tube and vacuum system

The crucial part of our experimental set up consists of glass discharge tube connected to the vacuum system. We used two discharge tubes with similar geometry – U-shaped cylinders with prolonged central part equipped with head-on planar windows for optical emission spectrometry (see fig. 3.1 for detailed dimensions). The discharge tubes were made out of different material to see the effect of the wall composition on the discharge chemistry and behaviour. One was made out of industrial pyrex glass, one from pure silica glass. The discharge electrodes were made from nickel cup on molybdenum wire, later replaced by platinum hollow cylinders on molybdenum wire. The central part was equipped with two pairs of cylindrical platinum probes (0.1 mm diameter).

The tube was connected with stainless steel system of valves and pumps. The pumping part consisted of turbomolecular pump Pfeiffer TMH O64 prepumped by a diaphragm pump Pfeiffer MVT 015-T with base pressure below 100 Pa. The base pressure of the system (around $2 \cdot 10^{-5}$ Pa) was measured using Pirani-Penning double gauge Pfeiffer PKR 261. The pressure of the filling was measured using capacitance gauge Balzers ACR 263.

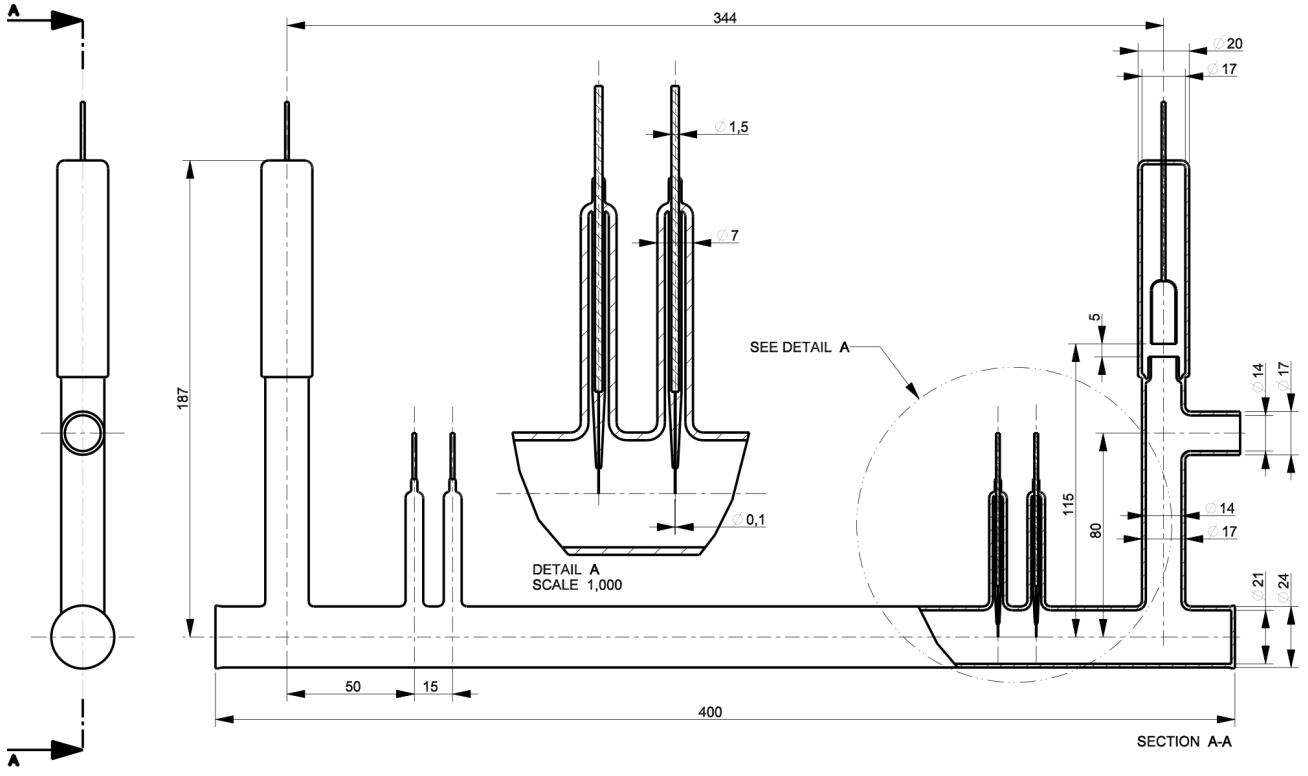

Figure 3.1: *Schematics of the discharge tube with measurements in mm.*

To supply the gas into the system, needle valves in series with globe valves were used. Filling gases were supplied in glass balloons made by Röderer GmbH containing pure oxygen and nitrogen (declared purity 10 ppm). The discharge was operated in steady-state regime (the tube was filled, sealed off and then the discharge was ignited).

To ensure purity of the system, the discharge tube with part of filling tubes were enclosed in an oven and heated to 420 °C while pumped prior to each set of measurements. The temperature was held still for at least an hour (longer after long pauses or adjustments on the vacuum system such as exchange of the gas balloons). The pressure after such treatment was always better than $4 \cdot 10^{-5}$ Pa. The necessity of such treatment and its effect on the presence of especially water impurities was discussed e.g. in [12].

The scheme of the discharge tubes id in Fig. 3.1. The schematics of the vacuum system are shown in Fig. 3.2.

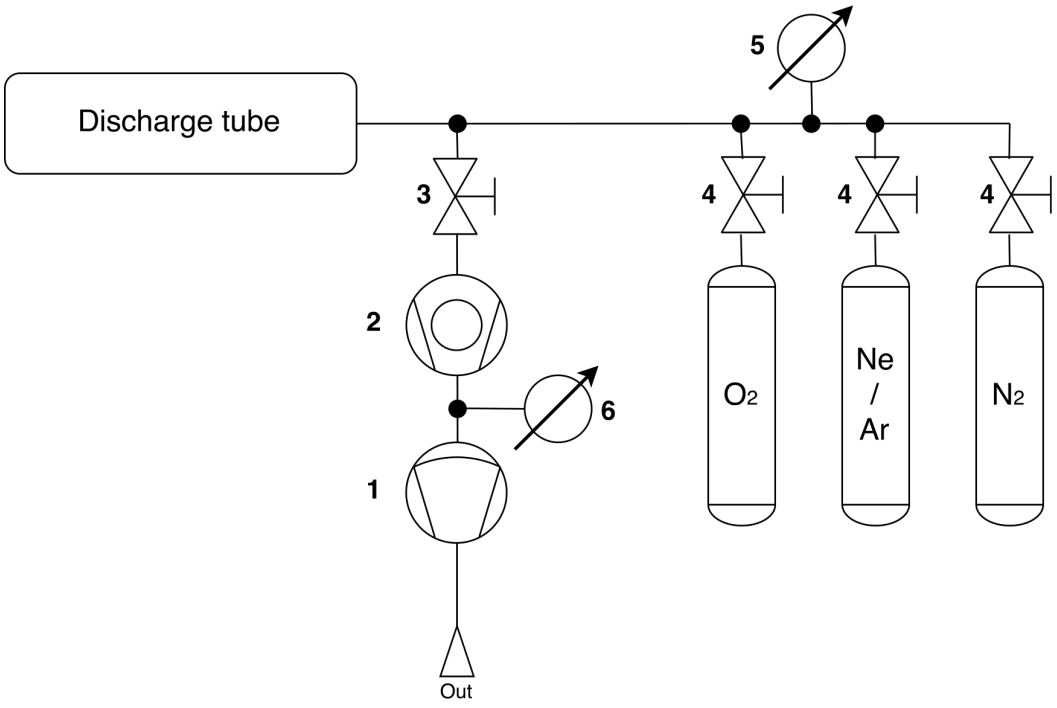

Figure 3.2: *Schematics of the vacuum system. 1 - Diaphragm pump, 2 - Turbomolecular pump, 3 - Manual valve, 4 - Needle valve with stopper, 5 - Capacitance gauge, 6 - Pirani-Penning gauge.*

3.2 Double probe

The central part of the discharge tube was equipped with two pairs of cylindrical Langmuir probes. The probes were made out of platinum wire with diameter of 0.1 mm and length of the part in connection to plasma of 10 mm. These were mainly used to determine the axial electric field strength, an important parameter of the positive column of the glow discharge. The compensation method was used as is described in section 2.1. The circuit used can be seen in Fig. 3.3, detail of the probes is in Fig. 3.1.

A set of alkaline batteries was used as a voltage source. Two multimeters were used for the determination of voltage and current in the circuit.

The same circuit was used to determine the double-probe characteristic of the discharge for electron density determination (see part 2.3.3).

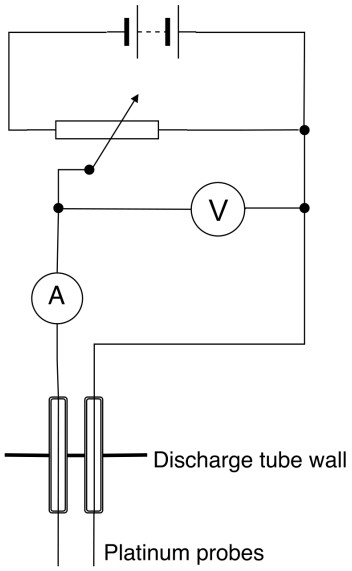

Figure 3.3: *Schematics of the electric circuit for the double probe measurements.*

3.3 Optical spectroscopy system

The main diagnostic method used was optical emission spectroscopy. As a passive method it has many advantages and disadvantages, covered in more detail in section 2.2. Three geometrical set-ups were used for determination of the properties of the discharge.

3.3.1 Longitudinal and perpendicular setup

In most measurements, the emitted light was collected perpendicularly to and along the axis of the central part of the discharge tube as is schematically shown in the figure 3.4. The co-axial set-up had the advantage of higher emitting volume scanned, resulting in much better spectra contrast and lower noise. On the other hand, the emitted light was collected from almost whole length of the positive column, mixing up emission from T-form and H-form, when both were present.

The perpendicular set-up had much better spatial resolution, enhanced by simple rectangular diaphragm placed near the discharge tube wall. The width of the opening was 1 mm measured along the discharge tube axis. The disadvantage of this set-up was significantly low signal gain, resulting in long exposition times (up to 100 s).

The emitted light was collected using bare optical fiber (silica glass core, diameter 0.2 mm, numerical aperture 0.22). The fiber was adjusted in a holder

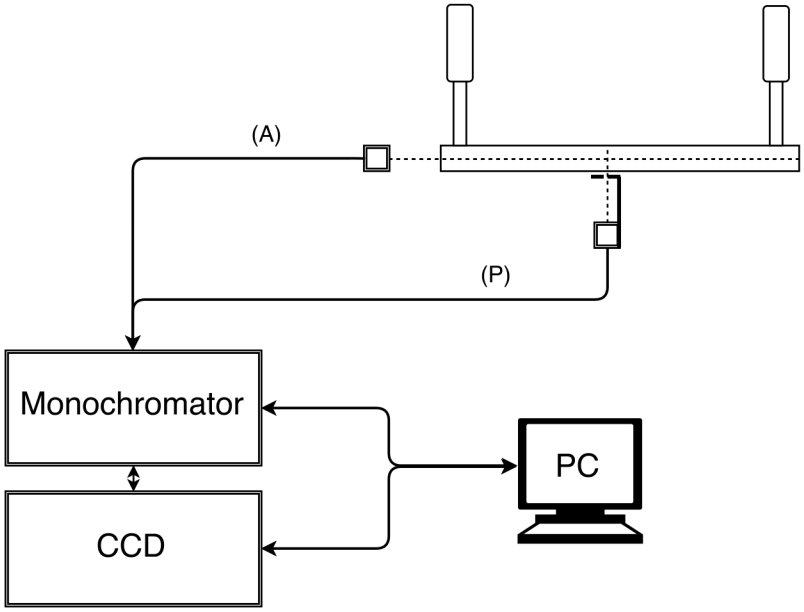

Figure 3.4: *Schematics of the optical measurements. The emitted light was collected along the discharge tube axis (A) and perpendicularly to it using a 1 mm diaphragm (P).*

5 cm from the discharge tube wall. The fiber led the emitted light to the Jobin-Yvon Spex Triax 550 monochromator with focal length of 550 mm, equipped with plane grating of 1200 grooves/mm, maximum spectral resolution 0.024 nm for the wavelength of 546.07 nm. The monochromator was equipped with an MTE CCD 1024x256-16 detector which was thermoelectrically cooled by means of a Peltier couple to the typical operating temperature of 255 K.

The perpendicular setup was successfully used in previous measurements of standing ionizing waves in CO_2 laser gas mixture [41]. Figure 3.8 shows range measured perpendicularly with the offset of the position denomination.

The collected spectra were processed in software shipped with the monochromator, which subtracted dark spectra collected before each measurement, corrected spectra for cosmic rays and enabled further postprocessing in Origin-like environment. This process is covered in more detail in the section 2.2.

3.3.2 Radial measurements system

The optical scanner for direct radial measurements was originally designed by Dr. Adolf Kaňka from our laboratory (see [42]). It consists of two conical mirrors positioned on common axis. Positive mirror is fixed, while negative ring mirror is adjustable along the common axis. This axis was set to be in line with discharge tube axis. By positioning the negative mirror with respect to the positive mirror, the light from a specified annulus was let through the system lens to output aperture where it was collected by the optical fibre and transferred to the monochromator. Therefore only light emitted in the discharge in between chosen

radii was collected, enabling the direct measurement of the radial dependence of emitted light spectra (see figure 3.5).The width of the annulus could be adjusted by fixed diaphragm. In the measurements presented in this work, it was set to 0.9 mm.

This system was not calibrated for the absolute measurements due to its complexity.

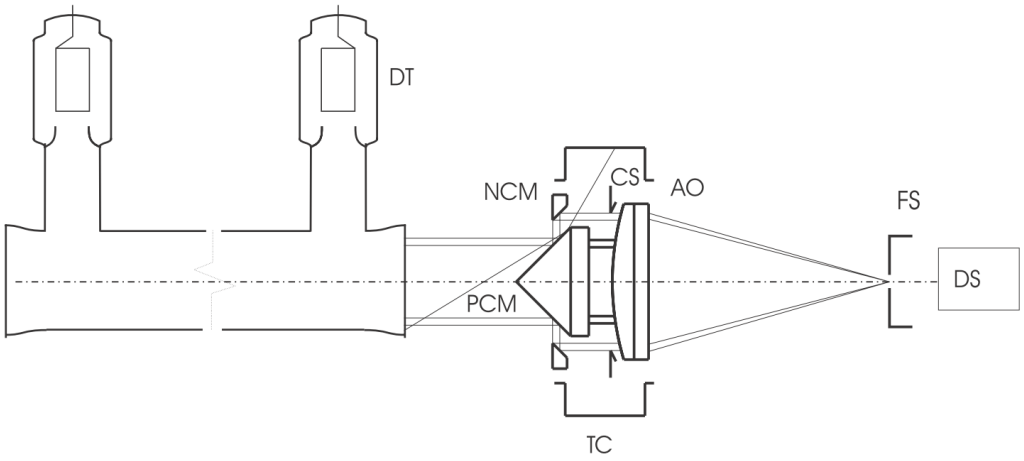

Figure 3.5: *Schematics of the radial scanner. (DT – discharge tube, NCM negative conic mirror, PCM – positive conic mirror, TC – toroidal cavity, CS – circular stop, FS – field stop, AO – achromatic objective, DS – detecting system). Image taken from [42].*

3.3.3 Calibration

In order to be able to calibrate absolute concentrations of the emitting particles, two-step calibration of the setup had to be made. For this purpose tungsten halogen calibration lamp LSK 116 (200 W, 6.6 A) made by L.O.T. Oriel GmbH was used. The irradiance calibration was made by Heraeus Noblelight GmbH laboratory. The calibration spectra provided by Heraeus were divided by measured spectra and spectral responsivity function (or after multiplication by spectral width of the datapoints, the apparatus function to convert counts per second to watts) was obtained (see fig. 3.6). The oscillations in the intensity starting at around 600 nm and increasing towards larger wavelengths are due to the so-called 'etaloning' effect of back-illuminated CCDs. The thin layer of the insulator on the back of the transistor through which the light has to travel in order to be registered behaves as a Fabry-Pérot etalon with width of few microns. More on this in [43].

During second step the concentration of the emitting species was calculated from the measured spectral power (see section 2.2.1, equation (2.2), page 11). The geometric coefficient C featured in the equation contains spectral responsivity of the detector and geometric effects of the setup, such as diffraction, the optical fiber aperture etc. It was obtained using ray-tracing 3D model made in Visual Basic by our collaborator ing. Jiří Čáp from ČVUT.

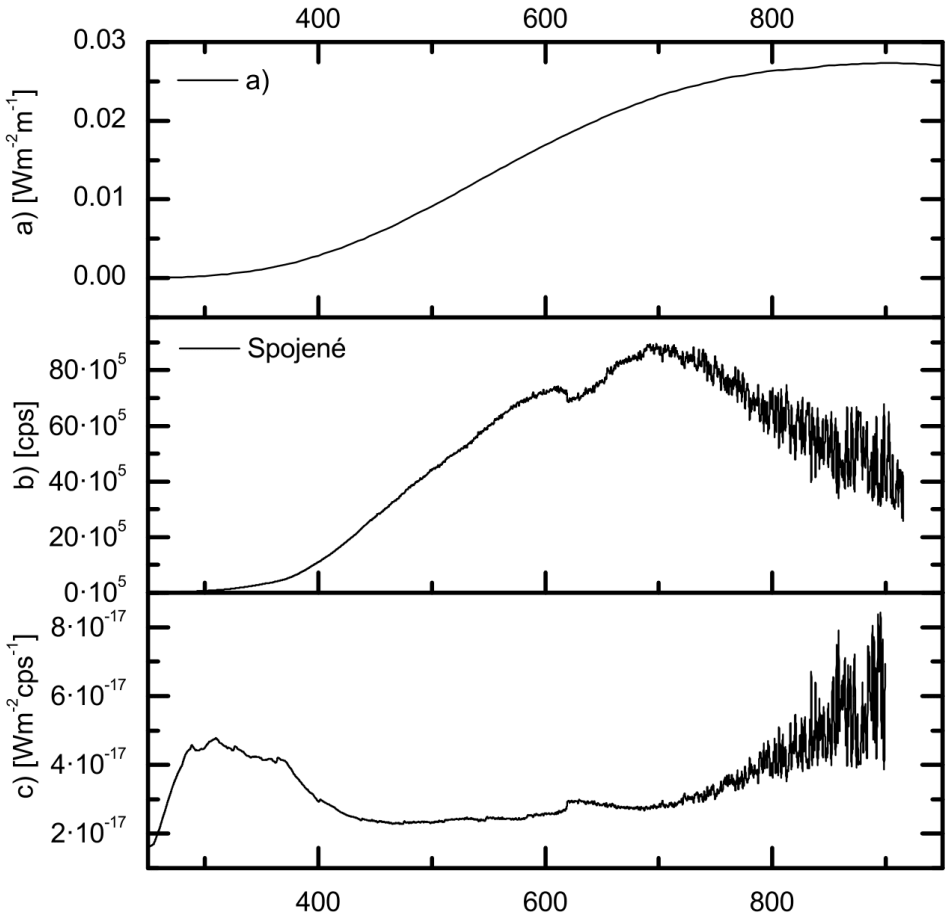

Figure 3.6: *The spectral density of calibration lamp LSK 116 - a) as measured by Heraeus Noblelight GmbH, b) as measured with our setup. The resulting responsivity function of our setup is shown under the letter c).*

The discharge tube was divided into 36 angular times 16 radial sectors (390 sectors along the axis), the face of the optical fibre collecting the radiation was divided into 6 angular times 3 radial sectors. Its position and glass transmitting function were taken into account, auto-absorption was neglected. Resulting coefficient enabled us to calculate the exact I_{if}^0 and from it the mean concentration of emitting species n_i. The estimated standard error of this overall method is better than 15 % (the obvious source of error is the uncertainty of the calibration curve, which is $\pm 8.2\%$ according to the report of the Heraeus Noblelight GmbH; additional 7 % were added due to the uncertainty in the measured irradiation curve).

The intensity profile measured for the 777 nm triplet of atomic oxygen was also implemented in the model. The profile was measured using radial scanner described in section 3.3.2.

3.4 Microwave toroidal resonator

Microwave toroidal resonator of our construction was used in order to determine electron concentration in the positive column of the discharge. The resonator was made out of brass and it was manufactured by Vakuum Praha. The dimensions of the resonator can be seen in Figure 3.7.

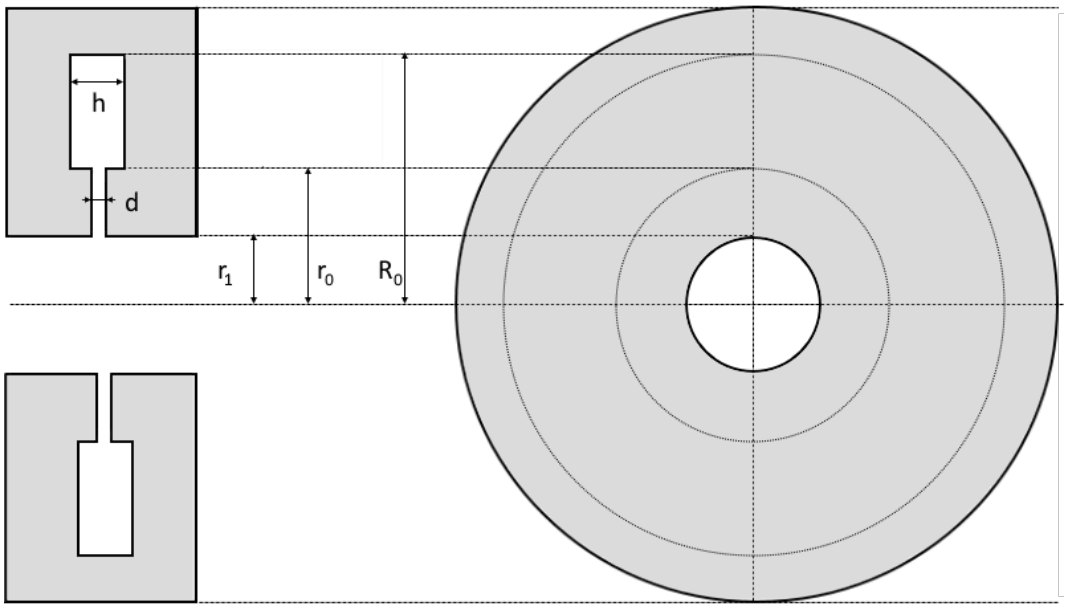

Figure 3.7: *Schematics of the toroidal resonator. Dimensions:* $R_0 = 40\ mm$, $r_0 = 20\ mm$, $r_1 = 13.5\ mm$, $h = 7\ mm$, $d = 2.06\ mm$, *calculated natural frequency* $f = 2253.5\ MHz$

The resonator was placed on movable table with micrometric screw, so it can be positioned on different precisely defined positions along the discharge tube axis. Due to the space restrictions (mainly the Langmuir probes' inlets), the positions in which we could measure the resonances were limited to the range of 51 mm to 196 mm (see figure 3.8)

The resonator was driven by Agilent Microwave Generator N9310A, internal magnetic field was measured using simple antenna from copper wire, connected to the selective nanovoltmeter Unipan type 237. The output was collected by multimeter Agilent U1251A and stored in the controlling computer. The whole setup was controlled via script in Agilent Vee. The driving frequency was set to 1 kHz, upon which the scanning frequency (approx. 2.2 GHz to 2.4 GHz) was superposed by the generator.

The resonance curve of the resonator with only silica discharge tube filled with pure oxygen, 1000 Pa (without discharge) is shown in fig. 3.9. The resonance frequency ν_c and quality Q were determined by fitting the characteristic with

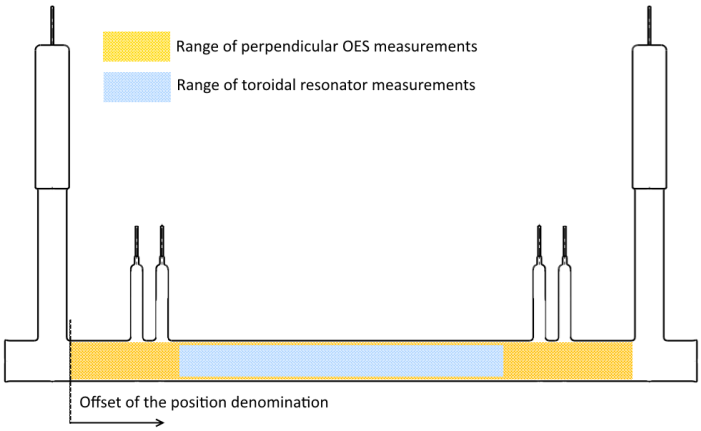

Figure 3.8: *The range of discharge tube scanned with perpendicular measurements and toroidal resonator.*

Lorentz peak function (3.1) and calculated from its definition:

$$y = y_0 + \frac{2A}{\pi} \frac{w}{4 \cdot (\nu - \nu_c)^2 + w^2}, \tag{3.1}$$

$$Q = \frac{\nu_c}{w}. \tag{3.2}$$

The theoretical characteristics of the resonator in vacuum and calculations of the parameters needed for the determination of the electron density were calculated in the section 2.3.

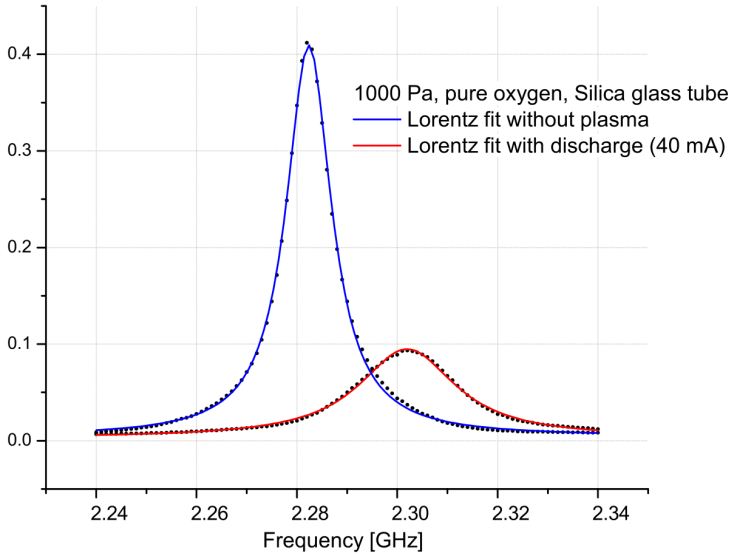

Figure 3.9: *The resonance characteristic of the resonator without and with plasma (filled only with discharge tube with gas). The resonance frequency ν_c was 2.282 GHz and 2.302 GHz and the quality Q was 209 and 98 respectively.*

4. Results

This chapter encompasses all experimental results obtained during the course of this work. The results are divided into sections and subsections as per the gas composition and diagnostic method used.

4.1 Results: Pure Oxygen

The H-form was present in the measurements for 650 Pa of total pressure in the whole discharge tube when the discharge was started at 40 mA of the discharge current. However, when started at 10 mA of the discharge current, the T-form was present in more than three quarters of the examined discharge tube. The region of the T-form shortened with raising discharge current and at around 35 mA the positive column "collapsed" to H-form in whole length. This can be clearly seen in the figure 4.1. The lower concentration of excited species is equivalent to the T-form present in the majority of the observed plasma volume. This is due to lower ionization due to lower axial electric field strength.

4.1.1 OES - Axial Measurements

The results obtained using optical emission spectrometry (see sections 2.2 and 3.3 for more detail) are presented in this subsection. These measurements offer relatively simple and not time-consuming way to check the conditions in the plasma. The main drawback of this method is the inlocality of the measurements, especially when both forms of positive column are present. The T-form was usually at the side of the collecting optical fibre, however since the T-form is much less bright than the H-form, the emission from H-form may be present in significant part.

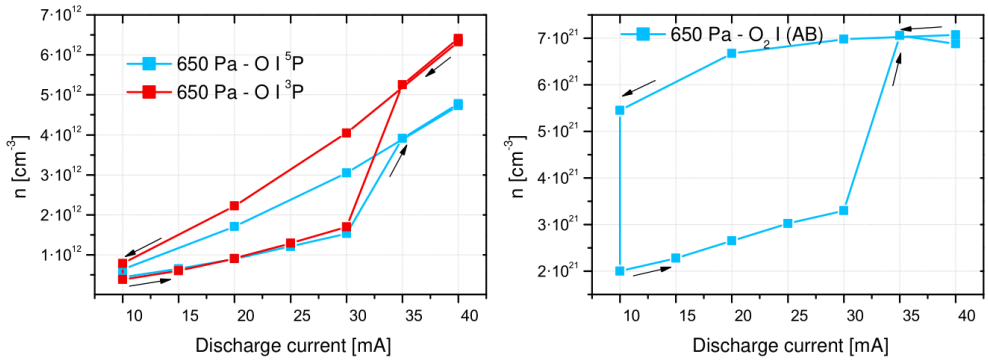

Figure 4.1: *The hysteresis of the positive column form as seen on the concentrations of the excited species O I (^3P), O I (^5P) and O_2 ($b\ ^1\Sigma_g^+$). The direction of discharge current change is shown with arrows, starting at 40 mA and 10 mA respectively. The discharge was turned off and reignited before switching the direction. Pure oxygen, silica discharge tube, total pressure before discharge breakdown 650 Pa.*

4.1.1.1 Rotational temperature

The rotational temperature of dioxygen calculated from optical emission spectra of so-called Atmospheric band (AB), namely the ${}^{P}P$ branch is shown in figure 4.2. The temperature also shows hysteresis due to the presence of H-T-form transition at 650 Pa (see figure 4.3). For higher pressures, the T-form lengthens occupying more and more volume of the discharge tube, so the results presented in the figure 4.2 can be taken as temperature in the T-form of the oxygen discharge for pressures $\geq$ 1000 Pa.

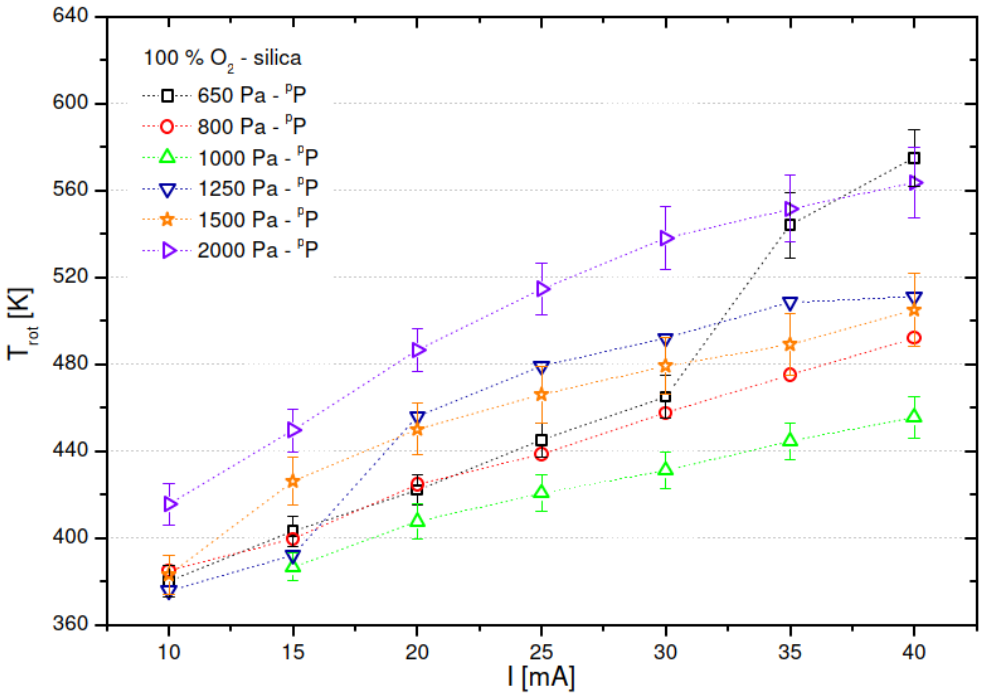

Figure 4.2: *The rotational temperature of oxygen molecules calculated from the Atmospheric band emission. Pure oxygen, silica discharge tube.*

The temperature rises with power fed to the discharge (i.e. with discharge current). The profile of temperature vs. pressure is non-uniform, first falling from 650 Pa to 1000 Pa and then rising to 2000 Pa. This effect was observed systematically a probably is due to the presence of the high-voltage H-form at lower pressures. Higher axial electric field means higher mean velocity of excited particles, which transfers to the rotational temperature of oxygen and neutral gas kinetic temperature. As H-form retracts from the examined volume around 1000 Pa of total pressure, only T-form temperature can be observed. This then rises with pressure as a result of higher power input (to keep the discharge current at chosen value, the driving voltage had to be higher).

4.1.1.2 Concentrations of excited particles

The concentrations of the excited species O I (${}^{3}P$), O I (${}^{5}P$) and O_2 ($b\ {}^{1}\Sigma_g^+$)) are presented in figures 4.4 - 4.6. Only measurements made in T-form at 650 Pa are presented (the "upwards" part from 4.1).

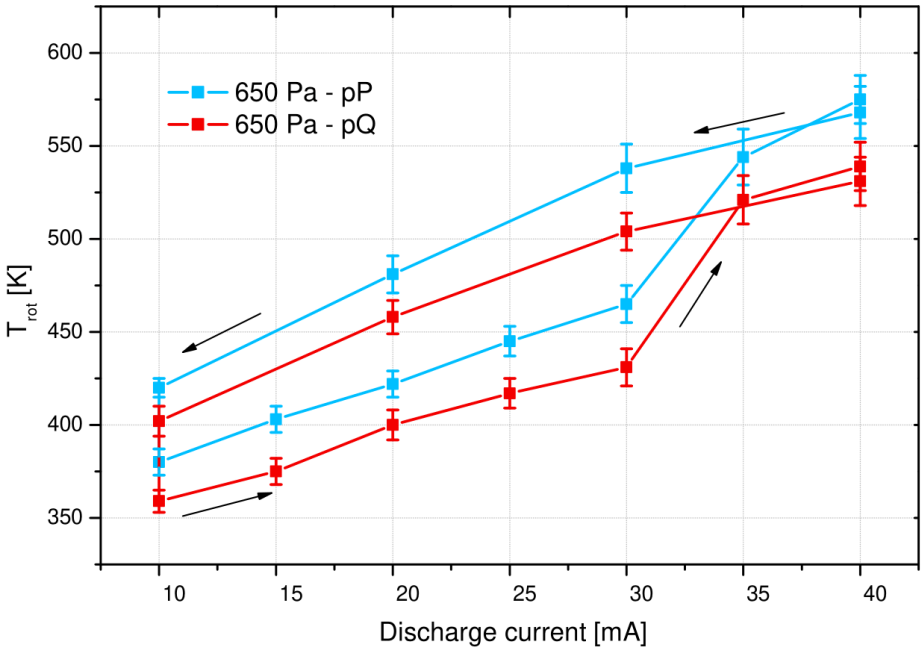

Figure 4.3: *The rotational temperature of oxygen molecules calculated from the Atmospheric band emission, ${}^{P}P$ and ${}^{P}Q$ branch, for pure oxygen, silica discharge tube, total pressure before discharge breakdown 650 Pa.*

The dependence of the concentration for all excited species rises with discharge current, which is simply a consequence of higher power input fed to the discharge. The concentration for the atomic oxygen is non-uniformly falling with rising total pressure. The only irregularity presents the measurements for the total pressure 1000 Pa, which we attributed to instabilities of the discharge, mainly ionization waves, which even made impossible to measure the spectra for 10 mA of discharge current. Second H-form forming near the anode was observed too. The T-form is very unstable when surrounded by H-form from both sides (it can be sustained, but every minor distortion like inserting voltage on the probes may cause collapse to uniform H-form). It can be seen that while the atomic oxygen concentrations are lower than would correspond to invertible fall with pressure, the concentration of molecular oxygen is much higher. The higher concentration of molecular oxygen and lower of atomic oxygen was attributed to the H-form and presented as one of the chemical differences between the forms by Dettmer [24].

Apart from the 1000 Pa, the concentrations uniformly fall with the raise of total pressure. This is due to the lowering of the reduced electric field E/N (from about 30 Td at 650 Pa to about 5 Td at 2000 Pa, for more details see section 4.1.4).

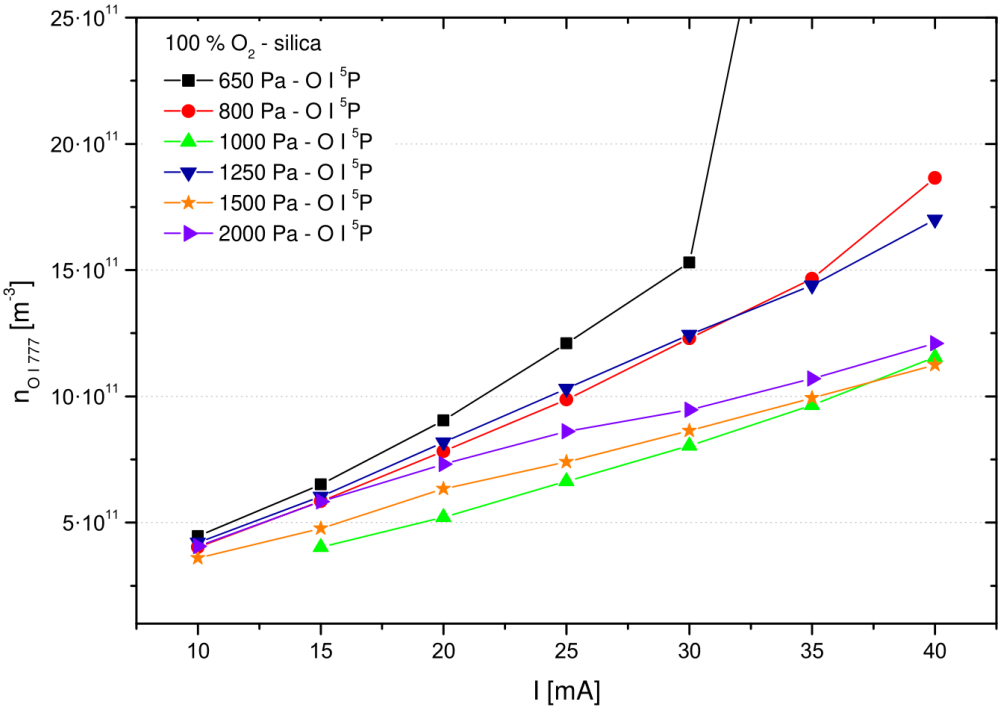

Figure 4.4: *The concentration of O I (^5P) as measured using calibrated optical emission spectrometer. The relative uncertainty of each datapoint is* ±15 %. *Pure oxygen, silica discharge tube.*

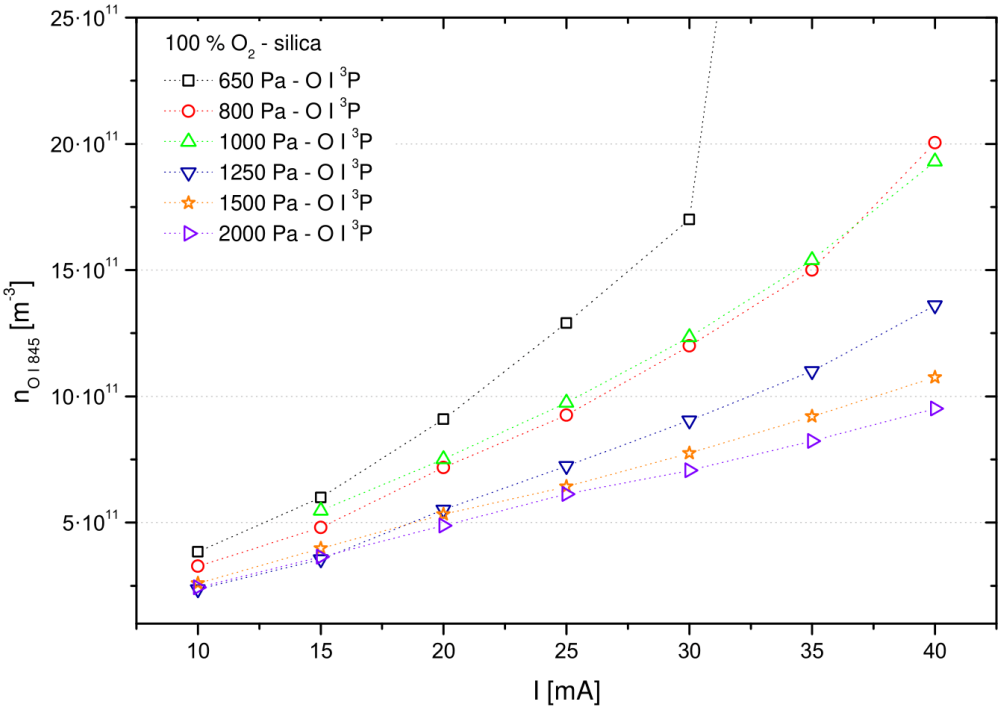

Figure 4.5: *The concentration of O I (^3P) as measured using calibrated optical emission spectrometer. The relative uncertainty of each datapoint is* ±15 %. *Pure oxygen, silica discharge tube.*

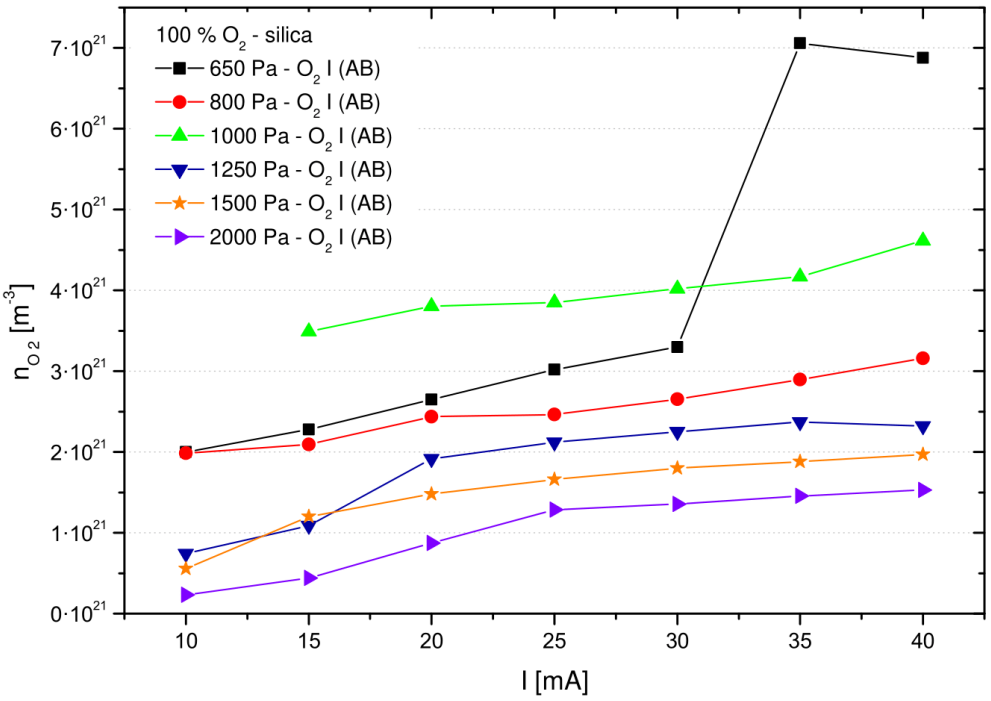

Figure 4.6: *The concentration of* O_2 $(b\ ^1\Sigma_g^+)$ *as measured using calibrated optical emission spectrometer. The relative uncertainty of each datapoint is* ± 20 %*. Pure oxygen, silica discharge tube.*

4.1.2 OES - Perpendicular measurements

In order to acquire some locality for our optical measurements, second geometry of experiment was used with the optical fiber positioned perpendicularly to the discharge tube axis. For even better spatial resolution, the fiber intake was equipped with rectangular diaphragm of the width of 1 mm (for more details see section 3.3.1).

The respective forms were discernible both in the overall intensity of collected spectra (as well as by naked eye) and in the spectra composition. Two main effects observed were increase in rotational temperature between T- and H-form and change in atomic oxygen concentration. For details see next subsections.

4.1.2.1 Rotational temperature

The rotational temperature of oxygen molecules was determined in the same fashion as for the co-axial measurements. The 'step' in the temperature between T- and H-form is clearly visible for all pressures where the transitional region was observable. The width of this step was in all cases about 20-25 mm as can be seen in Figure 4.7.

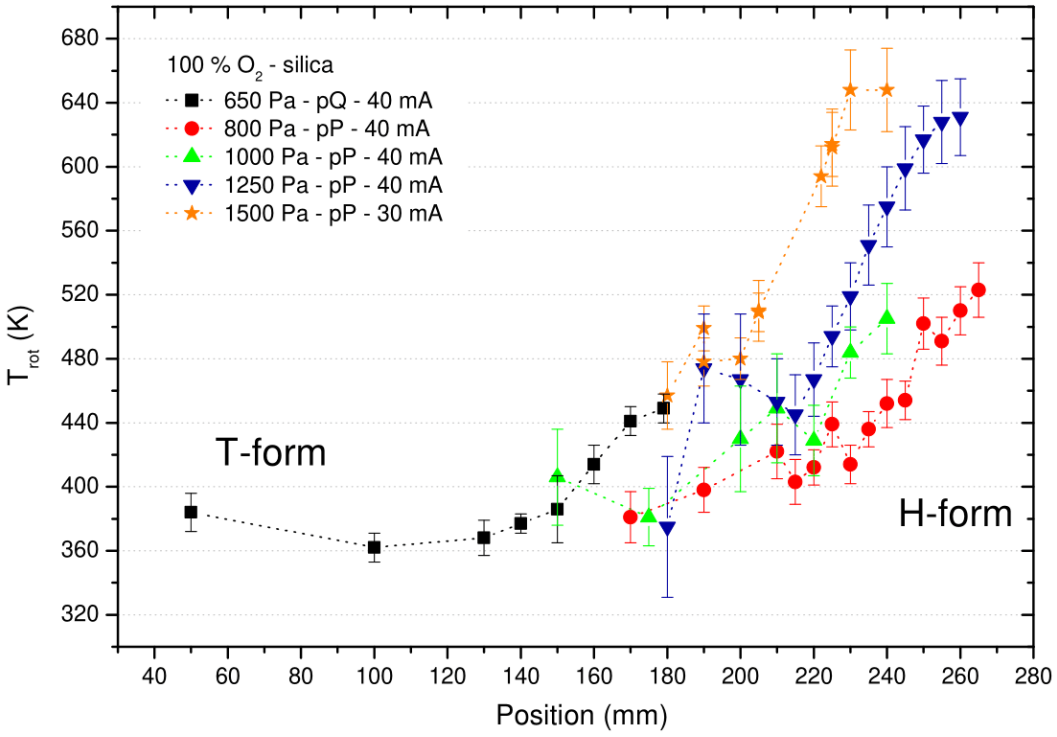

Figure 4.7: *The rotational temperature as calculated from the optical emission of O_2 ($b\ ^1\Sigma_g^+$) for various total pressures. Discharge current chosen to stabilize the T-H form transitional region in one place. Pure oxygen, silica discharge tube.*

The interesting fact is this implies significant thermal gradient along the discharge axis and the discharge tube itself. This gradient was observable even on the outer surface of the discharge tube with thermocouples. The higher temperature of the H-form is closely connected to higher energy dissipation to plasma and higher excitation due to higher axial electric field strength (see 4.1.4).

4.1.2.2 Concentrations of excited particles

The concentrations of the excited species O I (^3P), O I (^5P) and O_2 ($b\ ^1\Sigma_g^+$) are presented in figures 4.8 and 4.9 respectively. Due to more complicated geometry the calculations needed for absolute calibration were not performed and the presented data are shown only in arbitrary units.

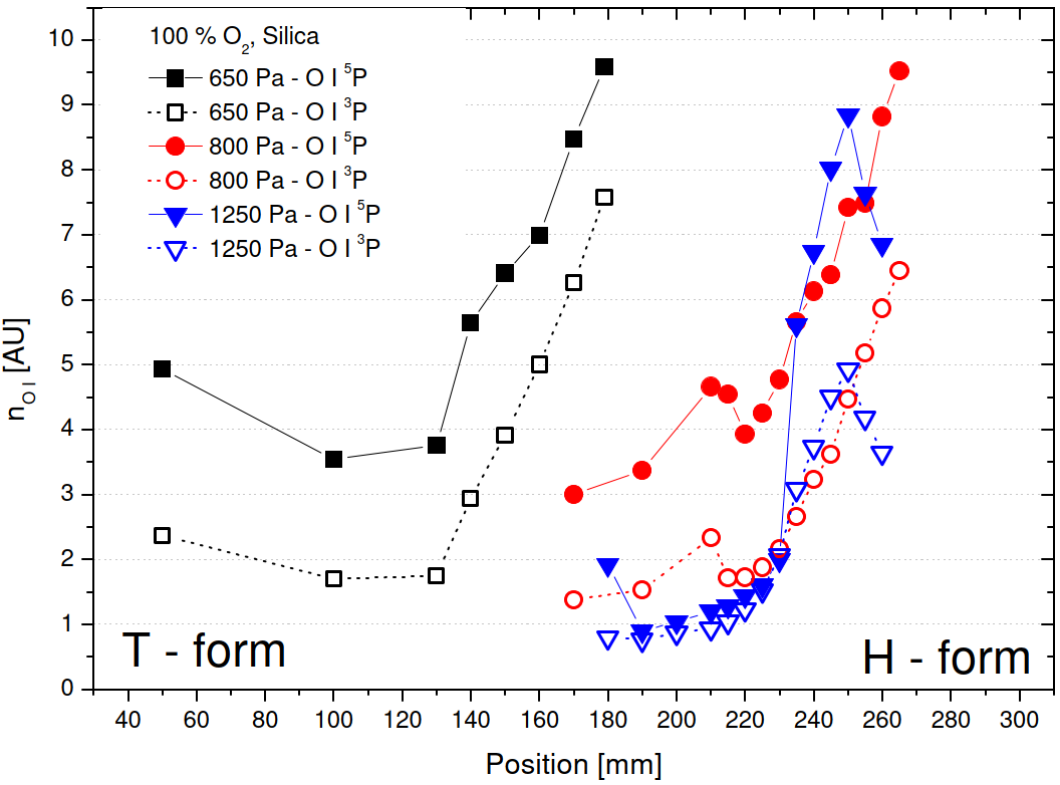

Figure 4.8: *The concentration of excited atomic oxygen in the O I (^3P) (empty symbols) and O I (^5P) (full symbols) states as measured using optical emission spectrometer for various total pressures. The relative uncertainty of each datapoint is ±30 %. Results are plotted using arbitrary units. Discharge current chosen to stabilize the T-H form transitional region in one place. Pure oxygen, silica discharge tube.*

The raise in concentrations of all studied excitation levels corresponds in position both one to another and to the raise in the rotational temperature. Since the rotational temperature is sensitive only to the relative intensity of lines used in calculation (see section 2.2.2) and not the absolute intensity, it can be inferred the concentration and temperature are indeed tied together with the form of the plasma of the positive column.

The position of the transition region itself with regard to the discharge tube is subject to many influences including the tube geometry, positioning of the Langmuir probes etc. and therefore no quantitative information can be deduced from the shift of this region with the increase of the gas pressure. Qualitatively we observed shift towards the cathode (i.e. prolongation of the T-form) with increasing total gas pressure. This is in agreement with previous observations that the T-form is preferred at higher pressures (see Chapter 1.2).

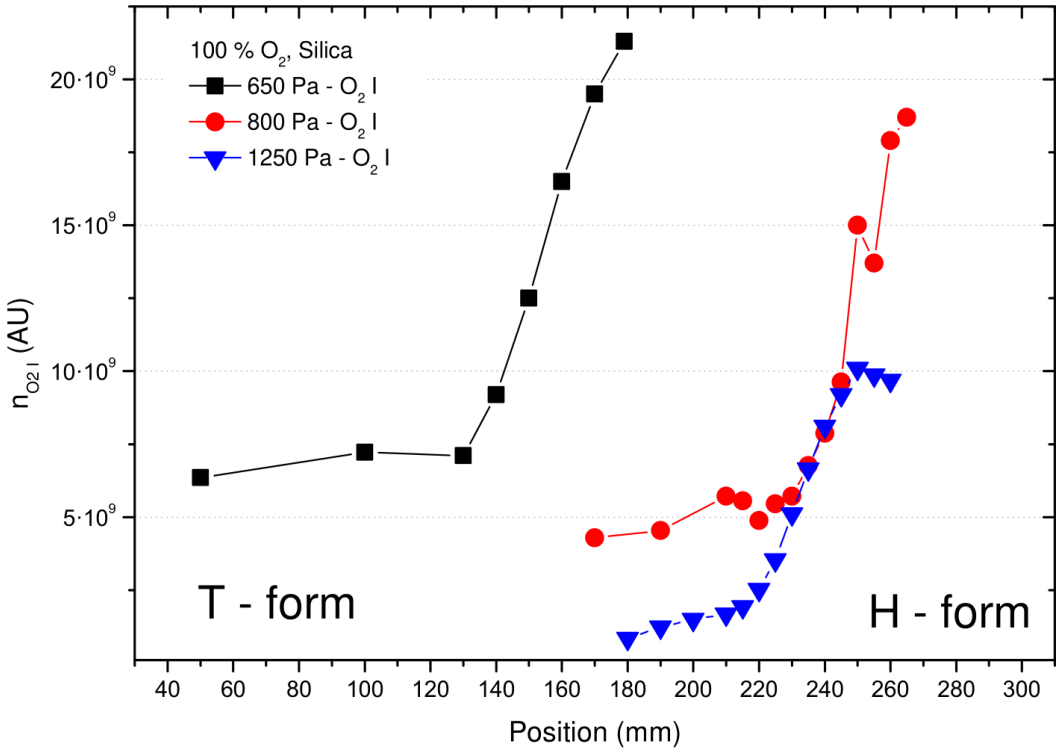

Figure 4.9: *The concentration of excited molecular oxygen in the* O_2 $(b\ ^1\Sigma_g^+)$ *state as measured using optical emission spectrometer for various total pressures. The relative uncertainty of each datapoint is* ± 30 *%. Results are plotted using arbitrary units. Discharge current chosen to stabilize the T-H form transitional region in one place. Pure oxygen, silica discharge tube.*

4.1.3 Toroidal resonator

Toroidal resonator was utilised as supplemental method to estimate the electron concentration in the respective forms and in the transitional region. The resonances were measured for total pressures of 800 Pa, 1000 Pa and 2000 Pa. A scan of burning discharge was done on chosen positions along the discharge axis. Afterwards the measurements of the resonances without the plasma were done for the same positions. The resulting resonance curves were fitted with the Lorentz bell curves. The calculated electron concentrations are shown in Fig. 4.10 - 4.12.

From literature it is well known, that the electron concentration is usually about an order higher in the T-form than in the H-form, which is usually explained by a change in the concentrations of negative ions (for more details see e. g. [20], [24]). This behaviour was also observed in our measurements.

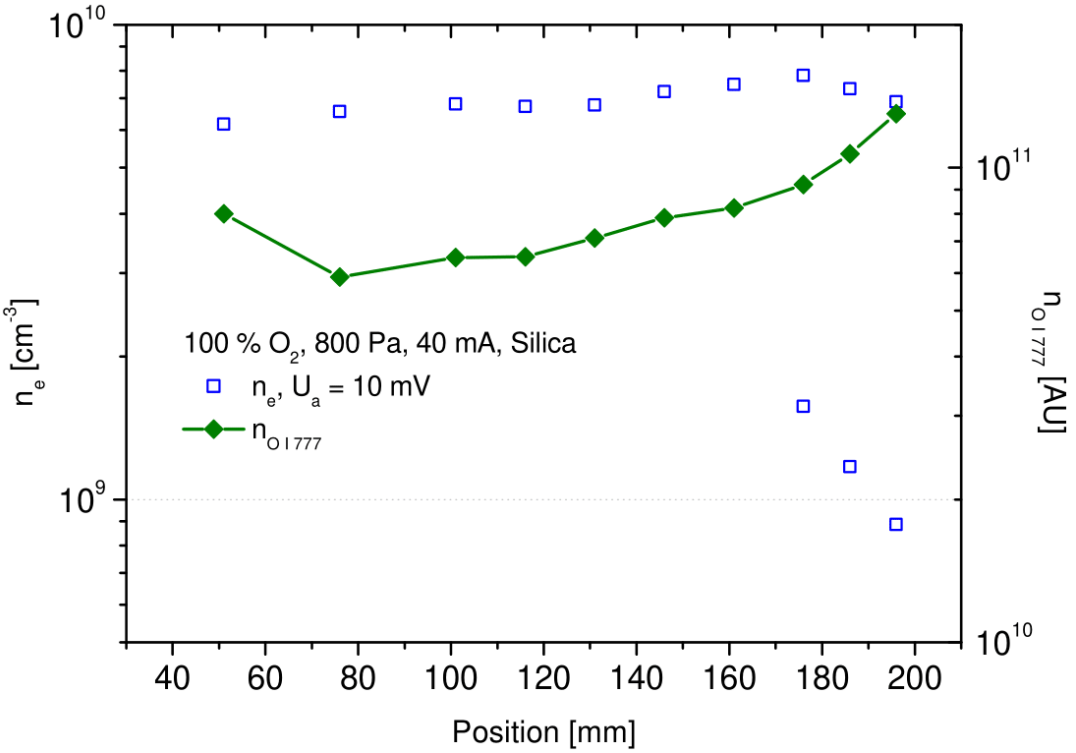

Figure 4.10: *The electron concentration measured using toroidal resonator (amplitude of the driving voltage 10 mV). The concentration of O I (^5P) as measured using optical emission spectrometer is shown for comparison of the position of the transitional region. The T-form is present on the left, H-form to the right. Pure oxygen, 800 Pa total pressure, 30 mA of discharge current, silica discharge tube.*

What was of more concern was the strange effect emerging in the transition region, where a resonance "doublepeak" was present - see Fig. 4.13. More so, with a change of the position along the axis, the height of the respective peaks changed so that one was rising while the other was falling - see Fig. 4.14. If we fit the doublepeak with two superimposed separate Lorentz curves and use these for the calculation of the electron concentration, we will get two separate concentrations for each such position on the discharge axis. Since the resonator is responsive only to an integral of the electric field over whole interaction region

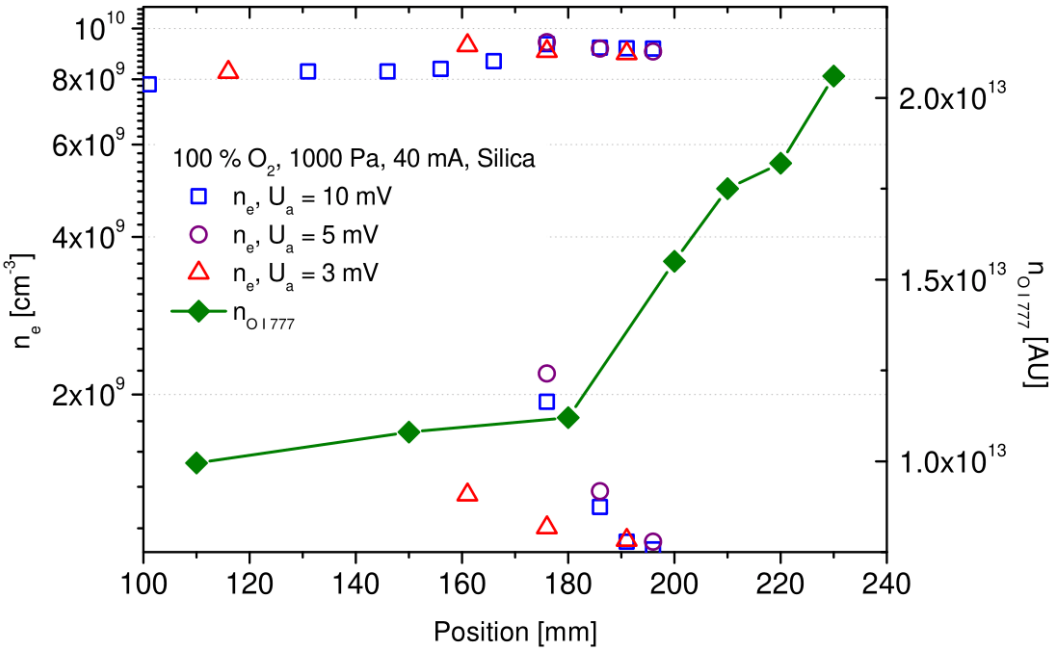

Figure 4.11: *The electron concentration measured using toroidal resonator with three different amplitudes of the driving voltage (3 mV, 5 mV and 10 mV). The concentration of O I (^5P) as measured using optical emission spectrometer is shown for comparison of the position of the transitional region. The T-form is present on the left, H-form on the right. Pure oxygen, 1000 Pa total pressure, 40 mA of discharge current, silica discharge tube.*

(see equations 2.6 and 2.7), it is technically impossible for it to measure two different concentrations.

The presence of the "double-resonation" may be explained, if the transitional region between the T- and H-form is in fact rather thin boundary, which is oscillating along the discharge axis. Since all our local measurements (be it perpendicular optical spectroscopy - see section 4.1.2 - or toroidal resonator) take rather long time (in the order of minutes), if the boundary between the forms is rapidly oscillating, we would not be able to neither register nor follow these oscillations. While scanning the resonance curve, we will in fact scan two resonance curves, each belonging to one of the respective forms, overlapping one over the other. That seems to be our case (see fig. 4.13).

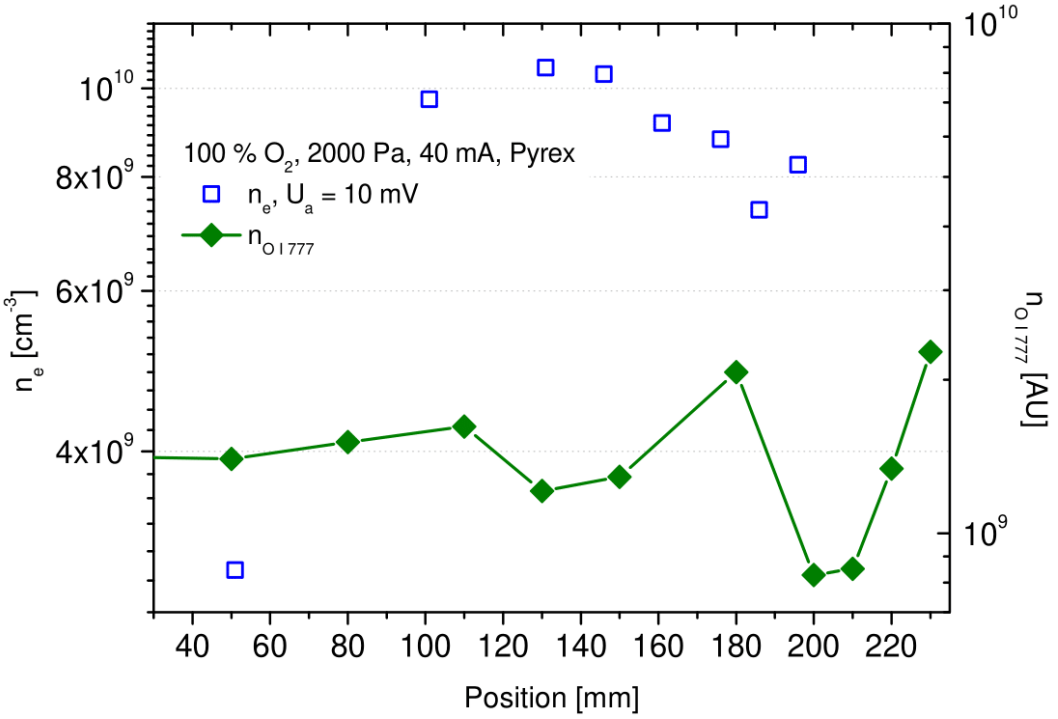

Figure 4.12: *The electron concentration measured using toroidal resonator (amplitude of the driving voltage 10 mV). The concentration of O I (^5P) as measured using optical emission spectrometer is shown for comparison of the position of the transitional region. The T-form is present in the whole observed region. Pure oxygen, 2000 Pa total pressure, 40 mA of discharge current, silica discharge tube.*

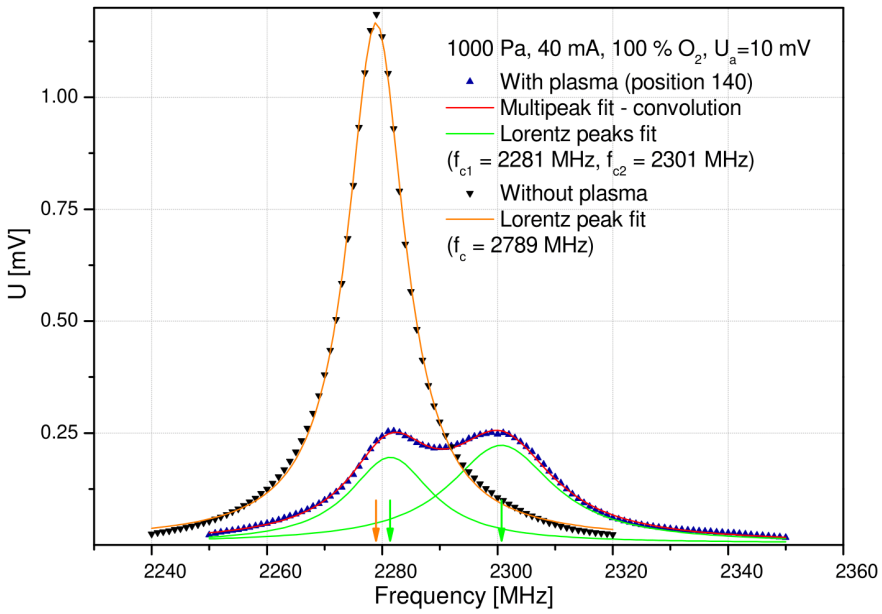

Figure 4.13: *The resonance curves as measured without and with plasma using the toroidal resonator. The fitting was done in the Origin 8 software. Positions of the maxima of the fitted peaks are denoted. Pure oxygen, 1000 Pa total pressure, 40 mA of discharge current, silica discharge tube, position 140 mm.*

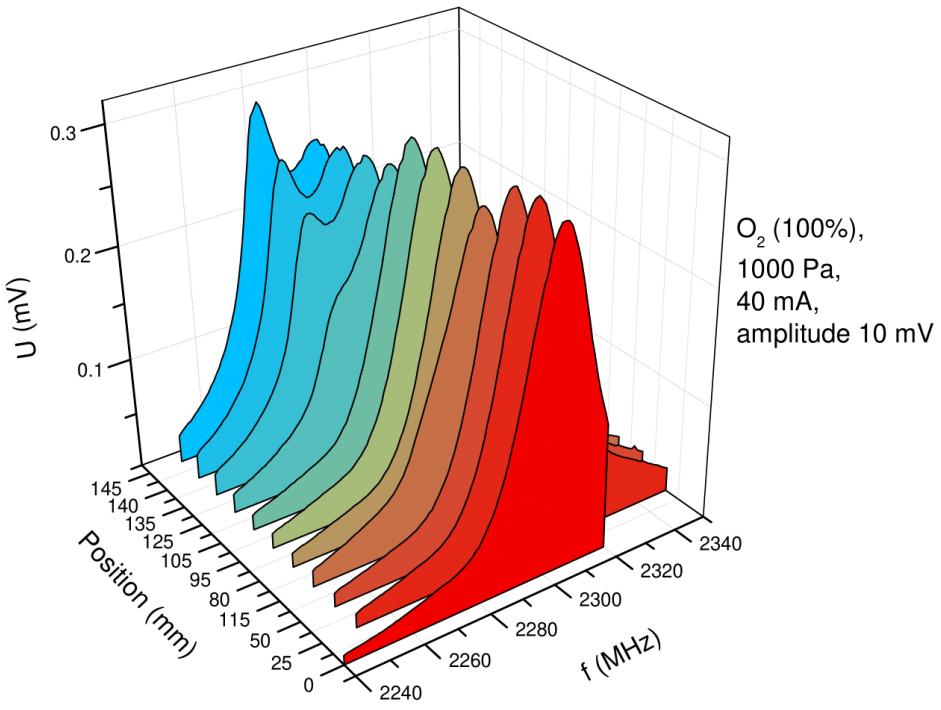

Figure 4.14: *Different resonance curves as measured with the discharge using the toroidal resonator over the transitional region between T- and H-form. The rise of the peak corresponding to the concentration electrons in the H-forms begins around the position of 125 mm. Pure oxygen, 1000 Pa total pressure, 40 mA of discharge current, silica discharge tube.*

4.1.4 Electrical properties

Axial electric field strength was measured in order to have independent control over the presence of the respective forms of the glow discharge positive column. Two pairs of Langmuir probes were utilized as described in the section 2.1. The results are shown in the Figure 4.16.

Two lines are always displayed for each initial pressure, which corresponds to the direction of the current change during measurements. Usually we measured the axial electric field strength starting at high current (40 mA) then lowering it to the minimum current where the discharge was sustainable. After that the discharge was put off and after three minute rest restarted at the last current measured (the minimum) then raised up to the maximum of 40 mA. The classical hysteresis of presence of T-form was observed, as can be clearly seen e.g. at 650 Pa at anode probe pair (fig. 4.16, top left) - when the discharge was broken down at 40 mA, the H-form was present in the whole tube down to the 10 mA of discharge current. However when the discharge was broken down at 10 mA, the T-form was present and disappeared while the discharge current reached approx. 33 mA.

When in H-form, the axial electric field strength showed signs of classical DC glow discharge field behavior, rising with lowering of the discharge current / power fed to the discharge. When in the T-form, the profile is much more flat and almost no rise is observed.

It needs to be noted, that the double probe measurements in the T-form have much higher uncertainty due to running oscillation waves present in the T-form (see Fig. 4.15, for more about oscillations in T-form see e.g. [19]). Oftentimes any certain value was unobtainable as the observed value jumped between two values approx. 10 V apart. These measurements were omitted and are not shown, however the actual uncertainty of the values depicted in Fig. 4.16 is about 10 % at higher discharge currents and up to 50 % at lower currents (10 - 15 mA).

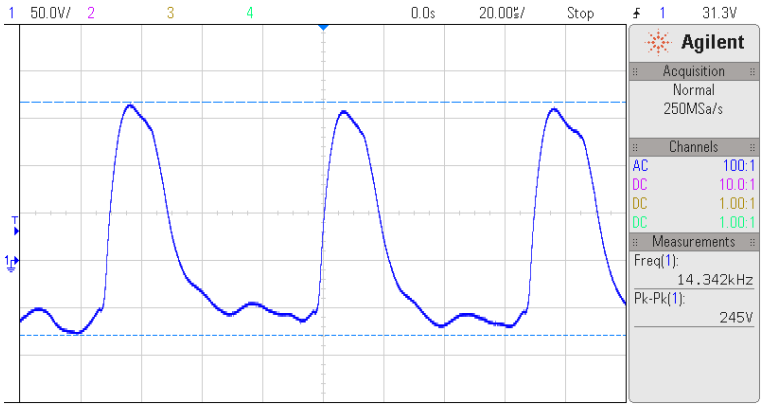

Figure 4.15: *Fast running oscillation waves as measured using Agilent DSO-X 2004A oscilloscope with Tektronix P5100 HV probe on one of the anode pair probes. Pure oxygen, 1000 Pa, 40 mA of discharge current. The T-form was present in about 1/3 of the discharge tube length around anode langmuir probe pair*

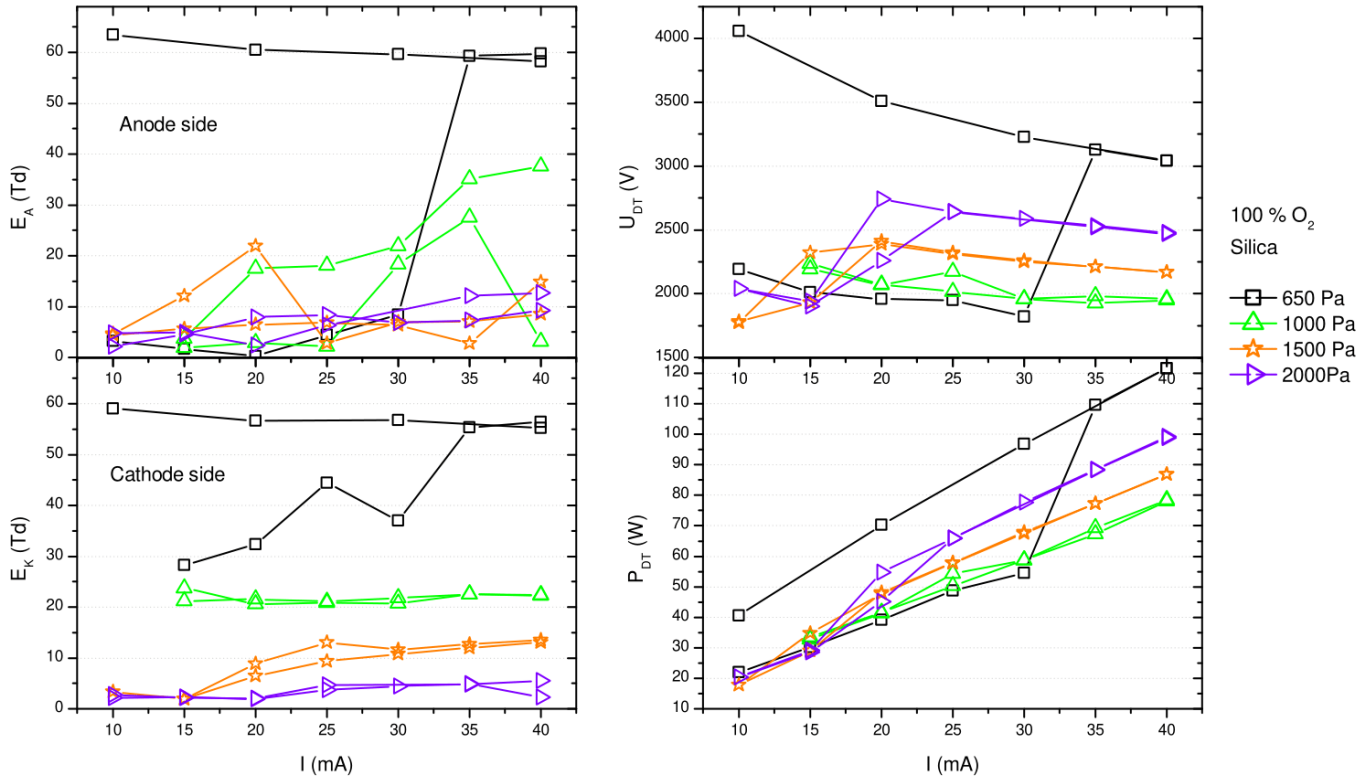

Figure 4.16: *Electric properties of the glow discharge column as measured in different pressures. Left top and bottom: Axial electric field strength measured using Langmuir doubleprobes. Right top: The voltage drop on the entire discharge calculated from generator voltage, excluding the stabilization resistor (kΩ). Right bottom: The power input on the discharge tube calculated as* $P = U_{DT} \cdot I$. *Pure oxygen, silica discharge tube*

4.1.5 Wall composition

In order to determine the effect of the wall composition on the discharge plasma, two discharge tubes with the same geometry but different glass composition were utilized in our experiments (see 3.1). In addition to the axial measurements, special radial scanner was used to determine the radial profile of the emission spectra and therefore the parameters obtainable from those (see 3.3.2 for more about the scanner). The absolute calibration of the scanner was not done due to the complexity of the optical setup, the results for concentrations of excited species are therefore shown only in arbitrary units.

4.1.5.1 OES - Integral

The axial measurements without the radial scanner were used to determine the rough differences between the two glasses as well as absolute concentrations of the excited species. As can be seen in the fig. 4.17, the temperatures are similar or higher in the Pyrex tube than in the Silica tube. The measurements for 650 Pa in Pyrex tube were taken in pure H-form of the discharge, whereas the set for 650 Pa in Silica tube shows transition between T-form and H-form in whole volume between the currents of 30-35 mA. The results for the Pyrex tube are therefore higher due to the presence of H-form. This effect was seen previously in our measurements in lower pressures (see e.g. [44], [45]) and can be explained as a result of difference in the thermal conductivity of Pyrex glass (1.14 W/mK) and Silica glass (1.38 W/mK) [46]. The thermal energy is lost at the wall in known surface processes, especially wall recombination and desorption (e.g. [47], see section 1.1).

This difference in the rotational (and therefore kinetic) temperature is mirrored by the populations of the excited species, see figures 4.18 and 4.19, however in the opposite way: the concentrations of excited oxygen atom and molecule respectively are higher in the Silica tube than in the Pyrex tube. Again, the measurements for 650 Pa, Pyrex tube were taken in pure H-form of the discharge, whereas the set for 650 Pa, Silica tube show transition between T-form and H-form in whole volume between the currents of 30-35 A. The results for the Pyrex tube are therefore higher due to the presence of H-form.

4.1.5.2 OES - Radial

The radial scanner was utilized to determine the radial dependent spectra of the discharge. The results are shown in figs. 4.20 - 4.26.

As can be seen in fig. 4.22, the temperature measured along the axis without the scanner agrees well with the one measured with radial scanner. This is mainly due to almost constant profile of the temperature (see fig. 4.20 - 4.23) with only steep fall near the wall. This steep could not be measured with better precision as the understandably low intensity of the emission needed wider region of emission collection (we used 1.8 mm width or 16 % of total radius). As the thermal conductivity of the glass (Pyrex glass: 1.14 W/mK; Silica: 1.38 W/mK) is sufficient to answer for a step of only few kelvins per the tube wall, we assume the temperature drops significantly in the tight vicinity of the wall.

The profile of the concentration of the excited species is shown in the fig.

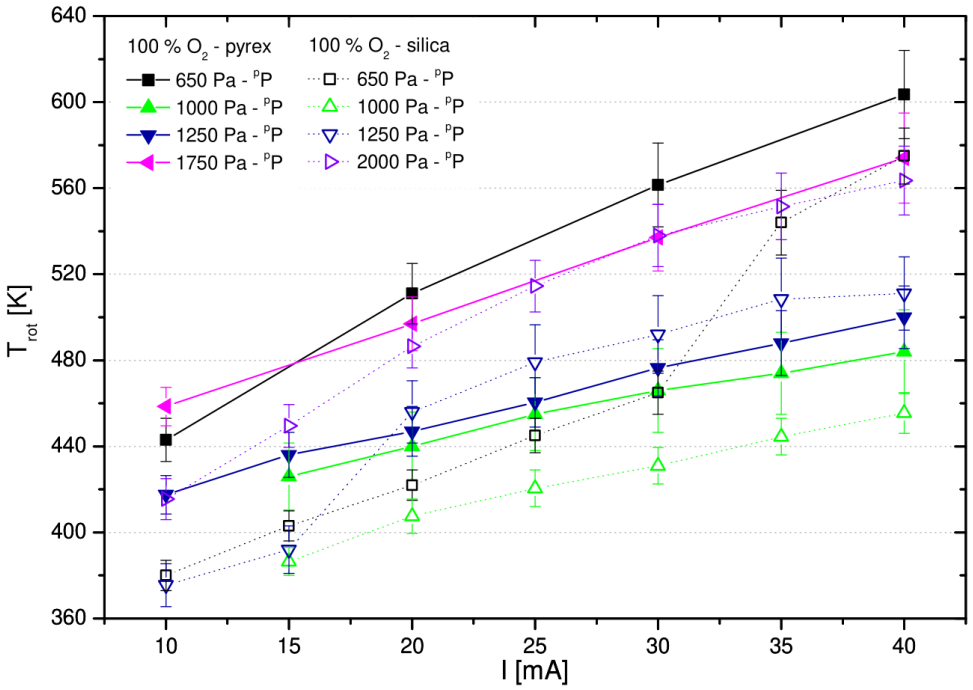

Figure 4.17: *The rotational temperature of oxygen molecules calculated from the spectra of the atmospheric band. Comparison of different composition of discharge tube wall, pure oxygen.*

4.25 and 4.26. The intensities were divided by the area of the respective annulus from which the emissions were taken, therefore corresponds to the actual concentrations. However since proper calibration would be arduous the results are presented only in the arbitrary units (and cannot be compared to the results presented in the section 4.1.1.2). The profiles show typical bell curve which is narrower for higher pressures - the result of the compression of the positive column similar to the effect described in [9], p. 239.

The profile of the atomic oxygen is qualitatively the same as that of the dioxygen. Since the plasma of the positive column is stable non-thermal quasineutral plasma, the coefficient of ambipolar diffusion between ions and electrons D_A^{eM} can be described using Einstein relation (see [9], p. 29):

$$D_A^{eM} = \mu_M \frac{kT_e}{e} = \frac{kT_e}{m_M \nu}, \tag{4.1}$$

where $\mu_M = \frac{e}{m_M \nu}$ is the mobility of the (single charged) ions, m_M their mass and T_e is the kinetic temperature of the electrons. Since $M_{O2} = 2M_O$, the ambipolar diffusion of the molecular oxygen should be twice as strong as that of the atomic oxygen, which should result in a flatter profile. The fact that this was not observed suggests that ambipolar diffusion is not main diffusional process. The main reason might be significantly lower electron concentration with respect to the concentration of the negative ions (which does not induce ambipolar diffusion due to the same mobility and temperature as positive ions).

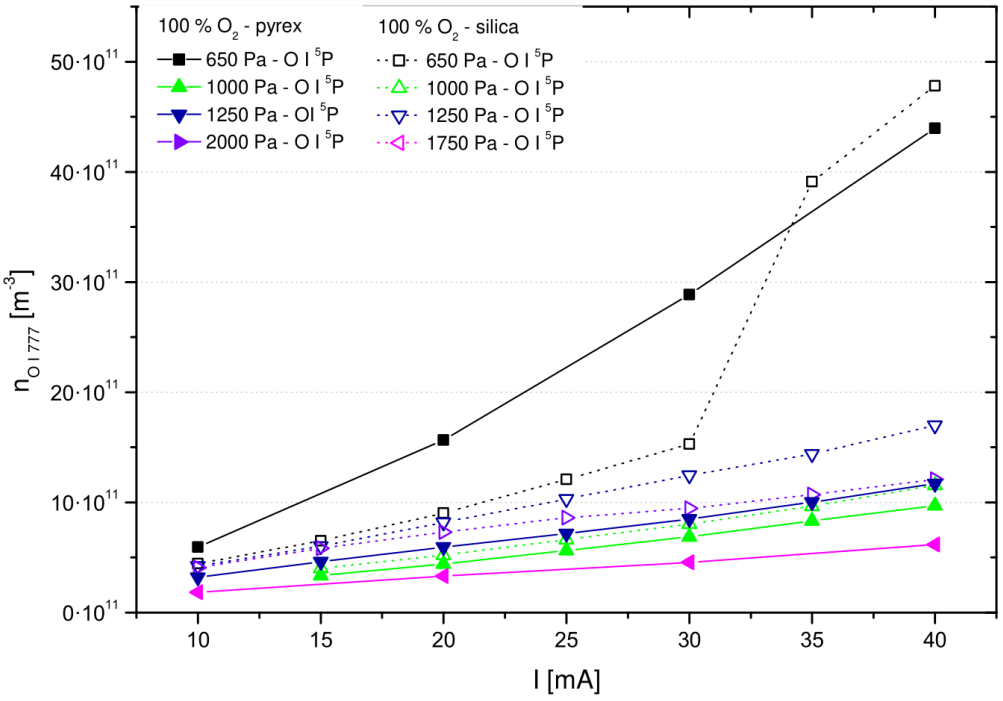

Figure 4.18: *The concentration of O I (^5P) as measured using calibrated optical emission spectrometer. The relative uncertainty of each datapoint is ±15 %. Comparison of different composition of discharge tube wall, pure oxygen.*

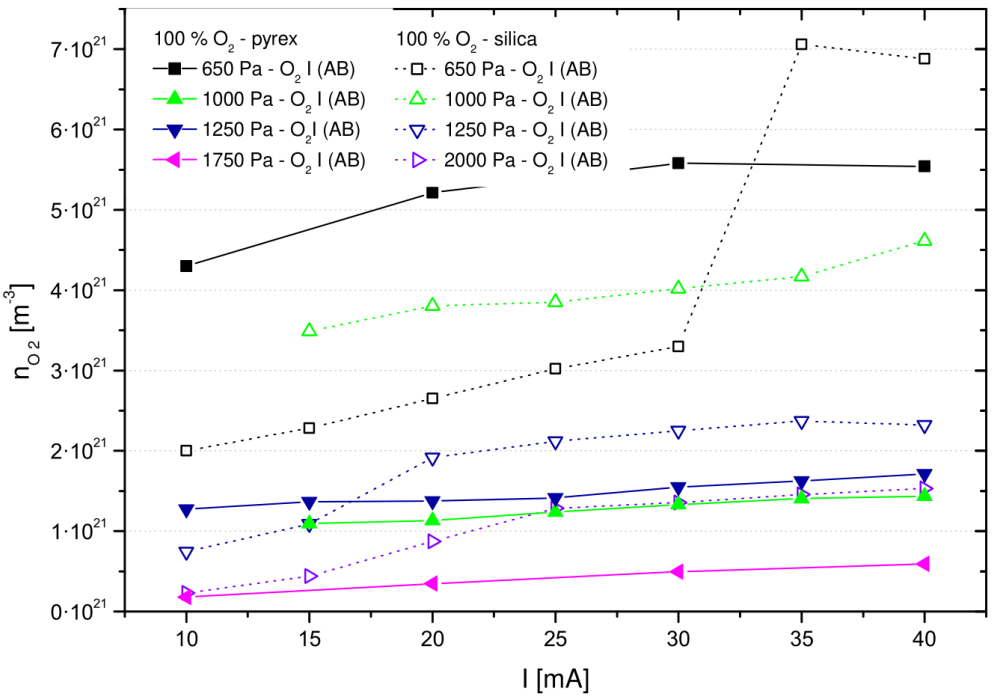

Figure 4.19: *The concentration of O_2 ($b\ ^1\Sigma_g^+$) as measured using calibrated optical emission spectrometer. Comparison of different composition of discharge tube wall, pure oxygen.*

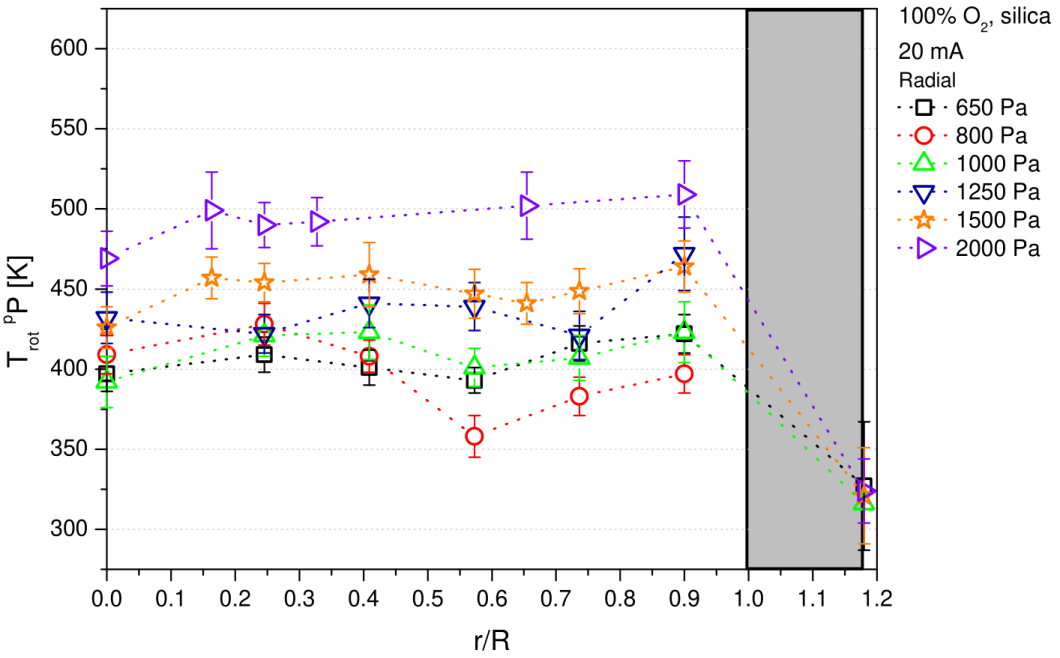

Figure 4.20: *The radial profile of the rotational temperature of oxygen molecules calculated from the spectra of the atmospheric band. Silica glass tube, 20 mA of discharge current, pure oxygen. The datapoints on the outer side of tube wall were obtained using IR thermometer.*

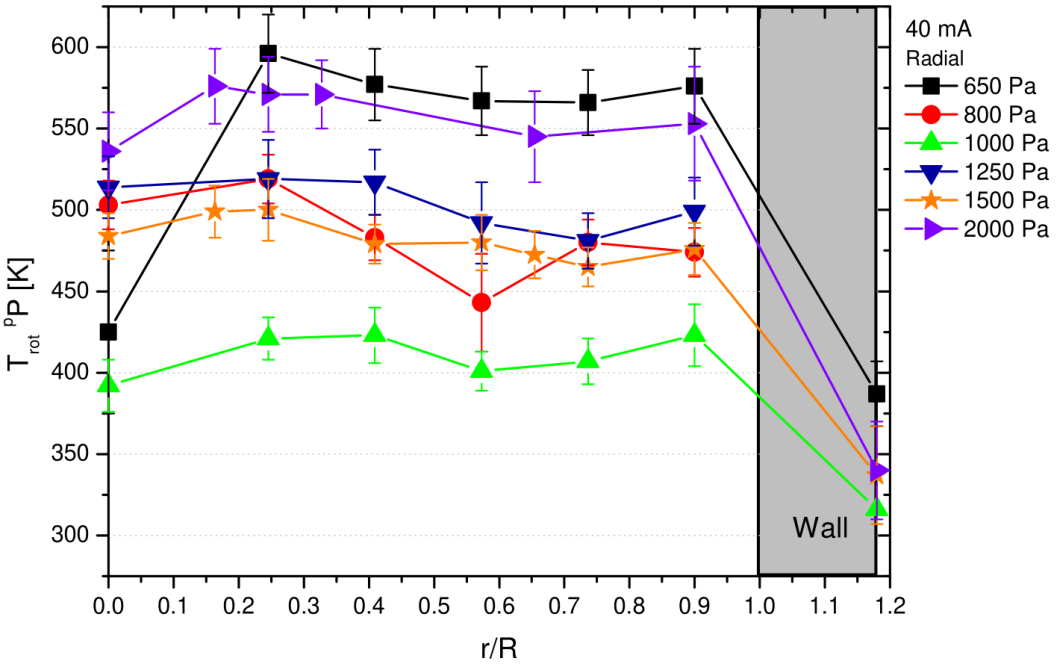

Figure 4.21: *The radial profile of the rotational temperature of oxygen molecules calculated from the spectra of the atmospheric band. Silica glass tube, 40 mA of discharge current, pure oxygen. The datapoints on the outer side of tube wall were obtained using IR thermometer.*

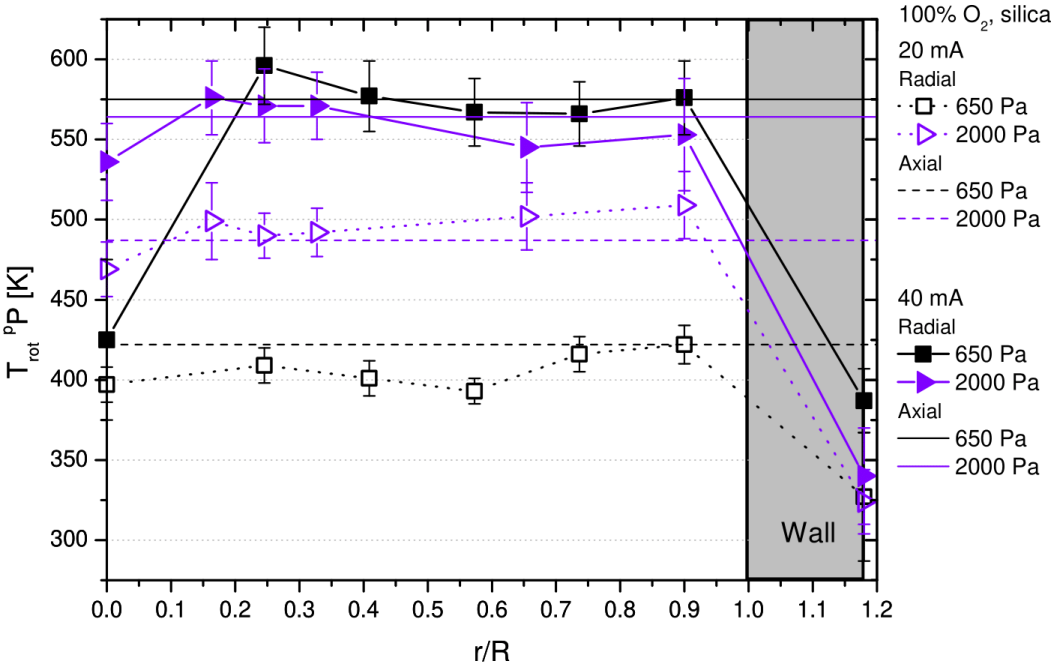

Figure 4.22: *The radial profile of the rotational temperature of oxygen molecules calculated from the spectra of the atmospheric band. Silica glass tube, 20 mA and 40 mA of discharge current, pure oxygen. The straight lines denote temperature measured along axis without the scanner. The datapoints on the outer side of tube wall were obtained using IR thermometer.*

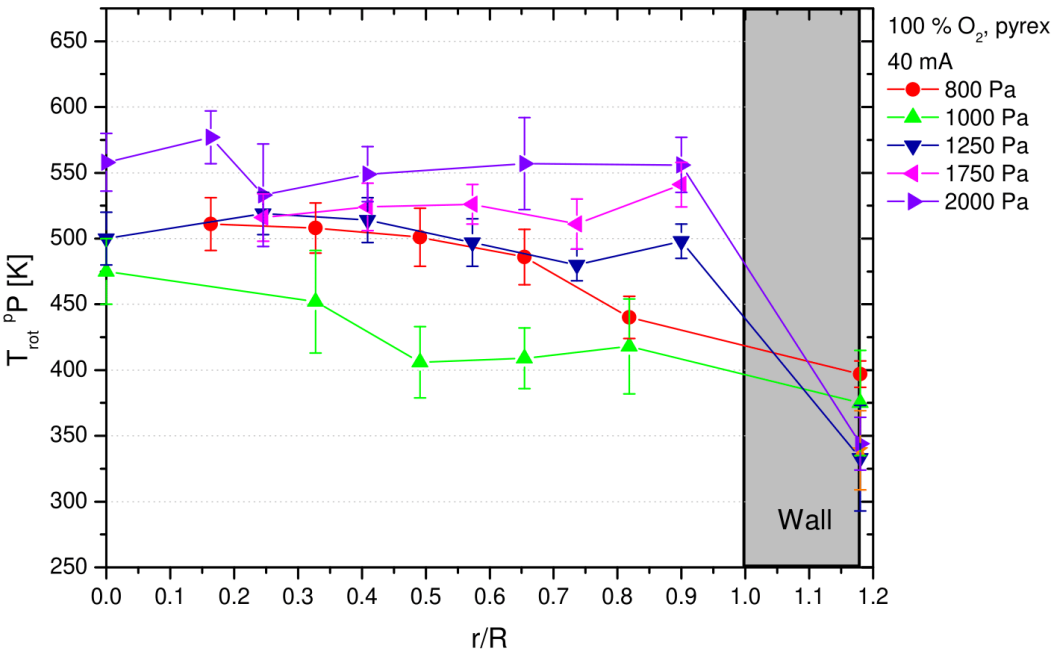

Figure 4.23: *The radial profile of the rotational temperature of oxygen molecules calculated from the spectra of the atmospheric band. Pyrex glass tube, 40 mA of discharge current, pure oxygen. The datapoints on the outer side of tube wall were obtained using IR thermometer.*

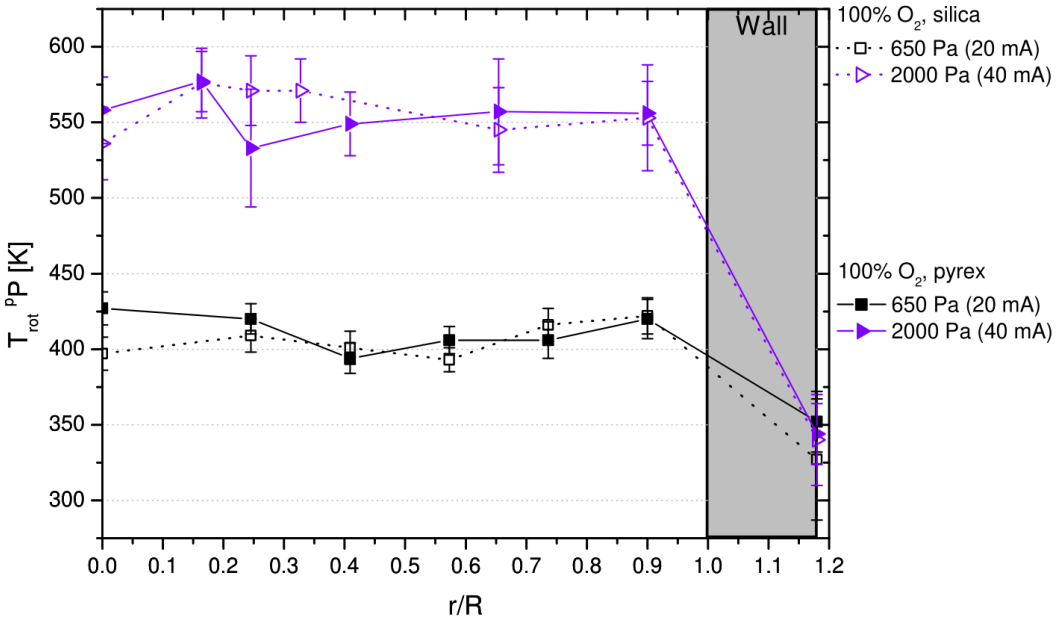

Figure 4.24: *The radial profile of the rotational temperature of oxygen molecules calculated from the spectra of the atmospheric band, comparison for Silica and Pyrex glass tube, 20 mA and 40 mA of discharge current, pure oxygen. The datapoints on the outer side of tube wall were obtained using IR thermometer.*

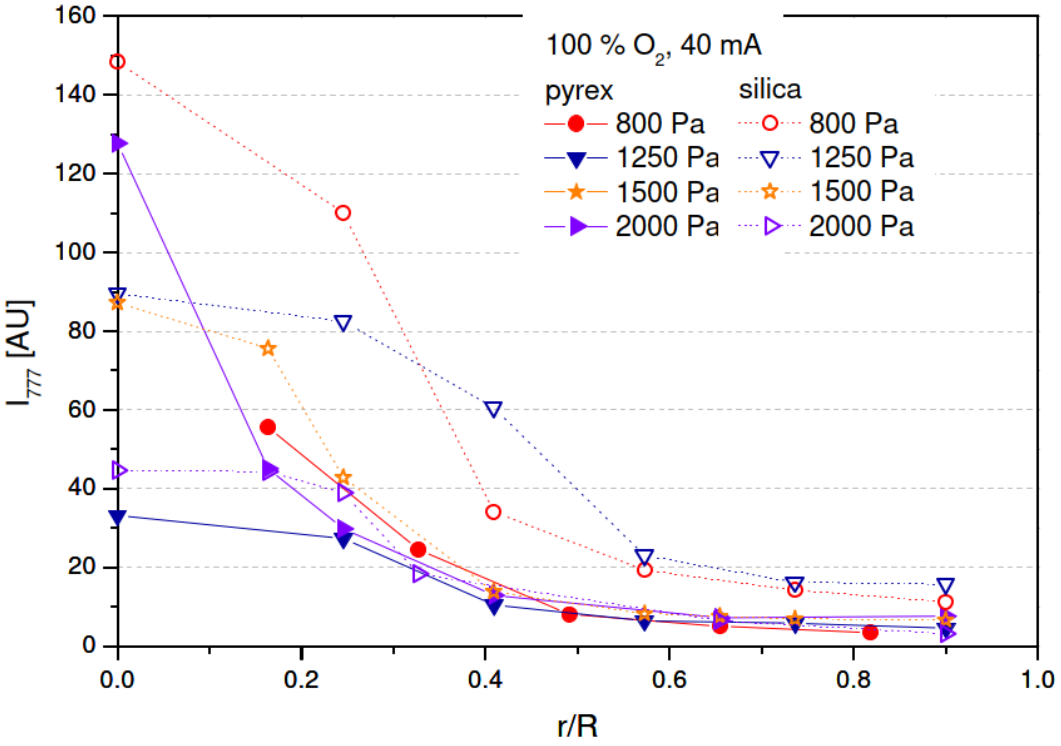

Figure 4.25: *The concentration of O I (^5P) as measured using radial scanner. The relative uncertainty of each datapoint is ±15 %. Comparison of different composition of discharge tube wall, pure oxygen.*

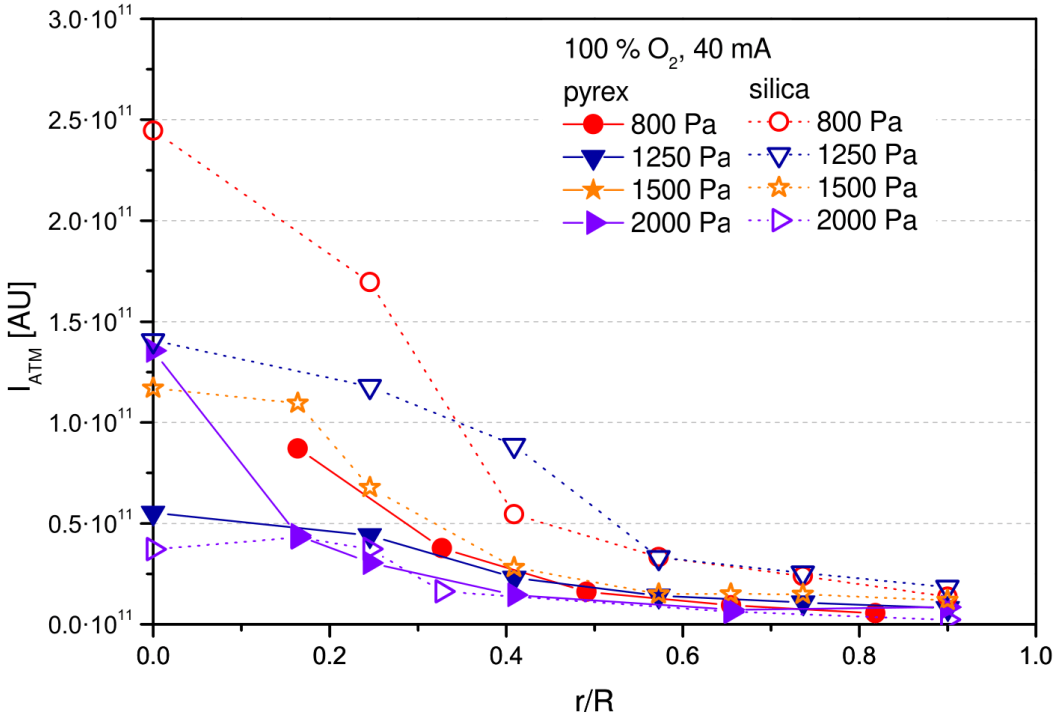

Figure 4.26: *The concentration of* O_2 $(b\ ^1\Sigma_g^+)$ *as measured using radial scanner. The relative uncertainty of each datapoint is* ± 15 *%. Comparison of different composition of discharge tube wall, pure oxygen.*

4.2 Results: O_2-N_2 mixture

4.2.1 OES - Axial measurements

The discharge showed distinctly different structure when even small amount (about 1 % of total pressure) of nitrogen is introduced. Due to high amount of energy that can be stored in the vibrations of N_2 molecule, the chemical composition and energetic balance change. Even to a naked eye the discharge looks different: the pure oxygen discharge is mainly grey (some people describe it as green-greyish) with almost no radial structure (apart from obvious thinning towards the walls of discharge tube). However the oxygen-nitrogen discharge has typically purple-grey "core" near the axis of the tube and green-grey "halo" filling the rest of the tube uniformly and extending even into the filling/pumping channel. This suggests the presence of long-living excited species.

The presence or strength of the halo corresponds to the occurrence of the H-form - when the T-form of the discharge was present, only small-to-none halo was observed.

The purplish colour of the core of the discharge is due to so-called Second Positive System of nitrogen molecule $C\ ^3\Pi_u \rightarrow B\ ^3\Pi_g$) with head at 380.4 nm for $v_i - v_f = 0$ and 375.4 nm for $v_i - v_f = 1$ [48]. The halo is mainly composed of nitrogen radiation.

4.2.1.1 Rotational temperature

The rotational temperature of oxygen molecule shows the same behaviour as described in pure oxygen (see 4.1.1.1), except the absolute temperatures are significantly higher (see fig. 4.27). This is due to the higher energy stored and re-released in the discharge from the nitrogen molecules.

4.2.1.2 Concentrations of excited particles

The concentrations of excited atomic oxygen and oxygen molecule are shown in fig. 4.28 - 4.30. Again, at 650 Pa the H-form filled most of the discharge tube driving the concentrations higher. In the T-form region, the concentrations did differ only slightly both with discharge current and pressure.

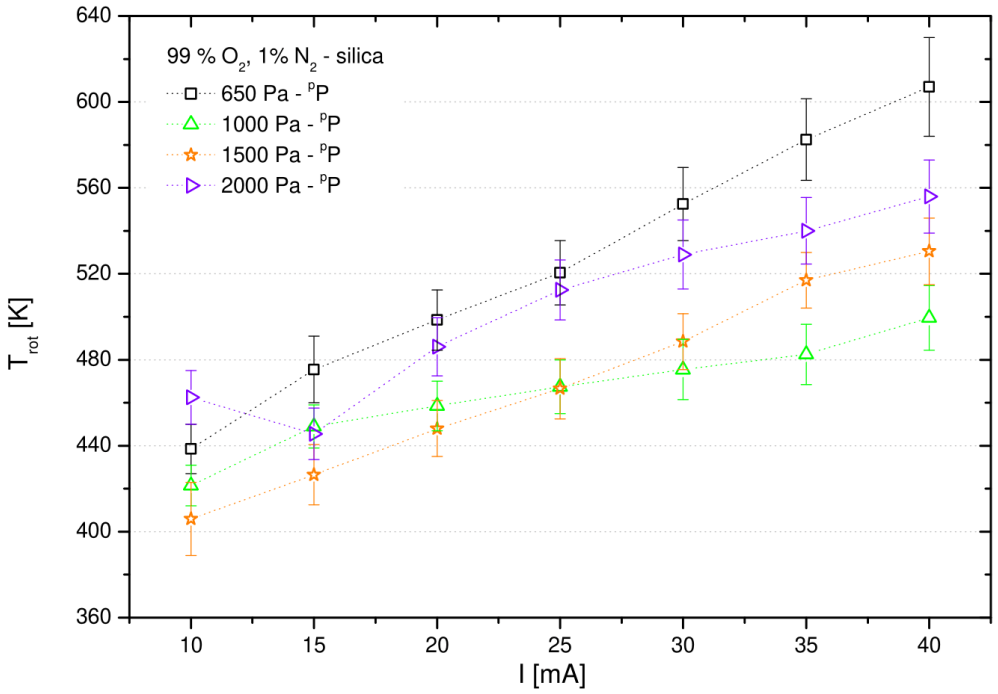

Figure 4.27: *The rotational temperature of oxygen molecules calculated from the Atmospheric band emission. Oxygen-nitrogen mixture (99:1), silica discharge tube.*

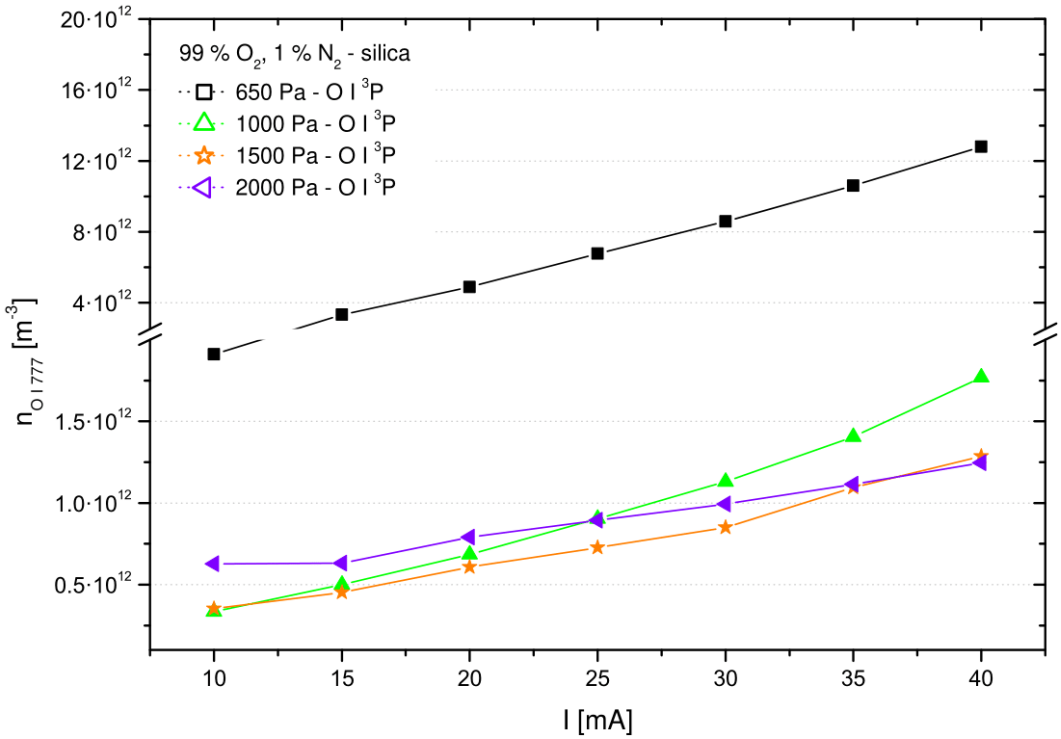

Figure 4.28: *The concentration of O I (^5P) as measured using calibrated optical emission spectrometer. The relative uncertainty of each datapoint is ±15 %. Oxygen-nitrogen mixture (99:1), silica discharge tube.*

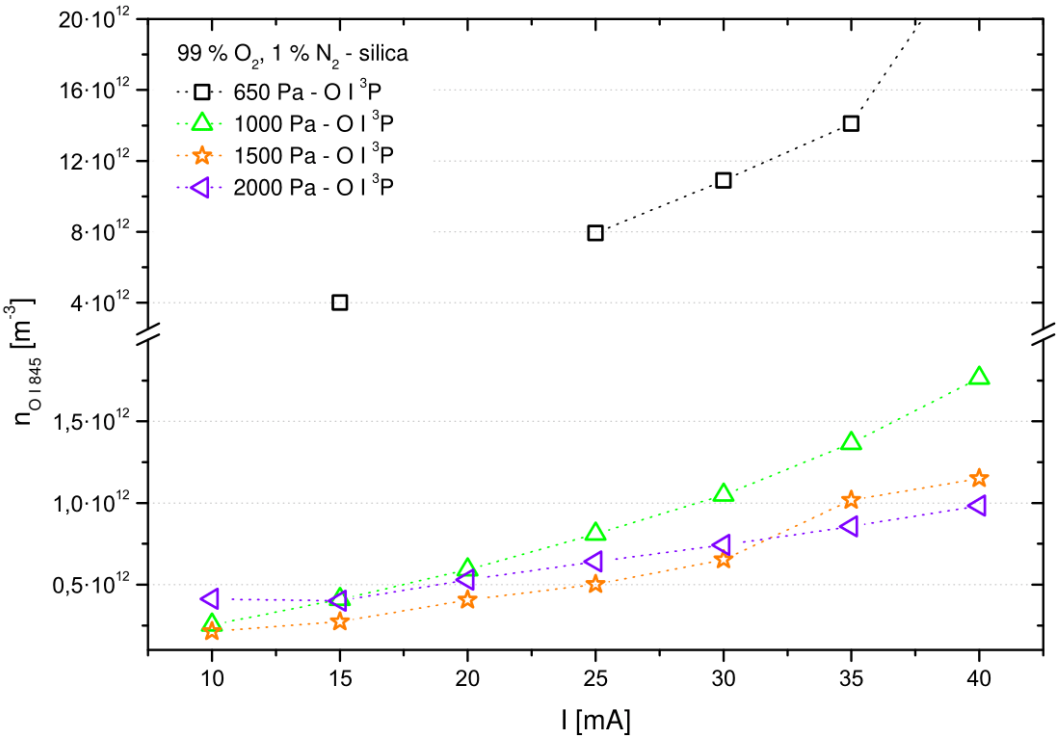

Figure 4.29: *The concentration of O I (^3P) as measured using calibrated optical emission spectrometer. The relative uncertainty of each datapoint is ±15 %. Oxygen-nitrogen mixture (99:1), silica discharge tube.*

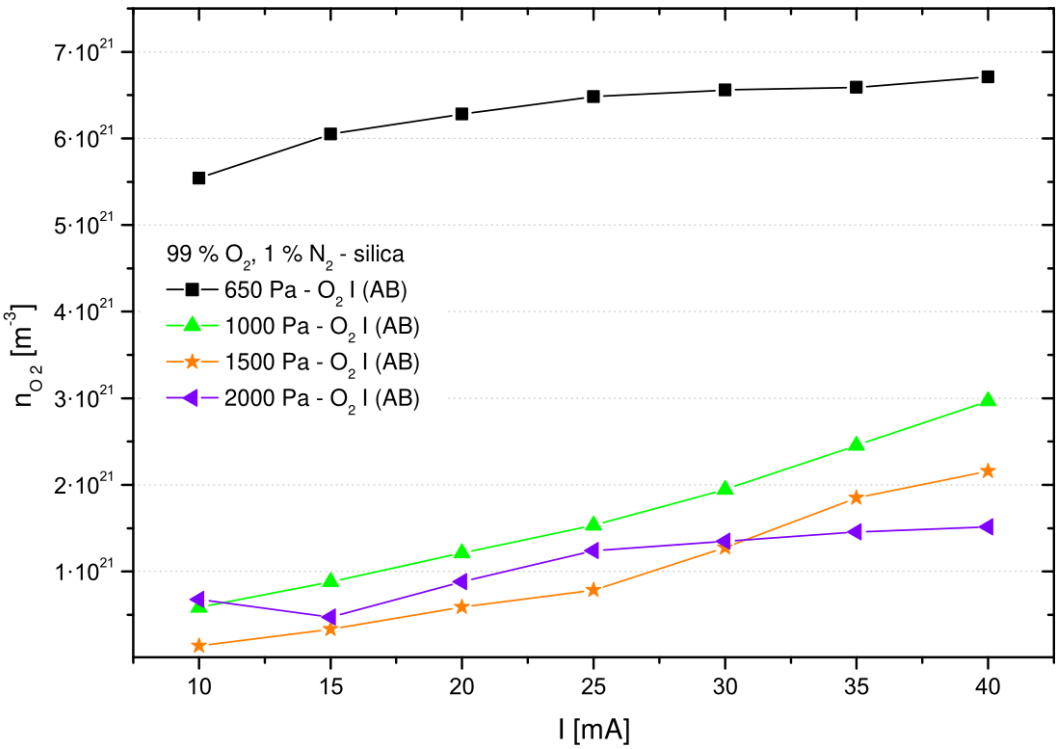

Figure 4.30: *The concentration of O_2 ($b\ ^1\Sigma_g^+$) as measured using calibrated optical emission spectrometer. The relative uncertainty of each datapoint is ±20 %. Oxygen-nitrogen mixture (99:1), silica discharge tube.*

4.2.2 OES - Perpendicular measurements

The addition of nitrogen changed not only the visual emissions, but clearly also changed the behaviour of the forms. Most notable is the spatial fuzziness of the transitional region, which was not always apparent in the perpendicular measurements, especially at higher pressures.

4.2.2.1 Rotational temperature

The rotational temperature as was calculated from the spectra is shown in the figure 4.31. The step in temperature associated with the transition between T-form and H-form in pure oxygen (see section 4.1.2.1) can be seen only in the data for 1000 Pa and 1500 Pa of total pressure and it is at position far to the cathode. More so it spans over at least 60 mm. Although the presence of the H-form can be confirmed by electrical measurements (see figure 4.36 on page 58), the data are not that conclusive. The axial electric field strength as measured with the double Langmuir probe is significantly lower on the cathode pair and even in the region of T-form for pressures over 1000 Pa. Thus we may infer that our inability to observe distinct forms with naked eye was only acknowledged by rotational temperature measurements.

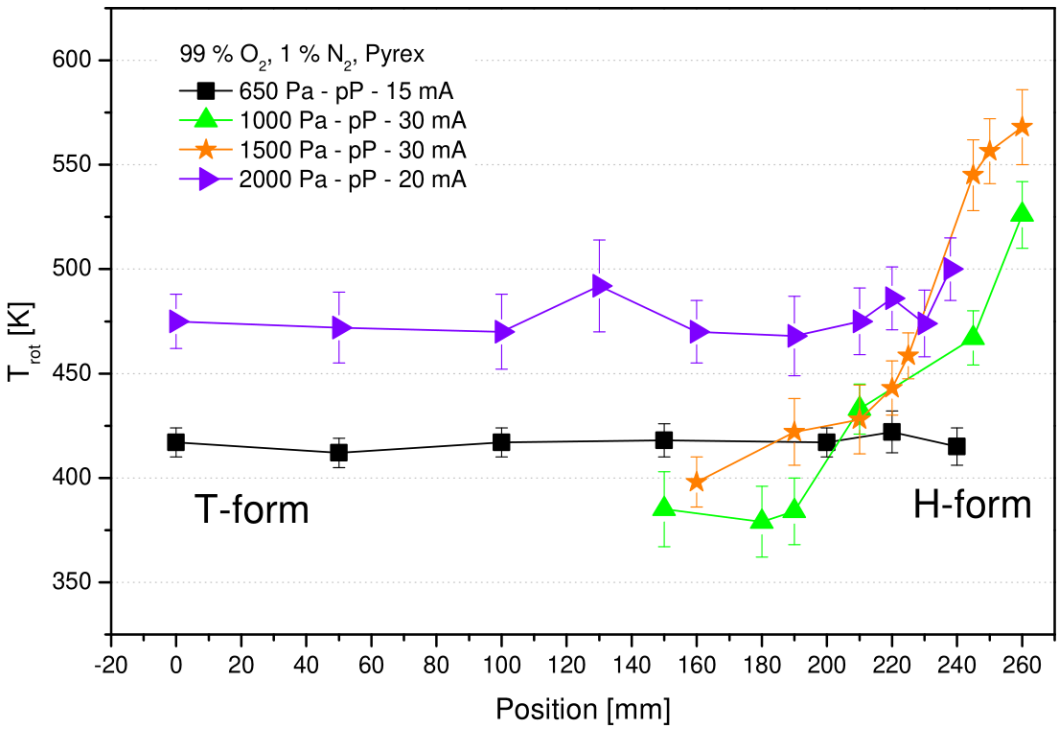

Figure 4.31: *The rotational temperature as calculated from the optical emission of O_2 ($b\ ^1\Sigma_g^+$) for various total pressures. Discharge current chosen to stabilize the T-H form transitional region in one place. Oxygen-nitrogen mixture (99:1), Pyrex discharge tube.*

4.2.2.2 Concentrations of excited particles

Similarly to the rotational temperature measurements, the concentration (or

more precisely the intensity of resulting emission lines) of studied states does not exhibit any remarkable behavior indicating on the presence of the transitional region - see Figures 4.32 and 4.33. Unlike in the pure oxygen, no clear spatial difference was observed. This in correspondence with the rotational temperature suggests that the transitional region was indeed not observable with the exception of the 1500 Pa pressure and to some extent 1000 Pa. There we see the same behavior of all concentrations and rotational temperature as we have observed with pure oxygen.

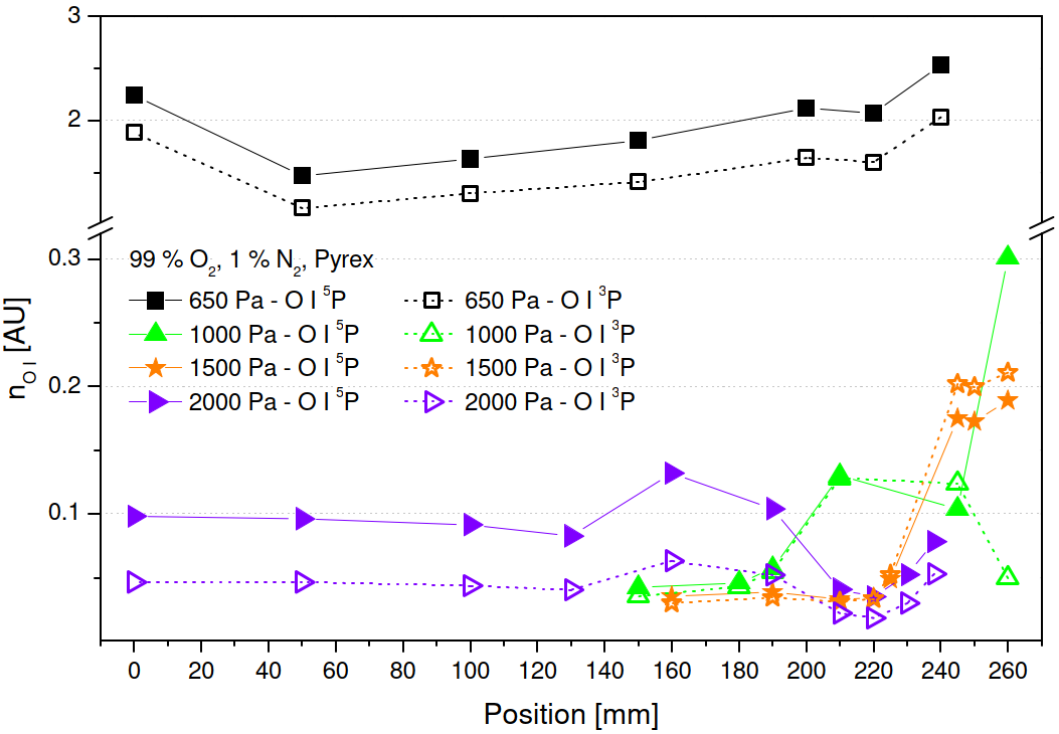

Figure 4.32: *The concentration of excited atomic oxygen in the O I (^3P) (empty symbols) and O I (^5P) (full symbols) states as measured using optical emission spectrometer for various total pressures. The relative uncertainty of each datapoint is ±30 %. Results are plotted using arbitrary units. Discharge current chosen to stabilize the T-H form transitional region in one place.Oxygen-nitrogen mixture (99:1), Pyrex discharge tube.*

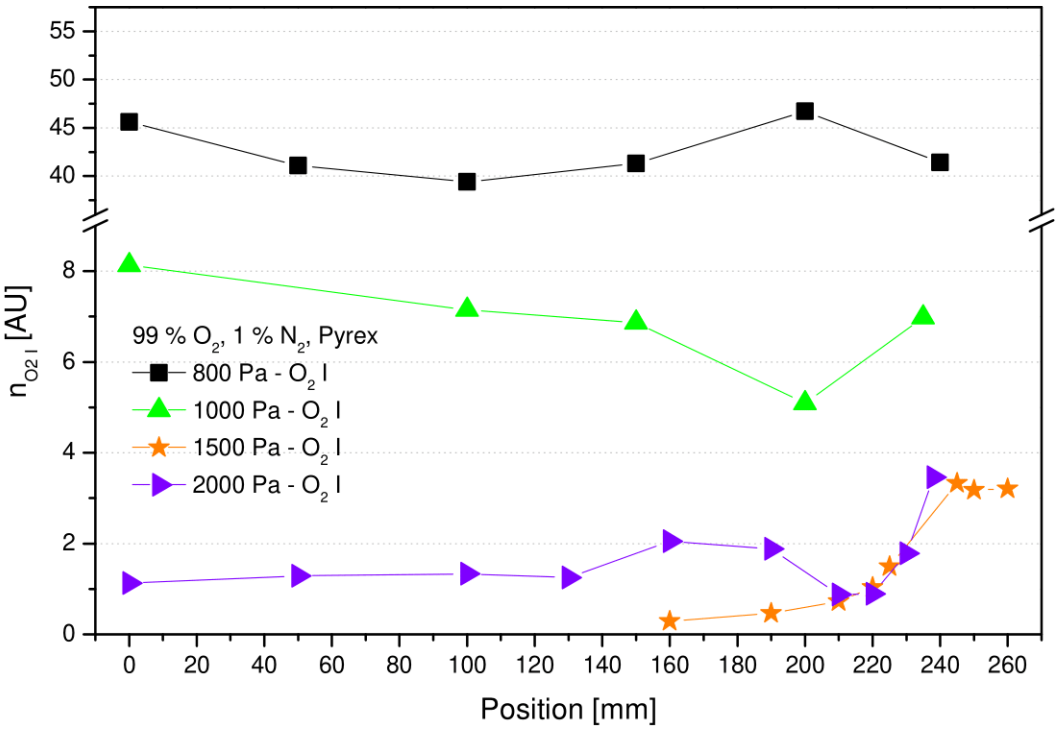

Figure 4.33: *The concentration of excited molecular oxygen in the* O_2 ($b\ ^1\Sigma_g^+$) *state as measured using optical emission spectrometer for various total pressures. The relative uncertainty of each datapoint is* ± 30 %. *Results are plotted using arbitrary units. Discharge current chosen to stabilize the T-H form transitional region in one place. Oxygen-nitrogen mixture (99:1), Pyrex discharge tube.*

4.2.3 Toroidal resonator

Toroidal resonator was utilised as supplemental method to estimate the electron concentration in the respective forms and in the transitional region. The resonances were measured for total pressures of 1000 Pa and 2000 Pa. A scan of burning discharge was done on chosen positions along the discharge axis. Afterwards the measurements of the resonances without the plasma were done for the same positions. The resulting resonance curves were fitted with the Lorentz bell curves. The calculated electron concentrations are shown in Fig. 4.34 and 4.35.

As mentioned before (see 4.1.3), the electron concentration is usually about an order higher in the T-form than in the H-form. Since we were not able to scan H-formed discharge with the resonator (the transitional region was to the far right out of its range, see Figure 3.8 on page 27), we were not able to confirm this fact in the gas mixture.

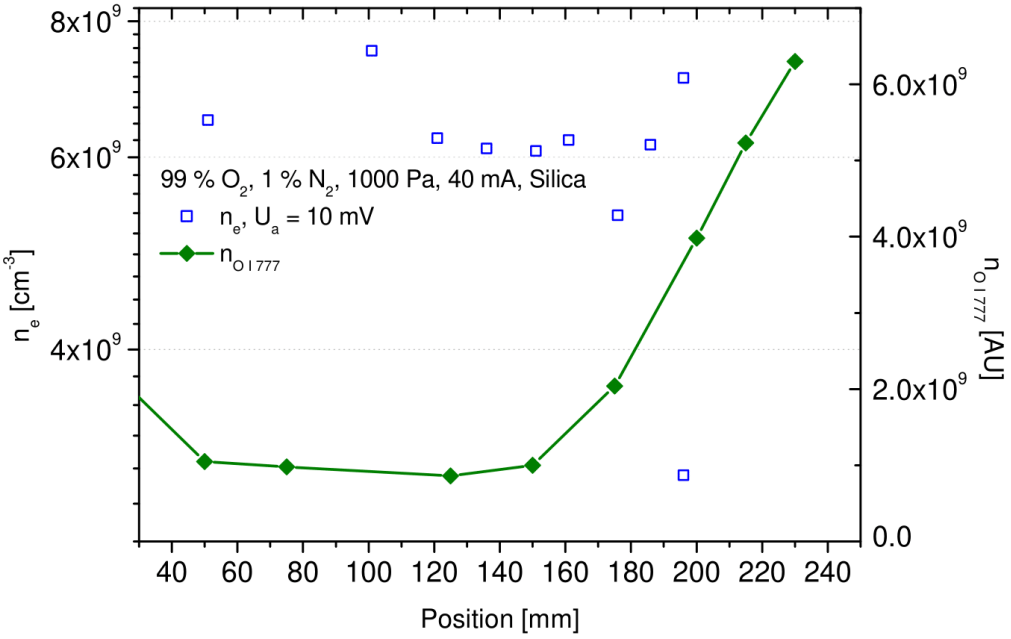

Figure 4.34: *The electron concentration measured using toroidal resonator (amplitude of the driving voltage 10 mV). The concentration of O I (^3P) as measured using calibrated optical emission spectrometer is shown for comparison of the position of the transitional region. The "doublepeak" was prominent only at the position of 196 mm. The T-form is present on the left, H-form to the right. Oxygen-nitrogen mixture (99:1), 1000 Pa total pressure, 40 mA of discharge current, silica discharge tube.*

The "doublepeak" mentioned in the section 4.1.3 was present only for one measurement at the 1000 Pa of total pressure, otherwise the resonances were normal. As mentioned above, we attributed this to the fact, that the transitional region was outside the range measureable with the resonator (as can be also seen e.g. from the O I (777) concentration curves).

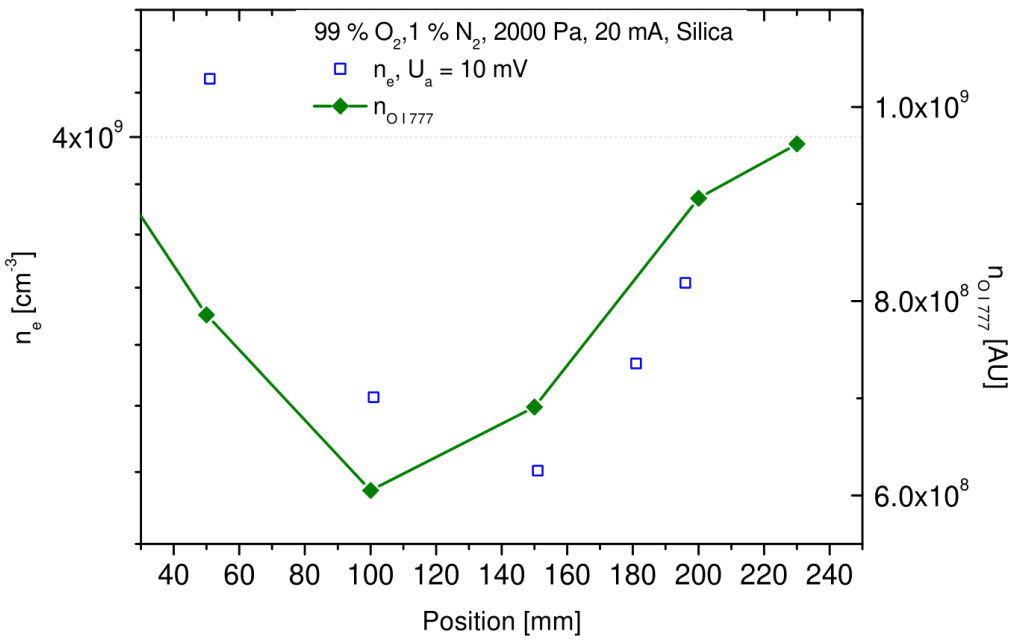

Figure 4.35: *The electron concentration measured using toroidal resonator (amplitude of the driving voltage 10 mV). The concentration of O I (^3P) as measured using calibrated optical emission spectrometer is shown for comparison of the position of the transitional region. The T-form is present on the left, H-form to the right. Oxygen-nitrogen mixture (99:1), 2000 Pa total pressure, 20 mA of discharge current, silica discharge tube.*

4.2.4 Electrical properties

Axial electric field strength was measured in order to have independent control over the presence of the respective forms of the glow discharge positive column. Two pairs of Langmuir probes were utilized as described in the section 2.1. The results are shown in the Figure 4.36.

There were almost no differences in axial electric field strength behavior observed in pure oxygen and in the oxygen/nitrogen mixture (see section 4.1.4). Only distinct feature was the power consumed in the discharge and subsequently the axial electric field strength were higher for pure oxygen, which is in agreement with the fact that N_2 molecule has vast system of metastable vibrational levels which facilitates step ionization and reduces the energy input needed to sustain the discharge.

Also the mixture seemed to be more easily stabilized in the T-form, however the problems with fast moving oscillations mentioned in 4.1.4 was much more prominent in the discharge, so the actual values have rather large uncertainty of few tens of percent. Since these measurements were meant only as auxiliary and were not in the main scope of the presented work, further investigations were not made.

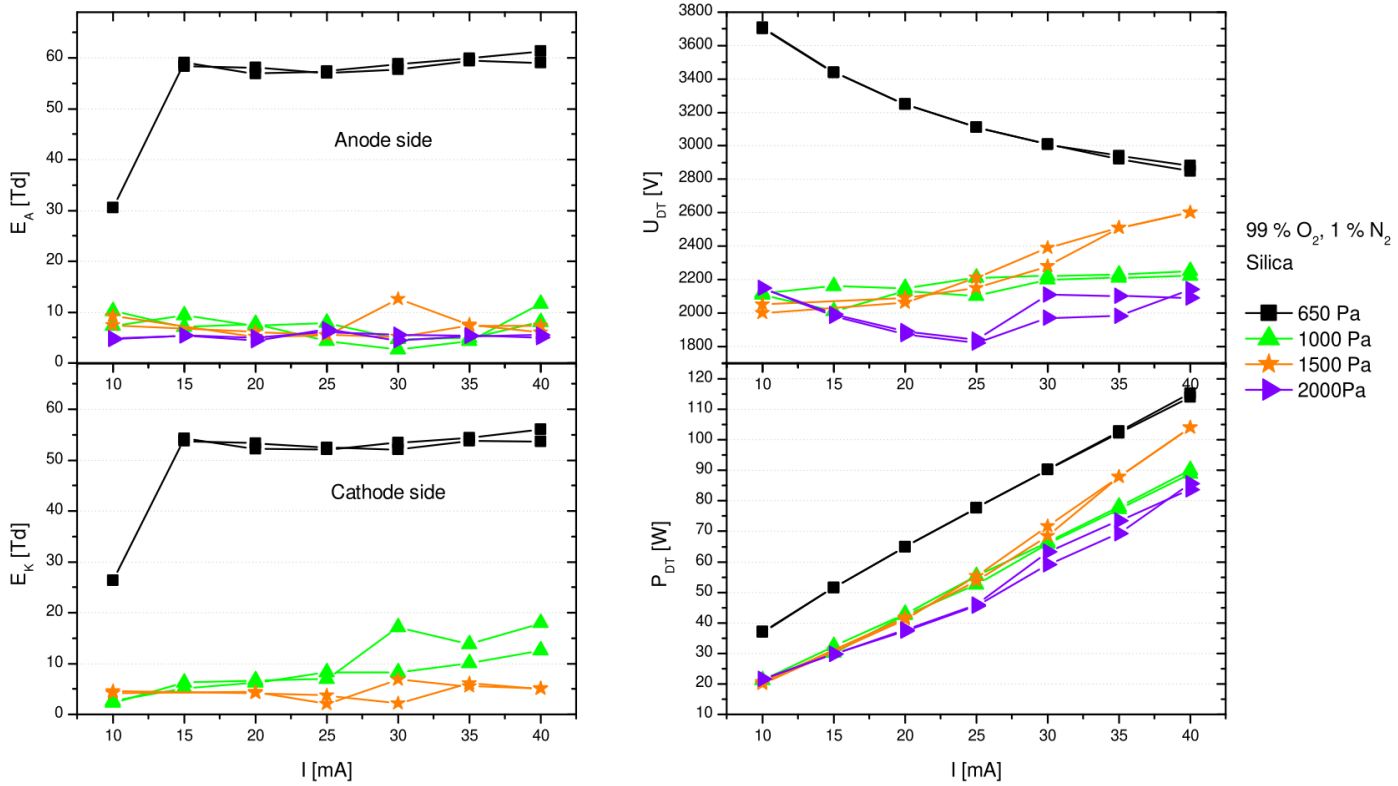

Figure 4.36: *Electric properties of the glow discharge column as measured in different pressures. Left top and bottom: Axial electric field strength measured using Langmuir doubleprobes. Right top: The voltage drop on the entire discharge calculated from generator voltage, excluding the stabilization resistor (kΩ). Right bottom: The power input on the discharge tube calculated as* $P = U_{DT} \cdot I$*. Oxygen-Nitrogen mixture (99:1), silica discharge tube*

4.2.5 Wall composition

The measurements in the two discharge tubes made out of pyrex and silica glass respectively were performed for selected discharge parameters in order to provide comparison with each other and with pure oxygen. The emission spectra were again collected along the discharge axis with plain optical fibre (see 4.2.5.1) and radial scanner (see 4.2.5.2).

4.2.5.1 OES - Integral

The results for the calculated rotational temperature are again higher in the pyrex tube than in the silica tube (see Fig. 4.37). Overall the temperatures are higher than in pure oxygen in both glasses. The effect of the wall composition is again prominent in whole pressure range.

Comparison of the excited species distribution is plotted in the Fig. 4.38 and 4.39. The results for the total pressure of 650 Pa before discharge breakdown are significantly higher due to the presence of the H-form positive column in a significant part of the discharge tube (more than one half of the tube length, usually in whole volume). The widening of the "gap" between the concentrations measured in silica and pyrex can be also attributed to the prolonging of the H-form to a significant portion of the measured volume (i. e. when the H-form starting from the cathode reached a region between the Langmuir probes pairs, see Fig. 3.1).

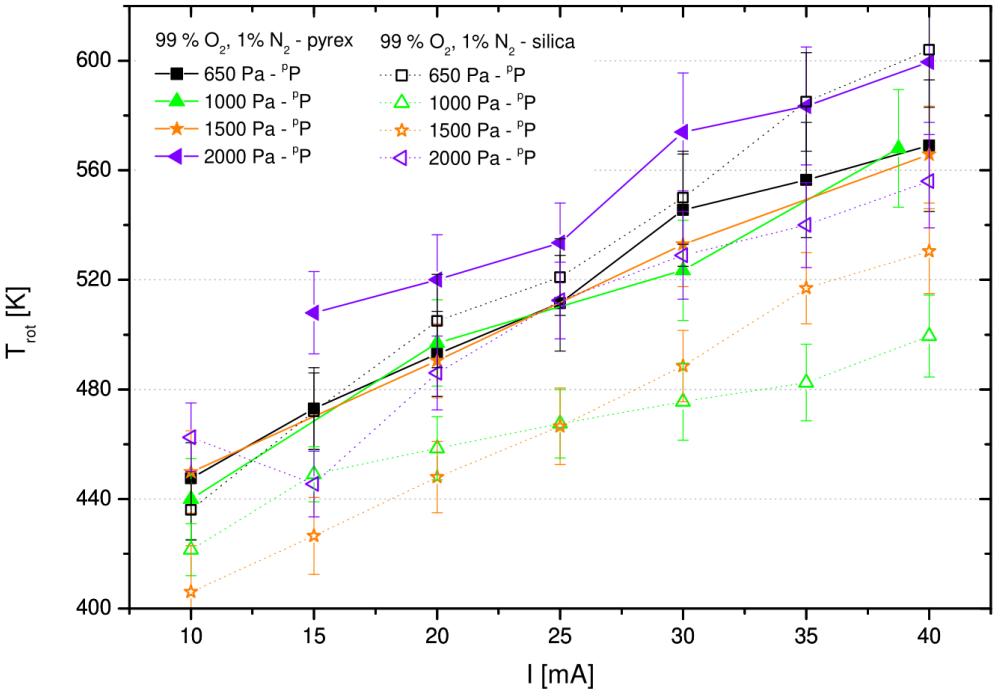

Figure 4.37: *The rotational temperature of oxygen molecules calculated from the spectra of the atmospheric band. Comparison of different composition of discharge tube wall, oxygen-nitrogen mixture (99:1).*

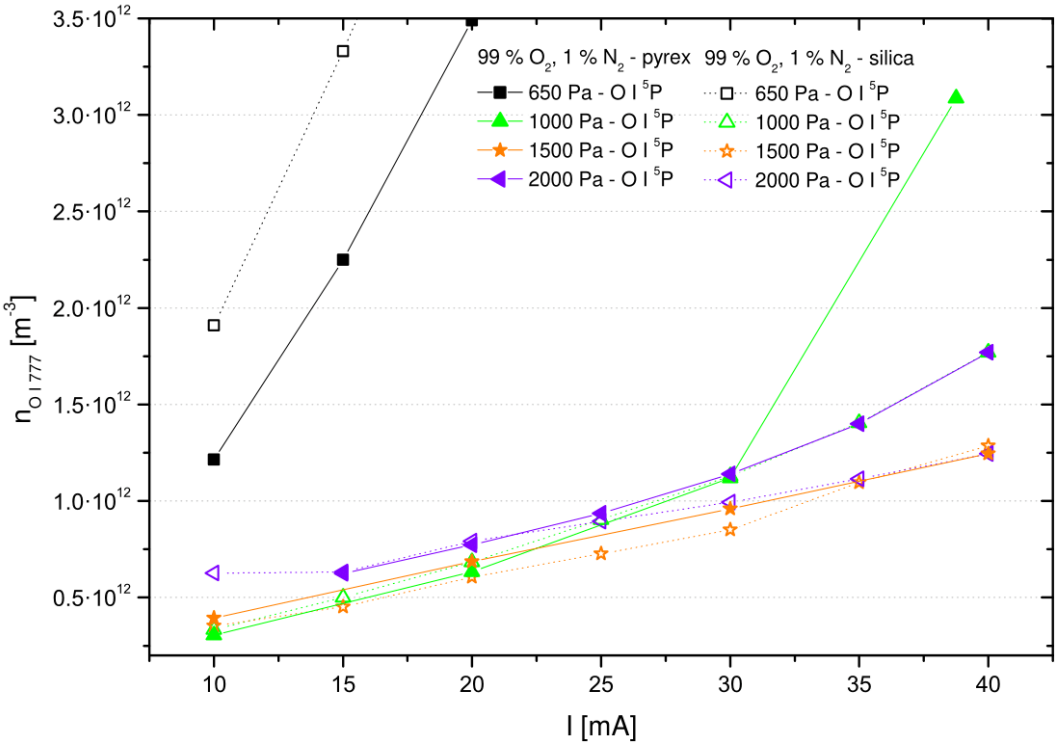

Figure 4.38: *The concentration of O I (^5P) as measured using calibrated optical emission spectrometer. The relative uncertainty of each datapoint is* ±15 %. *Comparison of discharge tube wall material, oxygen-nitrogen mixture (99:1).*

4.2.5.2 OES - Radial

The results of the radial profile of the rotational temperature are shown in Figs. 4.40 and 4.41. The temperature again has very flat profile, that corresponds to the temperature measured along the axis without the radial scanner (see Fig. 4.41). The measurements of the concentrations were unfortunately burdened with significant systematic error that prevented any meaningful comparison and therefore are not presented here.

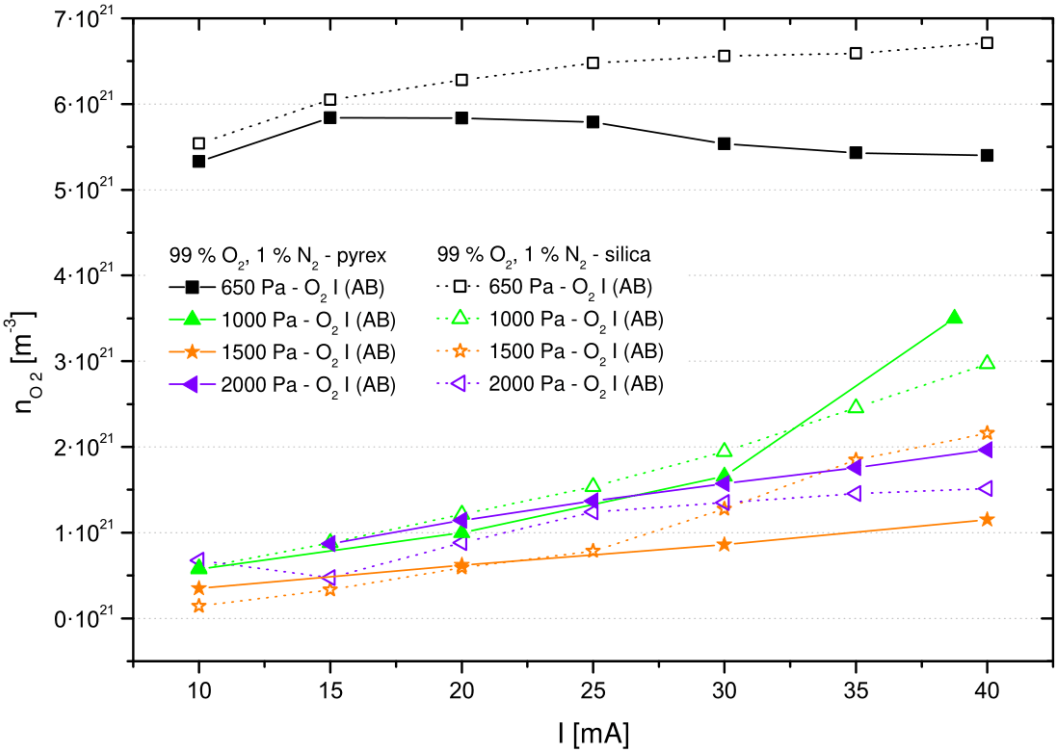

Figure 4.39: *The concentration of O_2 ($b\ ^1\Sigma_g^+$) as measured using calibrated optical emission spectrometer. Comparison of different composition of discharge tube wall, oxygen-nitrogen mixture (99:1).*

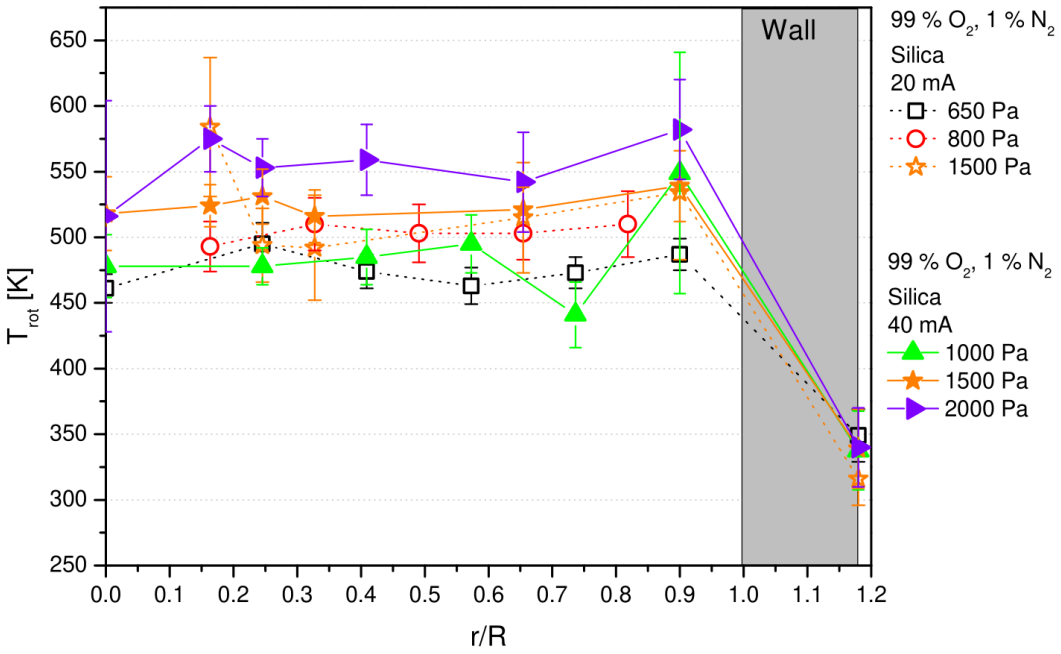

Figure 4.40: *The radial profile of the rotational temperature of oxygen molecules calculated from the spectra of the atmospheric band. Silica glass tube, 20 mA and 40 mA of discharge current, oxygen-nitrogen mixture (99:1). The datapoints on the outer side of tube wall were obtained using IR thermometer.*

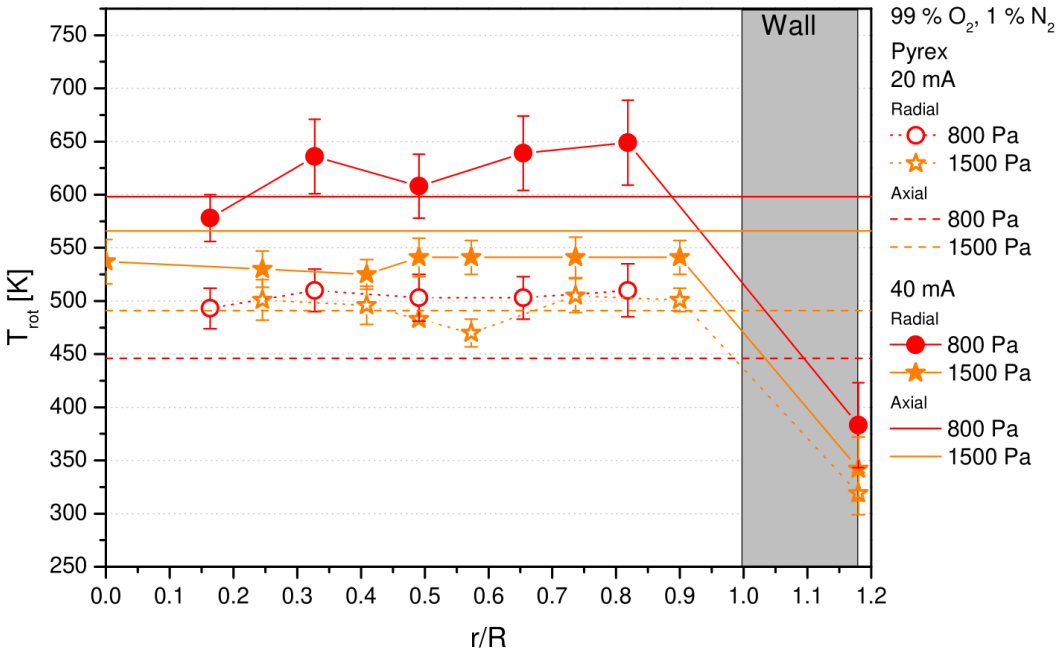

Figure 4.41: *The radial profile of the rotational temperature of oxygen molecules calculated from the spectra of the atmospheric band. Pyrex glass tube, 20 mA and 40 mA of discharge current, oxygen-nitrogen mixture (99:1). The datapoints on the outer side of tube wall were obtained using IR thermometer.*

4.3 Comparison of the O_2 and O_2-N_2 discharge

When we plot the results obtained in the pure oxygen and in the oxygen-nitrogen mixture next to each other, important differences show up, mainly in the rotational temperature. Complex computational model would be needed to explain directly the roots of these variances. The author is not aware of any model considering **both** H- and T-form of oxygen (and especially oxygen-nitrogen) discharge that could be used.

4.3.1 OES - Axial integral measurements

4.3.1.1 Rotational temperature

It can be seen in the figure 4.42 that the rotational temperature is significantly higher in the mixture than in the pure oxygen for pressures lower than 2000 Pa. The reason for this behaviour lies probably in the fact, that nitrogen molecule is relatively easily excited by electrons with various energy due to the vast system of vibrational bands. To sustain the discharge, higher energy must be fed into the discharge, resulting in higher discharge voltage and higher axial electric field strength even in the T-form (see 4.3.3).

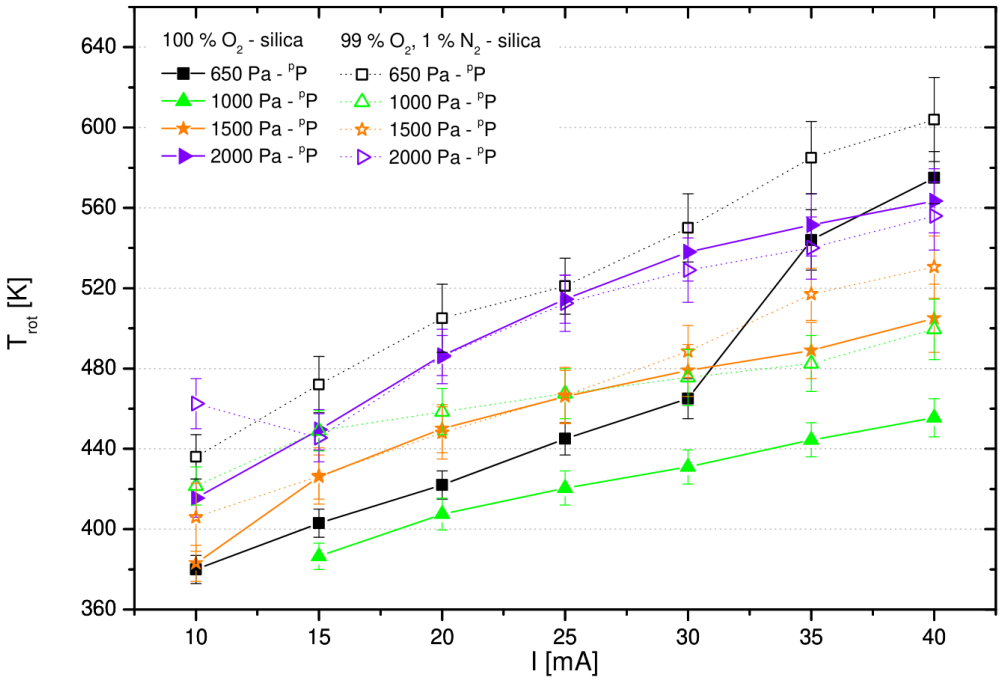

Figure 4.42: *The rotational temperature of oxygen molecules calculated from the Atmospheric band emission. Comparison of pure oxygen and oxygen-nitrogen mixture (99:1), silica discharge tube.*

4.3.1.2 Concentrations of excited particles

The comparison of excited atomic and molecular oxygen concentrations is shown in figures 4.43 - 4.45. These results are interesting in the fact that apart

from the 650 Pa measurements, which are affected by the presence of the H-form, the concentrations are almost the same in both gas compositions for higher pressures. This suggests that the excitation, deexcitation and dissociation of the oxygen happens with the same rates. At lower pressures, the concentrations in the mixture are lower, probably due to lower excitation of oxygen because of the presence of nitrogen and contraction of the discharge to the axis of the tube, which lowers the importance of wall interactions, which in turn are the main source of atomic species recombination to molecules (see equations (1.3) and (1.5)).

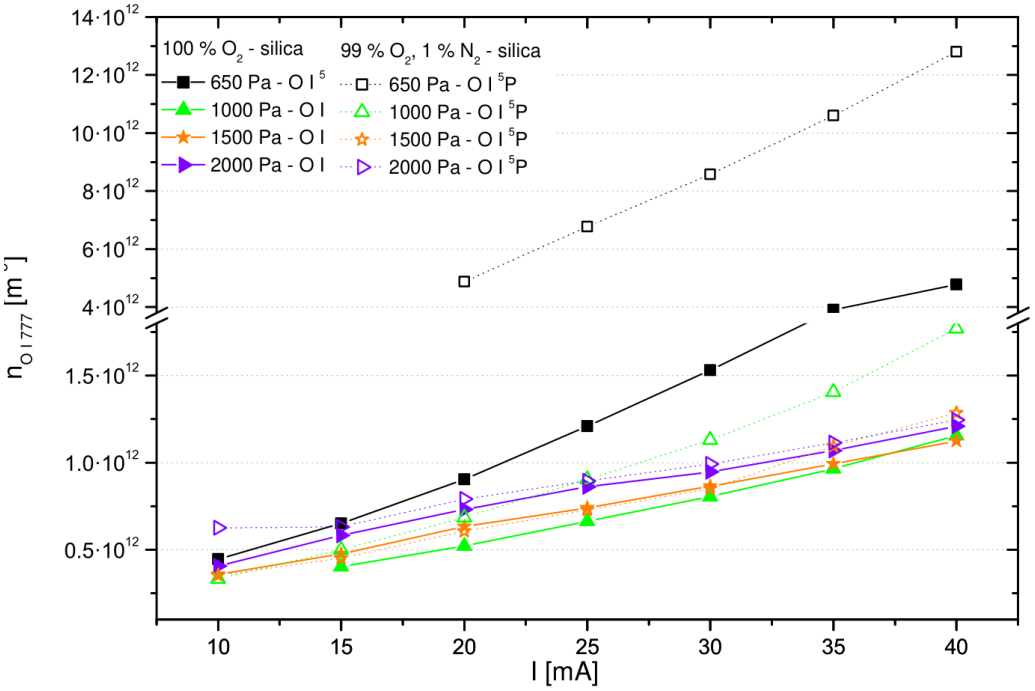

Figure 4.43: *The concentration of O I (^5P) as measured using calibrated optical emission spectrometer. The relative uncertainty of each datapoint is* ±15 %. *Comparison of pure oxygen and oxygen-nitrogen mixture (99:1), silica discharge tube.*

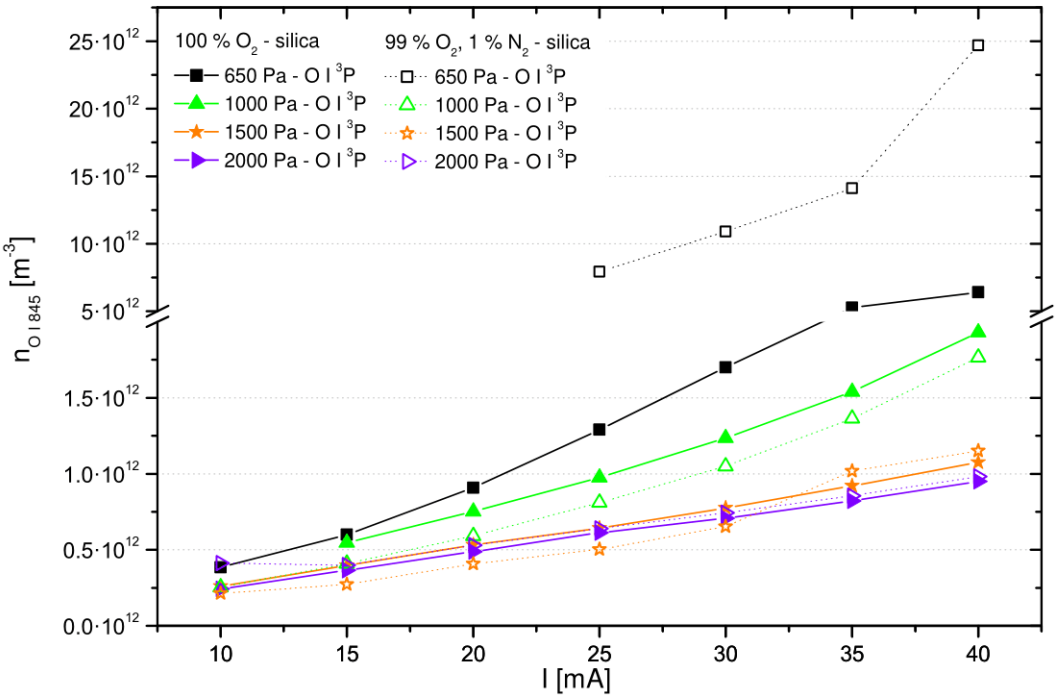

Figure 4.44: *The concentration of O I (^3P) as measured using calibrated optical emission spectrometer. The relative uncertainty of each datapoint is ±15 %. Comparison of pure oxygen and oxygen-nitrogen mixture (99:1), silica discharge tube.*

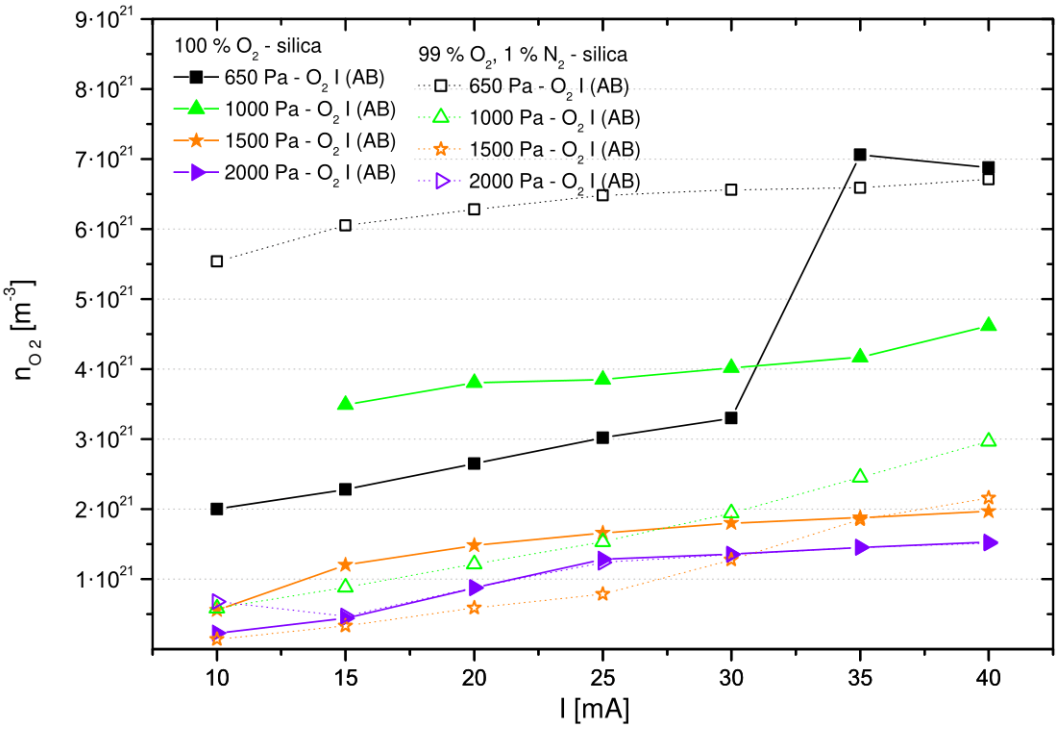

Figure 4.45: *The concentration of O_2 ($b\ ^1\Sigma_g^+$) as measured using calibrated optical emission spectrometer. The relative uncertainty of each datapoint is ±20 %. Comparison of pure oxygen and oxygen-nitrogen mixture (99:1), silica discharge tube.*

4.3.2 OES - Axial radial measurements

The effect of higher rotational temperature in the mixture with nitrogen compared to the pure oxygen was prominently observable even in the radial dependency measurements. Apart from that, the profiles of the temperature were comparably flat in both cases (see Fig. 4.46).

The comparison of radial profiles of the excited species O I (^3P) and O_2 ($b\,^1\Sigma_g^+$) are shown in the Fig. 4.47. It can be concluded, that the concentrations are higher in the pure oxygen as presumed. The presence of the easily excited nitrogen in the discharge leads to deflection of the energy of electrons towards excitation of the vibrations of the nitrogen molecules, therefore leading to decrease of excitation of the oxygen molecules and atoms.

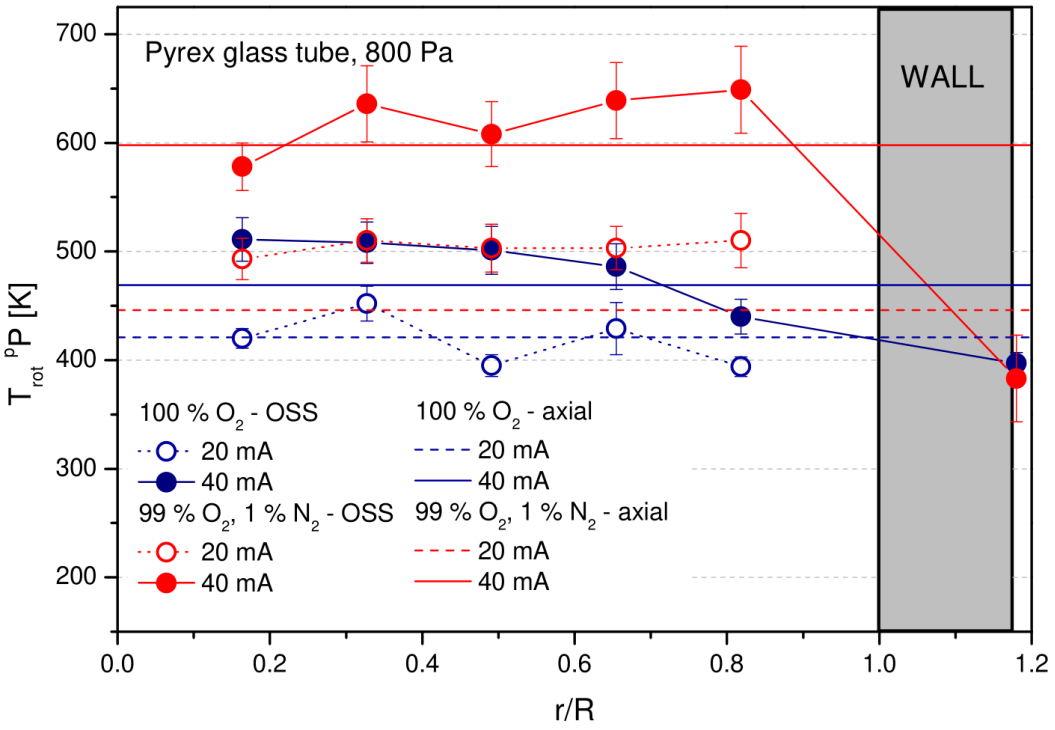

Figure 4.46: *The radial profile of the rotational temperature calculated from oxygen molecular atmospheric band as measured using radial scanner. Total pressure before breakdown 800 Pa. Comparison of pure oxygen and oxygen-nitrogen mixture (99:1), pyrex discharge tube.*

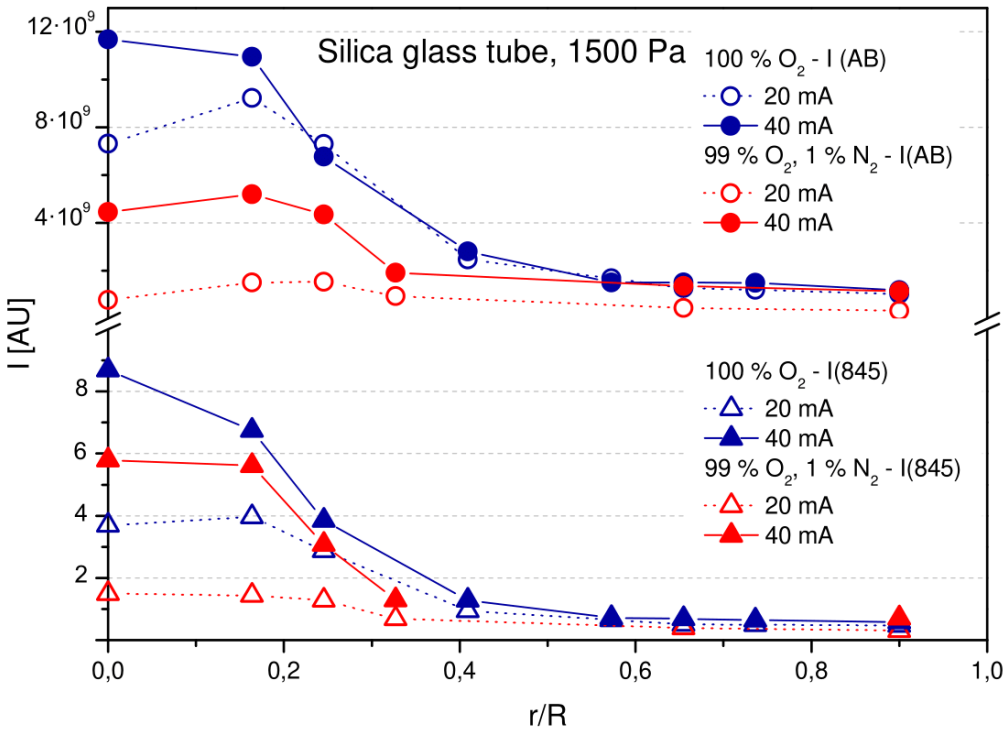

Figure 4.47: *The radial profile of the concentration of the O I (^3P) (triangles) and O_2 ($b\ ^1\Sigma_g^+$) (circles) as measured using radial scanner. Total pressure before breakdown 1500 Pa. The relative uncertainty of each datapoint is ±20 %. Comparison of pure oxygen and oxygen-nitrogen mixture (99:1), silica discharge tube.*

4.3.3 Electrical properties

The electrical properties, namely the axial electric field strength does indeed depend on the gas composition. It may be of interest that even low addition of nitrogen (1 % of total pressure) not only affects the emissions but the electric field strength as well as can be seen in Figure 4.48. Higher electric field strength was observed in pure oxygen compared with the mixture. This effect was observed before and described e.g. in [28]. The authors confirmed using model of oxygen-nitrogen discharge (H-form) that small addition of nitrogen in oxygen leads to higher concentrations of atomic oxygen, which has higher ionization energy than molecule (atomic - 13.62 eV, molecular - 12.07 eV; see [49]).

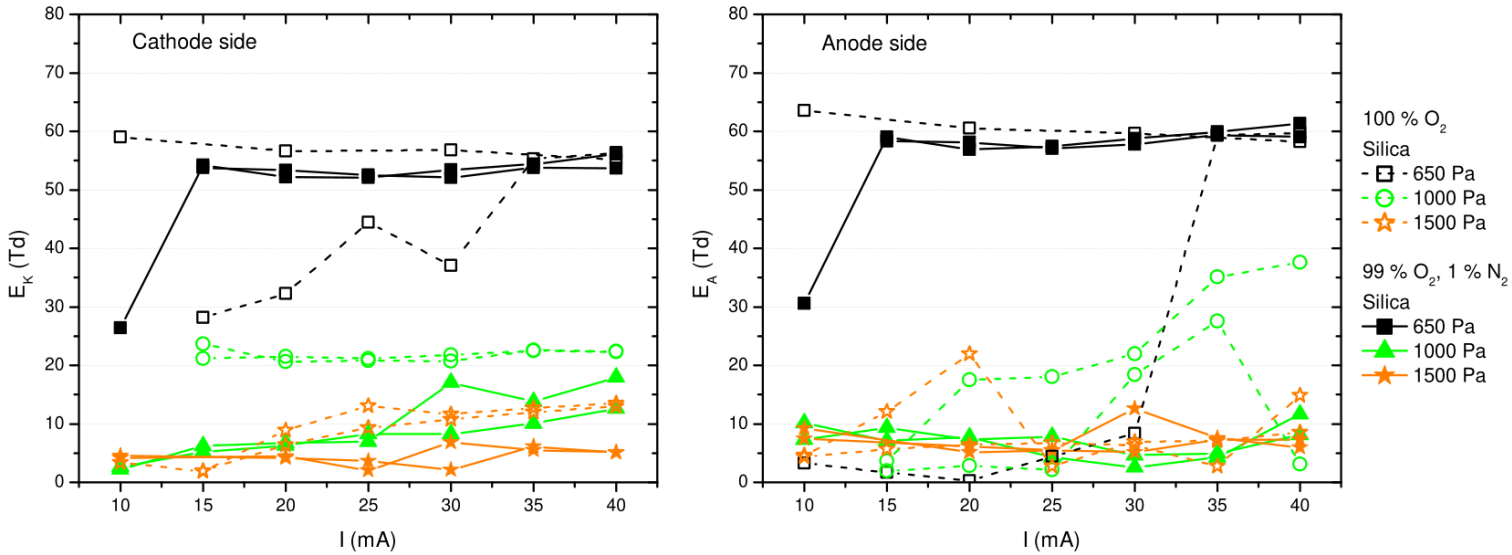

Figure 4.48: *Electric properties of the glow discharge column as measured in different pressures. Comparison of pure Oxygen and Oxygen-Nitrogen mixture (99:1), silica discharge tube. Double probe measurements at the Cathode (left) and Anode (right) side of the discharge tube.*

Discussion and Conclusion

The presented thesis brings comprehensive and systematic study of DC glow discharge in oxygen and oxygen-nitrogen mixture in medium pressures. The center topic of this study was the simultaneous occurrence of two forms of the positive column of the discharge, so-called H-form and T-form. The properties of discharge plasma were studied depending on the discharge parameters (namely total pressure and discharge current) and we used two discharge tubes made out of different type of glass (silica glass and pyrex).

This study concentrated on the transition region between the regions of said forms. We studied mainly optical emission of the discharge, with emphasis on the concentrations of selected atomic and molecular states that are easily obtainable from the spectra. Namely we studied the molecular oxygen in the state $b\ ^1\Sigma_g^+$, which forms well-known set of emission lines called "atmospheric band", and atomic oxygen in states O I (^3P) and O I (^5P), which form also easily recognizable set of lines with heads at 777.2 nm and 844.7 nm, respectively.

The concentrations showed higher dissociation rate of oxygen molecule for higher pressures, where the T-formed region filled increasingly larger part of the discharge volume, which is in agreement with previous studies made in our departement (e.g. [44], [50], [51]). Higher dissociation was also observed for higher discharge currents (due to higher energy fed to the discharge).

Optical emission was also used to calculate rotational temperature of the oxygen molecule, which can be said to be equal to kinetic temperature of the neutral gas. The temperature showed expected behaviour, rising with discharge current and with total pressure. The increase with pressure was mitigated in the region between 800 - 1250 Pa by extension of the T-form into larger part of the discharge volume, because the temperature in the T-form is significantly lower than in the H-form (see [25] (Attachment 2), [51]). Rise of temperature and concentrations of atomic species with the addition of nitrogen into discharge was also observed (see [52] (Attachment 6)).

In order to study the transitional region between said forms, we equipped the intake of optical spectrometer fiber with diaphragm and scanned the transitional region with spatial resolution of 5-10 mm. These measurements were never made before and showed us interesting properties of the plasma, namely that the width of the transitional region was about 20-25 mm, the rotational temperature increase together with the increase of the concentrations of studied excited particles (see [53] (Attachment 5)).

We also employed special radial scanner to measure the radial dependence of the optical emission and of the parameters obtainable from the optical spectra. We observed flat profile of the rotational temperature for the whole pressure range and discharge current range studied (see [54] (Attachment 4)). This was later employed as input for the computational model of oxygen plasma made by dr. Laca (see [14] (Attachment 1), [15]). The profiles of the excited species showed clear contraction of the discharge positive column to the axis with increasing pressure (see [55] (Attachment 3)).

Considering the discharge tube material, increased oxygen dissociation was observed in the pyrex tube. This effect was present in the whole studied pressure

region, however the difference between the materials decreased quickly with increasing pressure, most likely due to the contraction of the discharge to the axis of the tube mentioned above.

Considering the addition of nitrogen to the discharge gas mixture, even one percent affected the discharge in significant ways, triggering rise in the rotational temperature and decrease in both the excited dioxygen and atomic oxygen concentrations. Nitrogen addition also seemed to promote the formation of T-formed positive column, especially at higher pressures.

We accompanied our studies with auxiliary measurements of axial electric field strength using double Langmuir probe and measurements of the electron concentration using toroidal microwave resonator. The latter method provided interesting results and insight into the character of the transitional region, hypothesizing that the transitional region is in fact rather thin, but oscillating along the discharge axis. The presence of fast longitudinal ionization waves in the T-form is well known fact observed before (see e.g. [50]). We infer these might be the source of the transitional region blur. Since these measurements were meant only as auxiliary, closer examination was not performed, but can be a pointer for future studies.

Bibliography

[1] J. Musil, J. Matouš, and A. Rajský. Optical emission spectra from microwave oxygen plasma produced by surfatron discharge. *Czechoslovak Journal of Physics*, 43(5):533–540, may 1993.

[2] O. Kylian, P. Colpo, and F. Rossi. Experimental study of ICP in O2-N2-H2 mixtures for sterilization of bacterial spores. *Czechoslovak Journal of Physics*, 56(2):B1250–B1255, 2006.

[3] J. W. Coburn and M. Chen. Optical emission spectroscopy of reactive plasmas: A method for correlating emission intensities to reactive particle density. *Journal of Applied Physics*, 51(6):3134–3136, jun 1980.

[4] L. F. DiMauro, Richard A. Gottscho, and Terry A. Miller. Two-photon laser-induced fluorescence monitoring of O atoms in a plasma etching environment. *Journal of Applied Physics*, 56(7):2007–2011, oct 1984.

[5] Wen-An Loong and Hong-Long Chang. Oxidation of GaAs surface by oxygen plasma and its application as an antireflection layer. *Japanese Journal of Applied Physics*, 30(Part 2, No. 7B):L1319–L1320, jul 1991.

[6] G.K. Muralidhar, G.Mohan Rao, and S. Mohan. Fabrication and performance study of a YBa2Cu3O7-δ thin film varistor. *Thin Solid Films*, 238(1):115–118, jan 1994.

[7] G. Ceccone, D. Gilliland, O. Kylián, and F. Rossi. Experimental study of effect of low-pressure O2:H2 microwave discharge on protein films. *Czechoslovak Journal of Physics*, 56(S2):B672–B677, oct 2006.

[8] A N Vasiljeva, K S Klopovskiy, A S Kovalev, D V Lopaev, Y A Mankelevich, N A Popov, A T Rakhimov, and T V Rakhimova. On the possibility of O2(a 1 g) production by a non-self-sustained discharge for oxygen–iodine laser pumping. *Journal of Physics D: Applied Physics*, 37(17):2455–2468, aug 2004.

[9] Y. P. Raizer. *Gas discharge physics*. Springer-Verlag, Berlin-Heidelberg, 1991.

[10] H.D. Klotz, H. Drost, U. Timm, and W. Schulz. *Ann. Phys. 472*, page 301, 1966.

[11] H. Sabadil and S. Pfau. Measurements of the degree of dissociation in oxygen DC discharges: Comparison of the ozone method with the Wrede-Harteck method. *Plasma Chemistry and Plasma Processing*, 5(1):67–79, mar 1985.

[12] V. Hrachova, O. Kylian, and A. Kanka. Study of the vacuum purity influence on oxygen and nitrogen spectra properties in DC glow discharge. *Vacuum*, 76(4):433 – 436, 2004.

[13] G Gousset, C M Ferreira, M Pinheiro, P A Sa, M Touzeau, M Vialle, and J Loureiro. Electron and heavy-particle kinetics in the low pressure oxygen positive column. *Journal of Physics D: Applied Physics*, 24(3):290–300, mar 1991.

[14] Marek Laca, Matěj Jan Morávek, Lukáš Schmiedt, Věra Hrachová, and Adolf Kaňka. Fluid model of H-form of the positive column in DC oxygen glow discharge. *Contributions to Plasma Physics*, 57(8):336–350, sep 2017.

[15] Marek Laca, Adolf Kaňka, Lukáš Schmiedt, Věra Hrachová, and Matěj Jan Morávek. Fluid model of the positive column in argon-oxygen direct current glow discharge. *Contributions to Plasma Physics*, 59(9):e201800190, jun 2019.

[16] A Güntherschulze. *Zeitschrift der Physik*, (42):763, 1927.

[17] R. Seeliger and A. Wichman. *Annalen der Physik*, (9):235, 1951.

[18] R. W. B. Pearse and A. G. Gaydon. *The identification of Molecular Spectra*. TBD, 1976.

[19] L. Pekárek and M. Šícha. The connection between low-gradient form of the positive column in oxygen and moving striations. *Czechoslovak Journal of Physics*, 1960.

[20] V. Řezáčová. Electron density in the oxygen discharge plasma. *Czechoslovak Journal of Physics B*, 20(1):126–131, Jan 1970.

[21] H. Drost, U. Timm, and H. Pupke. *Ann. Phys.*, (467):186, 1963.

[22] H. Keren, P. Avivi, and F. Dothan. Positive ion mass spectra of a glow discharge in oxygen. *Physics Letters A*, 56(2):85–86, mar 1976.

[23] P. Kocian and J.M. Mayor. In *Proceedings of 13rd ICPIG*, page 253, Berlin, Germany, 1977.

[24] J. W. Dettmer. *Discharge processes in the oxygen plasma*. PhD thesis, Aero Propulsion Laboratory, Wright Patterson Air Force Base, Ohio, 1978.

[25] Lukáš Schmiedt, Matěj Jan Morávek, Adolf Kaňka, and Věra Hrachová. T- and H- forms of dc oxygen discharge at medium pressures: spectroscopic study. *Open Chemistry*, 13(1), jan 2015.

[26] B Gordiets and A Ricard. Production of N, O and NO in N2-O2 flowing discharges. *Plasma Sources Science and Technology*, 2(3):158–163, aug 1993.

[27] V Guerra and J Loureiro. Non-equilibrium coupled kinetics in stationary N2-O2 discharges. *Journal of Physics D: Applied Physics*, 28(9):1903–1918, sep 1995.

[28] V Guerra and J Loureiro. Self-consistent electron and heavy-particle kinetics in a low-pressure - glow discharge. *Plasma Sources Science and Technology*, 6(3):373–385, aug 1997.

[29] B Gordiets, C M Ferreira, J Nahorny, D Pagnon, M Touzeau, and M Vialle. Surface kinetics of N and O atoms in discharges. *Journal of Physics D: Applied Physics*, 29(4):1021–1031, apr 1996.

[30] A Hibbert, E Biemont, M Godefroid, and N Vaeck. E1 transitions of astrophysical interest in neutral oxygen. *Journal of Physics B: Atomic, Molecular and Optical Physics*, 24(18):3943–3958, sep 1991.

[31] Paul H. Krupenie. The spectrum of molecular oxygen. *Journal of Physical and Chemical Reference Data*, 1(2):423–534, apr 1972.

[32] Gerhard Herzberg. *Molecular Spectra and Molecular Structure. I. Spectra of Diatomic Molecules*. Van Nostrand, Princeton, 1950.

[33] M Touzeau, M Vialle, A Zellagui, G Gousset, M Lefebvre, and M Pealat. Spectroscopic temperature measurements in oxygen discharges. *Journal of Physics D: Applied Physics*, 24(1):41, 1991.

[34] Robert Schlapp. Fine structure in the 3Σ ground state of the oxygen molecule, and the rotational intensity distribution in the atmospheric oxygen band. *Phys. Rev.*, 51:342–345, Mar 1937.

[35] J.H. Miller, R.W. Boese, and L.P. Giver. Intensity measurements and rotational intensity distribution for the oxygen a-band. *Journal of Quantitative Spectroscopy and Radiative Transfer*, 9(11):1507–1517, nov 1969.

[36] M. Sicha, J. Pilar, J. Gajdusek, Jar Novak, V. Fuchs, and P. Lukac. A contribution to the measurement of the electron density of discharge plasma by means of a toroidal resonator. *Czechoslovak Journal of Physics*, 17(1):48–66, jan 1967.

[37] M. Šícha, G. G. Cloutier, and R. Bolton. Characteristics of a toroidal resonator for plasma diagnostics. *Canadian Journal of Physics*, 45(12):3979–3989, dec 1967.

[38] N. A. Kapcov. *Elektronika*. Vydavatelstvo Slovenskej akademie vied, Bratislava, 1959.

[39] Wolfram Research, Inc. Mathematica online, Version 12.0, retreived 2015-09-11. Champaign, IL, 2015.

[40] M Sicha, J Gajdusek, and S Veprek. Comparison of microwave and probe methods of plasma diagnostics. *British Journal of Applied Physics*, 17(11):1511–1514, nov 1966.

[41] M.J. Moravek, L. Schmiedt, A. Kanka, and V. Hrachova. Influence of CO2-laser mixture composition on the distribution of energy in nitrogen spectrum. *Vacuum*, 86(6):780–784, 2012.

[42] A. Kanka and V. Hrachova. Equipment for measurements of radial profiles of excited species in DC glow discharge. *Czech. J. Phys.*, 56(6):619–628, 2006.

[43] Princeton Instruments. Etaloning in back-illuminated CCDs. *Technical note 7*, 2000.

[44] Lukáš Schmiedt, Matěj Jan Morávek, Adolf Kaňka, and Věra Hrachová. Study of rotational temperature of oxygen DC glow discharge in silica and pyrex discharge tubes. *Vacuum*, 84(1):72 – 74, 2009. 12th Joint Vacuum Conference, 10th European Vacuum Conference and 7th Annual Meeting of the German Vacuum Society (JVC-12/EVC-10/AMDVG-7), Balatonalmadi, Hungary, 22 - 26 September 2008.Organised by Roland Evtvvs Physical Society, Hungary in collaboration with the Vacuum Societies of Austria, Croatia, Czech Republic, Germany, Hungary, Slovakia and Slovenia.

[45] O. Kylián, A. Kaňka, and V. Hrachová. Spectroscopic determination of oxygen DC glow-discharge temperature: Radial profile of gas temperature. *Czechoslovak Journal of Physics*, 53(3):219–227, Mar 2003.

[46] Kylián O. PhD thesis, Charles University in Prague, 2003.

[47] G Cartry, L Magne, and G Cernogora. Atomic oxygen recombination on fused silica: experimental evidence of the surface state influence. *Journal of Physics D: Applied Physics*, 32(15):L53–L56, jul 1999.

[48] Russ R. Lager Gilmore, Forrest R. and Patrick J. Espy. Franck-condon factors, r-centroids, electronic transition moments, and Einstein coefficients for many nitrogen and oxygen band systems. *J. Phys. Chem. Ref. Data*, 21(5):1005–1107, 1992.

[49] Peter Linstrom. Nist chemistry webbook, NIST standard reference database 69. *NIST Standard Reference Database*, 69, 1997.

[50] L. Schmiedt, A. Kanka, and V. Hrachova. Study of properties of O-2-Ar mixture in dc glow discharge at medium pressures. *Czech. J. Phys.*, 56:B1040–B1044, 2006.

[51] L. Schmiedt, A. Kanka, and V. Hrachova. Study of rotational temperature of oxygen molecules in H and T forms of dc glow discharge sustained in pure oxygen. *Vacuum*, 85(12):1093–1095, 2011.

[52] M. J. Morávek, A. Kaňka, J. Čáp, and V. Hrachová. Atomic oxygen concentration observation by optical emission spectrometry in O2 and O2–N2 dc glow discharge. *WDS'15 Proceedings of Contributed Papers — Physics*, page 227–232, 2015.

[53] M. J. Moravek, A. Kanka, V. Hrachova, and J. Cap. Determination of concentration of excited oxygen particles by optical emission spectroscopy. *WDS'16 Proceedings of Contributed Papers - Physics*, pages 137–143, 2016.

[54] M. J. Morávek, M. Laca, A. Kaňka, and V. Hrachová. Radial distribution of the temperature in the t-form of oxygen dc glow discharge. *WDS'17 Proceedings of Contributed Papers — Physics*, pages 71–75, 2017.

[55] M J Morávek, L Schmiedt, M Laca, A Kaňka, and V Hrachová. Radial profiles of the emission spectra of dc glow discharge sustained in molecular gases at medium pressures. *Physica Scripta*, T161:014056, may 2014.

List of Figures

List of Abbreviations

n_e	electron density
n	density of neutral gas
E/N	reduced electric field strength
p	pressure
k_B	Boltzmann thermodynamic constant
n^+	density of O2+ positive molecular ion
J_0	Bessel function of the zero order
r	distance from the axis of the discharge tube
R	discharge tube radius
E	electric field strength
I_{if}^m	measured emitted intensity of transition from state i to f
I_{if}^0	actual intensity emitted by transition from state i to f
C	geometric coefficient of experimental setup
n_i	concentration of the emitting species
A_{if}	Einstein coefficient of spontaneous emission from state i to f
ν_{if}	corresponding frequency of the emission from state i to f
λ_{if}	wavelength of the emission from state i to f
$I_{J_iJ_f}$	intensity of transition between rotational states J_i and J_f
$\nu_{J_iJ_f}$	frequency of transition between rotational states J_i and J_f
S_J	Hoenl-London factor
F_J	the energy of the quantum state J
T_{rot}	rotational temperature
E_J	rotational energy levels
ω_0	circular resonance frequency of resonator
ω_{np}	circular resonance frequency of resonator without plasma
Q_0	quality of resonator
n_0	concentration of electrons on the discharge axis
ν	collision frequency of electrons with heavy particles
$U_0(z)$	potential distribution along the axis of symmetry z
$U_0(z)^{(2n)}$	even derivatives of potential distribution in the position z
D_A^{eM}	coefficient of ambipolar diffusion between ions and electrons
μ_M	mobility of single charged ions
m_M	mass of single charged ions
T_e	kinetic temperature of electrons

List of all author's publications

Publications in impacted journals

- Laca, M; Kaňka, A; Schmiedt, L; Hrachová, V; Morávek, MJ: Fluid model of the positive column in argon-oxygen direct current glow discharge, Contrib. Plasma Phys., 59 (9): Art. No. e201800190 (16 pages), 2019.

  doi:10.1002/ctpp.201800190

- Laca, M; Morávek, MJ; Schmiedt, L; Hrachová, V; Kaňka, A: Fluid model of H-form of the positive column in DC oxygen glow discharge, Contrib. Plasma Phys., 57 (8): 336–350, 2017.

  doi:10.1002/ctpp.201600063

- Schmiedt, L; Moravek, MJ; Kanka, A; Hrachova, V: T- and H- forms of dc oxygen discharge at medium pressures: spectroscopic study, Open Chem., 13 (1): 399–403, 2015.

  doi:10.1515/chem-2015-0050

- Moravek, MJ; Schmiedt, L; Laca, M; Kanka, A; Hrachova, V: Radial profiles of the emission spectra of dc glow discharge sustained in molecular gases at medium pressures, Phys. Scr., 2014 (T161): Art. No. 014056 (5 pages), 2014.

  doi:10.1088/0031-8949/2014/T161/014056

- Moravek, MJ; Schmiedt, L; Kanka, A; Nikiforov, A; Leys, C; Hrachova, V: Comparison of low-pressure DC glow discharge and dielectric barrier discharge in CO_2-laser mixture by optical emission spectroscopy, Vacuum, 90 (Apr): 135–140, 2013.

  doi:10.1016/j.vacuum.2012.04.048

- Moravek, MJ; Schmiedt, L; Kanka, A; Hrachova, V: Influence of CO_2-laser mixture composition on the distribution of energy in nitrogen spectrum, Vacuum, 86 (6): 780–784, 2012.

  doi:10.1016/j.vacuum.2011.07.065

- Schmiedt, L; Moravek, MJ; Kanka, A; Hrachova, V: Study of rotational temperature of oxygen DC glow discharge in Silica and Pyrex discharge tubes, Vacuum, 84 (1): 72–74, 2009.

  doi:10.1016/j.vacuum.2009.04.018

Publications in Conference Proceedings

- Moravek, MJ; Laca, M; Kanka, A; Hrachova, V: Radial Distribution of the Temperature in the T-form of Oxygen DC Glow Discharge, WDS'17 Proceedings of Contributed Papers — Physics, Prague, Matfyzpress, 71–75, 2017.

- Moravek, MJ; Kanka, A; Hrachova, V; Cap, J: Determination of Concentration of Excited Oxygen Particles by Optical Emission Spectroscopy, WDS'16 Proceedings of Contributed Papers — Physics, Prague, Matfyzpress, 137–143, 2016.

- Moravek, MJ; Cap, J; Kanka, A; Hrachova, V: Atomic Oxygen Concentration Observation by Optical Emission Spectrometry in O_2 and O_2–N_2 DC Glow Discharge, WDS'15 Proceedings of Contributed Papers — Physics, Prague, Matfyzpress, 227–232, 2015.

- Moravek, MJ; Laca, M; Kanka, A; Hrachova, V: Radial Distribution of the Temperature in the T-form of Oxygen DC Glow Discharge, WDS'14 Proceedings of Contributed Papers — Physics, Prague, Matfyzpress, 267-270, 2014.

- Moravek, MJ; Schmiedt, L; Kanka, A; Hrachova, V: Spectroscopic Study of T- and H-form of O_2 and O_2-N_2 DC Glow Discharge, WDS'13 Proceedings of Contributed Papers — Physics, Prague, Matfyzpress, 115-119, 2013.

Attachments

Relevant attached publications:

1. Laca, M; Morávek, MJ; Schmiedt, L; Hrachová, V; Kaňka, A: Fluid model of H-form of the positive column in DC oxygen glow discharge, Contrib. Plasma Phys., 57 (8): 336–350, 2017.

   doi:10.1002/ctpp.201600063

2. Schmiedt, L; Moravek, MJ; Kanka, A; Hrachova, V: T- and H- forms of dc oxygen discharge at medium pressures: spectroscopic study, Open Chem., 13 (1): 399–403, 2015.

   doi:10.1515/chem-2015-0050

3. Moravek, MJ; Schmiedt, L; Laca, M; Kanka, A; Hrachova, V: Radial profiles of the emission spectra of dc glow discharge sustained in molecular gases at medium pressures, Phys. Scr., 2014 (T161): Art. No. 014056 (5 pages), 2014.

   doi:10.1088/0031-8949/2014/T161/014056

4. Moravek, MJ; Laca, M; Kanka, A; Hrachova, V: Radial Distribution of the Temperature in the T-form of Oxygen DC Glow Discharge, WDS'17 Proceedings of Contributed Papers — Physics, 71–75, 2017.

5. Moravek, MJ; Kanka, A; Hrachova, V; Cap, J: Determination of Concentration of Excited Oxygen Particles by Optical Emission Spectroscopy, WDS'16 Proceedings of Contributed Papers — Physics, 137–143, 2016.

6. Moravek, MJ; Cap, J; Kanka, A; Hrachova, V: Atomic Oxygen Concentration Observation by Optical Emission Spectrometry in O_2 and O_2–N_2 DC Glow Discharge, WDS'15 Proceedings of Contributed Papers — Physics, 227–232, 2015.